ABSTRACT

Title of Thesis: CHARACTERIZATION OF THE SPATIAL DIFFERENCES IN HYDROLOGICAL FUNCTIONING IN A TIDAL MARSH, PATUXENT RIVER, MD: A FRAMEWORK FOR UNDERSTANDING NUTRIENT DYNAMICS

Karen Elizabeth Phemister, Master of Science, 2004

Thesis directed by: Dr. Karen L. Prestegaard
Department of Geology

This study investigates spatial variations in sediment hydraulic conductivity (K), network channel shape and horizontal groundwater flux magnitude toward tidal network channels in a freshwater tidal marsh. Results showed the average value of K at zero meters from the creekbank was significantly higher than the K at both 5 and 15 meters from the network channel creekbank. Creekbank gradient did increase with increasing distance from the main channel and some data indicated that channel width-to-depth ratio (F), which is inversely related to creekbank gradient, correlates well with K. In addition, horizontal groundwater flux magnitude at a depth of 11 cm was significantly greater than flux magnitude at 22 cm below the ground surface at the first-order network channel location. Horizontal flux magnitude was also significantly higher from 5 to 0 meters than from 15 to 5 meters from the network channel creekbank at both the first- and second-order channel locations.

CHARACTERIZATION OF THE SPATIAL DIFFERENCES IN HYDROLOGICAL FUNCTIONING IN A TIDAL MARSH, PATUXENT RIVER, MD: A FRAMEWORK FOR UNDERSTANDING NUTRIENT DYNAMICS

by

Karen Elizabeth Phemister

Thesis submitted to the Faculty of the Graduate School of the
University of Maryland, College Park in partial fulfillment
of the requirements for the degree of
Master of Science
2004

Advisory Committee:

Professor Karen L. Prestegaard, Chair
Professor Philip A. Candela
Professor Roberta L. Rudnick

ACKNOWLEDGEMENTS

This study was funded by a Graduate Research Fellowship grant from NOAA's National Estuarine Research Reserve System. In addition to paying me, they allowed me to perform my research at the beautiful Jug Bay Wetland Sanctuary. Especially during the heat of summer, kayaking along the Jug Bay tidal channels to install and check my equipment was an absolute pleasure. Thank you for the opportunity and the experience!

I would also like to thank the members of my thesis committee: Dr. Phil Candela for his advice and assistance regarding error analysis and for always being available to talk when I was uncertain how to proceed, and Dr. Roberta Rudnick for her attention to detail and encouragement to aim for perfection.

Most of all, I would like to thank my thesis advisor, Dr. Karen Prestegaard, who has provided endless advice, support and assistance during both my undergraduate and graduate studies at the University of Maryland. Without Dr. Prestegaard as my mentor, this research would not have been possible.

TABLE OF CONTENTS

LIST OF TABLES

LIST OF FIGURES

INTRODUCTION

Statement of the problem

Nutrient loads from urban and agricultural sources are carried by streamflow into the Chesapeake Bay. Excessive levels of nutrients in the Bay have historically resulted in algal blooms which decreased dissolved oxygen levels and killed other forms of aquatic life. It has been suggested that tidal marshes serve as sinks for both sediments and nutrients brought in via tidal waters (Seitzinger, 1988; Comin et al, 1997). At high-tide events, channel water overflows the creekbanks, flooding these marshes. The decreasing flow velocity of the flood water as it moves away from the channel results in sediments dropping out of suspension. In addition, as the tidally-introduced water infiltrates into the organic-rich marshland sediments, nutrients such as nitrogen and phosphorous adsorb onto the soil organic matter and/or are consumed by wetland microbes or flora. In this way, the wetland sediments become a nutrient-filter for tidally-introduced groundwater.

There are at least two factors that determine how efficiently a tidal marsh filters nutrients: 1) the level of nutrient demand, and 2) the dominant driver of vertical groundwater fluxes. Obviously, if more nutrient consumers (i.e. plants and microbes) draw their sustenance from the tidal marsh groundwater system, a higher level of nutrients can potentially be removed from tidally-introduced groundwater. However, for the nutrients within the tidal water to become available for consumption, the tidal water must infiltrate into the marshland sediments and become part of the groundwater system. Therefore, marshes with a higher proportion of tidal-source groundwater would have a greater potential to filter nutrients from that water.

Previous studies have concluded that, at relatively short distances from a tidal creekbank, horizontal groundwater movement is negligible. Conservative estimates put this distance at 15 meters (Harvey et. al., 1987; Nuttle, 1988). If groundwater flux is only vertical, changes in sediment pore water pressures could be due to evapotranspiration, infiltration of tidal water during times of flooding, influx of water from an underlying aquifer, or a combination of these three. (See Figure 1.)

If evapotranspiration is the dominant engine for tidal marsh groundwater flux, then nutrients will accumulate in marsh sediments. They will infiltrate with each occurrence of tidal flooding. Once the tide goes back out, evapotranspiration will lower the water table, taking away the water but not the substances dissolved in the water. Each time flooding occurs, this process will repeat, causing nutrients carried in the tidal waters to build up in the marshland sediments.

However, if influx from an upland unconfined aquifer is the dominant component of groundwater flow, then as evapotranspiration removes water from sediment pores, aquifer water will come in to reestablish an equilibrium pore pressure. When tidal flooding occurs, the sediments, already saturated with aquifer water, will not accept much

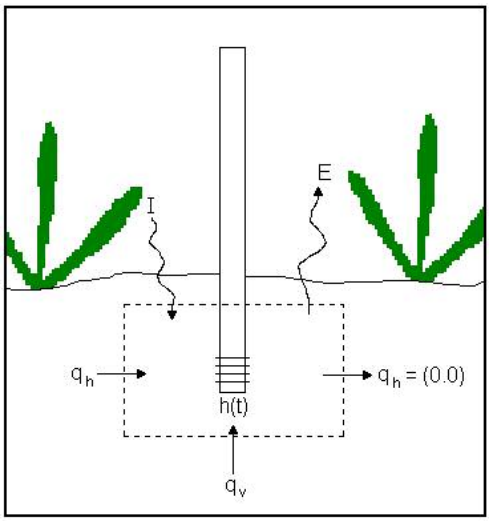

Figure 1: Groundwater fluxes within tidal marsh sediments. At distances greater than approximately 15 meters from a tidal creek, horizontal groundwater fluxes (q_h) are essentially zero. Therefore, changes in sediment pore pressure over time [h(t)] are due to vertical groundwater fluxes driven by evapotranspiration (E), tidal water infiltration (I) and/or upland aquifer influx (q_v). This figure is modified from Nuttle and Harvey, 1995.

infiltration from above. As a result, constituents of tidal waters would not tend to concentrate as much in the marsh sediments, assuming the aquifer water is nutrient depleted with respect to the tidal water.

So, the hydrologic functioning within a tidal marsh can be a significant determinant in how efficiently the marsh acts as a nutrient filter for tidally introduced waters. Depending on how much tidal water infiltrates into the marsh sediments and what happens to that water once it has infiltrated, the marsh may act as a nutrient sink or a nutrient source. In addition, the source/sink behavior of a marsh may change seasonally as hydrologic flux rates change.

Tidal marsh terminology

Tidal marsh systems are not homogeneous. A simple map or aerial photograph of these systems illustrates a complex array of areas; some with a high density of tidal network channels and others with no network channels at all. Within a tidal marsh, two different types of channels may exist: a main channel and a series of network channels. The main tidal channel is a stream that passes adjacent to the marsh. Tidal network channels are fully contained within the area of the marsh and feed into the main tidal channel. All freshwater tidal marshes contain at least one main channel thatconveys the tidal flow into the marsh, but the density of tidal network channels varies greatly from marsh to marsh. Some marshes fringe the main channel and have no network channels; others contain elaborate network channel structures with stream orders as high as 4^{th}- to 5^{th}-order. (See Figure 2.)

The most widely used method for determining stream channel order was developed by Horton in 1945. In this method, stream head waters are designated as first-

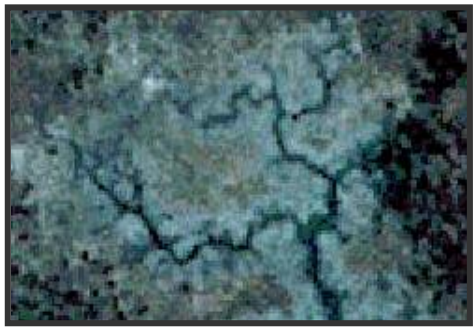

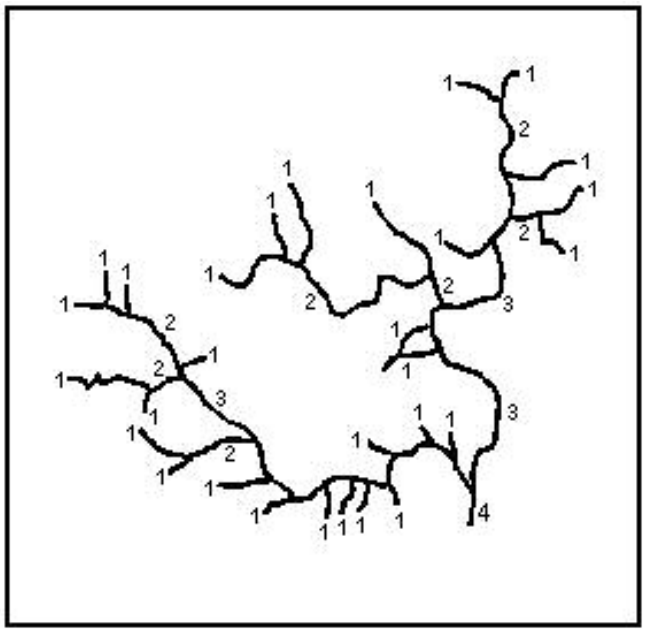

Figure 2: The organization and order of tidal network channels. (Right) Tidal network channels can have very complex structures, as shown by this channel map adapted from Smith-Hall (2002). The numbers give the stream order for each channel segment. (Above) This network system, shown in a high-resolution DOQ aerial photograph, is located along the Patuxent River approximately 2 ½ miles north of Jug Bay, MD.

order channels. When two first-order channels meet, the stream channel downstream of that juncture is designated a second-order channel; when two second-order channels meet, the stream channel downstream of that juncture is designated a third-order channel; etc. In general, higher order channels have larger cross-sectional areas. With regard to tidal network channels, because higher stream orders within a single network system are closer to the main tidal channel, they overflow their banks more frequently and obtain higher flood stages.

Purpose of the study

The most frequently used method for determining the magnitude of nutrient fluxes to and from tidal marshes is measuring the flow of tidal water into and out of a marsh and the nutrient concentrations of these waters. Results from these types of studies have been inconsistent. For example, Jordan and Correll (1991), who studied two marshes along the Rhode River, near Edgewater, MD determined that the lower marsh

had a net import of total organic nitrogen (TON), total organic phosphorous (TOP) and nitrate, and a relatively constant budget of total organic carbon (TOC), while the upper marsh had a net export of TON and TOC, and a relatively constant budget of TOP and nitrate. A similar study conducted by Hassen in 2001 at the Fier d'Ars Bay in France led to the conclusion that the lower marsh exported nitrate + nitrate (NN), phosphorous and dissolved organic carbon (DOC), while the upper marsh imported NN and DOC and remained relatively constant in phosphorous.

One possible explanation for these variations in net nutrient fluxes is differing hydrologic behaviors within tidal marshes related to differences in marsh geomorphology and hydrology. Currently, we do not understand the details, or even many of the basics, of tidal marsh hydrology. Numerous studies conducted in tidal marshes have focused on nutrient fluxes, but tidal marsh hydrology has been examined to a far lesser degree. To understand the specifics of nutrient fluxes, we must first understand the underlying driving mechanism, the hydrologic cycle within the marsh. The purpose of this study is to better define groundwater movement within tidal marshes. More specifically, it examines spatial variations in hydrologic functioning with respect to proximity to a tidal channel.

Previous work by Williams & Zedler (1999), Smith-Hall (2002) and Williams et al. (2002) has shown that geomorphic properties of tidal network channels can be highly predictable can thus provide a framework for examining hydrological and geochemical fluxes. (See 'Tidal channel geomorphology' subsection under 'Previous Studies'.)

Although vertical groundwater fluxes (driven primarily by evapotranspiration) determine to what degree tidal water constituents will become concentrated in the marsh

sediments, near-channel horizontal fluxes deliver groundwater to the tidal channel. As a result, the presence of tidal network channels within a tidal marsh would, logically, act to accelerate the filtration of tidal waters though the marsh sediments. In addition, the size, length and density of these channels would influence the amount of groundwater seeping into them.

Therefore, the tidal network system will be used as the framework for studying tidal marsh groundwater fluxes. Variations in sediment hydraulic conductivity, network channel shape and horizontal groundwater flux magnitude toward the network channel will be investigated. Because the magnitude and direction of groundwater flux is a function of sediment hydraulic conductivity and the hydraulic pressure gradient, all of these factors contribute to the amount of tidally-introduced floodwater than can infiltrate into the marsh sediments and then return to the channel through the groundwater system.

Hypotheses

Spatial organization of hydrologic properties

Research conducted in a freshwater tidal marsh by Pasternack et al. (2000) concluded that, with increasing distance from the main tidal channel, the percentage of particles adjacent to the channel that fall within the silt-clay range increases. Neglecting the effects of bioturbation, pore spaces between grains tend to decrease with decreasing grain-size (Wise & Myers, 2002). This decreased pore space can act to restrict groundwater flow, reducing the hydraulic conductivity (K) within the sediments. Therefore, it seems reasonable that the findings by Pasternack et al. of decreasing average grain-size with increasing distance from the main tidal channel would correlate with decreasing hydraulic conductivity with increasing distance from the main tidal channel.

As over-bank flooding occurs, fine sediments are carried with the flood waters and, as the velocity of the floodwater decreases, finer and finer sediments drop out of suspension. Because over-bank flooding occurs to a lesser extent around channels of lower order, finer sediments are carried to a lesser distance from the network channel with increasing distance measured up the network channel from the main channel. As a result, even though finer sediments will be carried further up the network channel, they will not be carried as far away from the channel bank when over-bank flooding occurs. (See Figure 3.) Therefore, hypothesis #1 (H1) is:

With increasing distance from the main channel, measured up the network channel, the hydraulic conductivity (K) in the sediments at a constant distance from the network channel creekbank will decrease.

Similar to Pasternack et al., Schumm's 1960 work on alluvial streams revealed that, with increasing channel width-to-depth ratio (F) the percentage of silt-clay fraction in the channel and channel banks decreases exponentially. (See Figure 4A.)Assuming

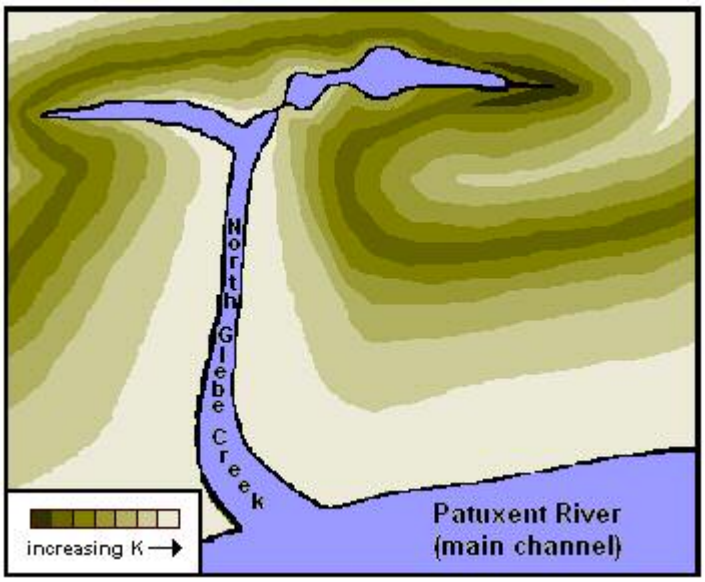

Figure 3: Cartoon illustrating hypothesis #1 (H1). We expect that the finding by Pasternack et al. (2000) of an increasing sediment silt-clay fraction with increasing distance from the main tidal channel will translate to decreasing sediment hydraulic conductivity (K) with increasing distance from the main channel. This cartoon shows the confluence of North Glebe Creek (a tidal network channel) and the Patuxent River (the main tidal channel) in North Glebe Marsh at the Jug Bay Wetland Reserve.

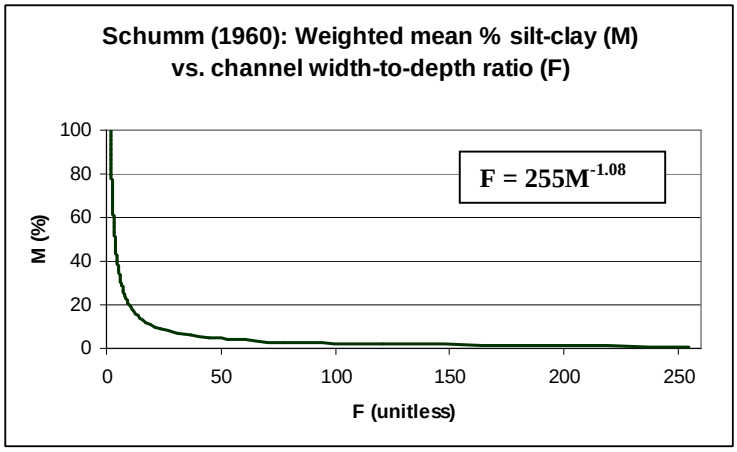

Figure 4A: Schumm's relationship between F and M. As the width-to-depth ratio (F) of an alluvial channel increases, the silt-clay fraction (M) in the channel sediments decreases according to the equation: $F = 255M^{-1.08}$.

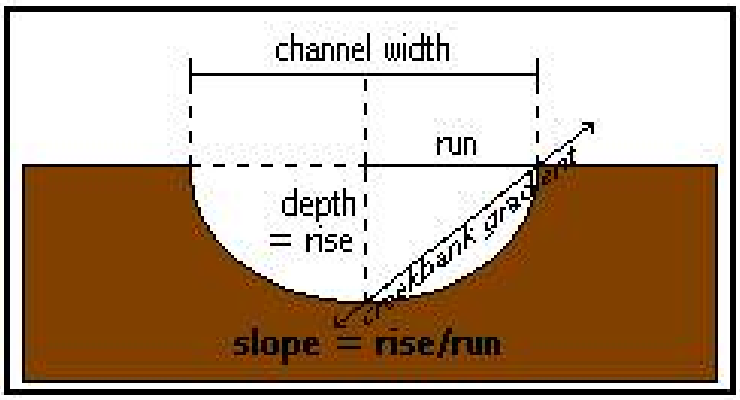

Figure 4B: Relationship between creekbank gradient and F. The channel creekbank gradient is the slope of the line from the deepest part of the channel to the top of the creekbank. Since the slope of a line is the rise / the run, and the rise is equal to the channel depth and the runs is equal to ½ the channel width, the creekbank gradient is equal to the channel depth / ½ the channel width. Since F = width / depth, creekbank gradient = 2/F.

that the channel is symmetrical and the deepest part of the channel is half-way across, the creekbank gradient can be related to Schumm's F:

creekbank gradient = slope = rise/run = depth / ½ width = 2(d/w)

F = w/d,

Therefore, creekbank gradient = 2/F

where d is the maximum depth of the channel and w is the width across the top of the channel. (See Figure 4B.) Therefore, F is inversely related to gradient and Schumm's finding of a decreasing silt-clay fraction adjacent to a channel of increasing F would translate to a decreasing silt-clay fraction adjacent to a channel with a decreasing creekbank gradient.

Combining this finding with that of Pasternack et al. (who found an increasing sediment silt-clay fraction with increasing distance from the main tidal channel), we would expect to find that the tidal network channel creekbank gradient will increase with increasing distance from the main channel. Therefore, hypothesis #2 (H2) is:

With increasing distance up a tidal network channel from the main tidal channel, the gradient of the network channel creekbank will increase.
(See Figure 5.)

Groundwater flux

In 1988, Nuttle observed that, in tidal marshes, significant horizontal groundwater flux is restricted to within 15 meters of a creekbank. Beyond that distance, groundwater flux is essentially only vertical. It seems reasonable that this 15 meter cut-off is not constant and that the distance from the channel to which horizontal groundwater flux is significant would correlate with distance up the network channel from the main channel.

Darcy's Law is the equation used to describe groundwater flow and is stated:

$$Q = -KA(dh/dL)$$

where Q is flux (in units of volume/time), K is hydraulic conductivity (in units of

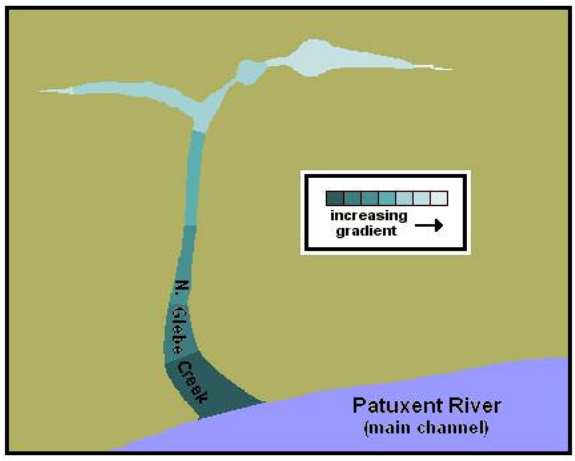

Pasternack: ⬆ distance ➡ ⬆ S-C
Schumm: ⬆ F ➡ ⬇ S-C
F ∝ 1/gradient
Schumm (revised): ⬇ gradient ➡ ⬇ S-C
OR: ⬆ gradient ➡ ⬆ S-C
➡➡ ⬆ distance ➡ ⬆ gradient

Figure 5: Explanation of hypothesis #2 (H2). Above, a combination of research from Pasternack et al. (2000) and from Schumm (1960) leads to the conclusion that, with increasing distance up the tidal network channel from the main channel, we will observe an increasing creekbank gradient. 'Distance' is from the main channel and 'S-C' is the sediment silt-clay fraction.

distance/time), A is the cross-sectional area through which flux is being calculated (in units of length-squared) and dh/dL is the hydraulic gradient (unitless). The hydraulic gradient is the change in sediment pore pressure with distance and is physically defined as the difference in hydraulic head between two locations, measured with a piezometer, divided by the distance between the two locations. The negative sign in Darcy's equation is directional and demonstrates that groundwater moves from areas of higher pressure to areas of lower pressure. From the equation, we can see that groundwater flux magnitude is maximized when both K and dh/dL are high.

Assuming that hypothesis #1 (decreasing K with increasing distance from the main channel) is correct, the decreasing hydraulic conductivities around the network channels should result in decreasing fluxes within the near-channel sediments. On the other hand, an increasing creekbank gradient, as suggested by hypothesis #2, could translate to increasing groundwater flux toward the network channel.

In an unconfined aquifer, as top-loading pressure from the overlying sediments increases, pore-pressure increases. Assuming a homogeneous medium (constant density), pore-pressure would increase linearly with increasing depth below the ground surface (Serway, 1996). Using the equation for the variation of pressure with depth:

$$P = P_o + \rho g h$$

where P is pore-pressure, P_o is the top-loading pressure, ρ is the sediment density, g is the rate of acceleration due to gravity and h is depth below the ground surface, we see that if g and ρ are constant, this equation becomes a linear function that varies based on changes in h:

$$P = P_o + (C \times h)$$

where C is the product of two constants ($\rho \times g$). Therefore, in a homogeneous medium, pore-pressure should increase linearly with increasing depth below the ground surface.

Creekbank gradient is a function of both the width and the depth of the channel. The gradient may increase because 1) the channel depth is increasing and/or 2) the channel width is decreasing. Although over short stretches, the channel depth may increase with increasing distance from the main channel, overall, the channel depth must decrease simply because it is approaching zero at the channel head. For the same reason, network channel width must also decrease overall with increasing distance from the main channel. So, assuming H2 is correct and the network channel creekbank gradient does increase with increasing distance from the main channel, the channel width must decrease at a faster rate than the channel depth and as the creekbank gradient increases, the dh/dL between the channel and the adjacent sediments increases. (See Figure 6.)

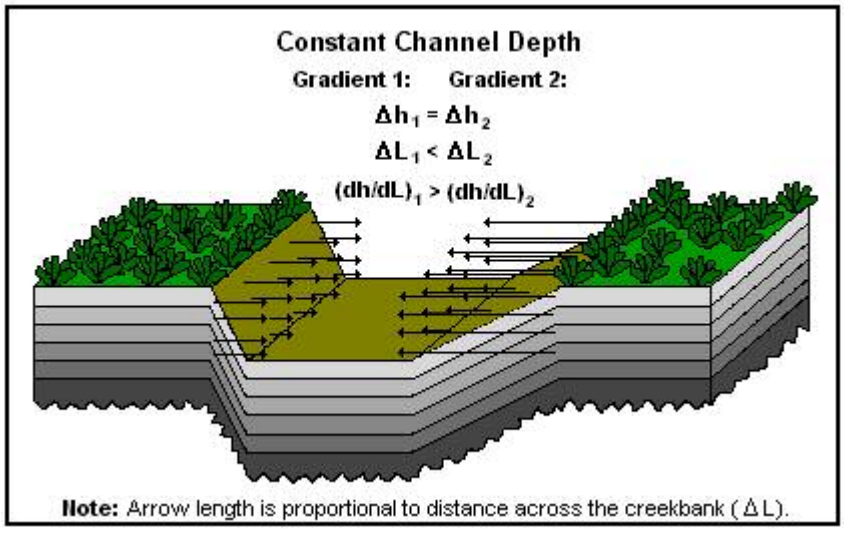

Figure 6: The effect of creekbank gradient change on horizontal groundwater flux. Assuming a linear increase in pore-pressure with increasing depth below the ground surface, a steeper creekbank gradient would produce a greater dh/dL between the empty channel and the adjacent sediments. Increasing dh/dL increases groundwater flux magnitude.

Therefore, the two main controls on changing groundwater flux magnitude with increasing distance from the main tidal channel, K and dh/dL, are working in opposite directions. While decreasing K should have the effect of decreasing groundwater flux, increasing creekbank gradient should produce an increasing dh/dL around the channel, thereby increasing the magnitude of groundwater flux. Up until this point, I have not discussed the creekbank area through which groundwater can flux horizontally into the network channel. Decreasing channel width would create a smaller area (A) through which vertical flux could enter the channel, but decreasing channel depth would create a smaller area through which horizontal flux could enter the channel. Therefore, this decreasing channel depth would act to decrease the magnitude of horizontal groundwater flux to the network channel. So, decreasing channel depth and decreasing K around the channel both act to decrease horizontal groundwater flux to the channel, and only increasing dh/dl acts to increase horizontal groundwater flux to the network channel with increasing distance form the main channel. So my prediction is that the effects of both decreasing K and decreasing A will out-weigh the effects of increasing dh/dL and hypothesis #3 (H3) is:

> *The magnitude of near-channel horizontal groundwater fluxes will decrease with increasing distance from the network channel creekbank and the rate of this decrease will increase with increasing distance from the main tidal channel.* (See Figure 7.)

Previous studies

Spatial organization of hydraulic conductivity

Previous studies on hydraulic conductivity (K) distributions in wetland sediments have focused primarily on vertical trends. In 1987, Knott et al. measured K-values over a depth profile of 1.6 meters in two Massachusetts salt marshes. Values ranged from 10^{-5} to

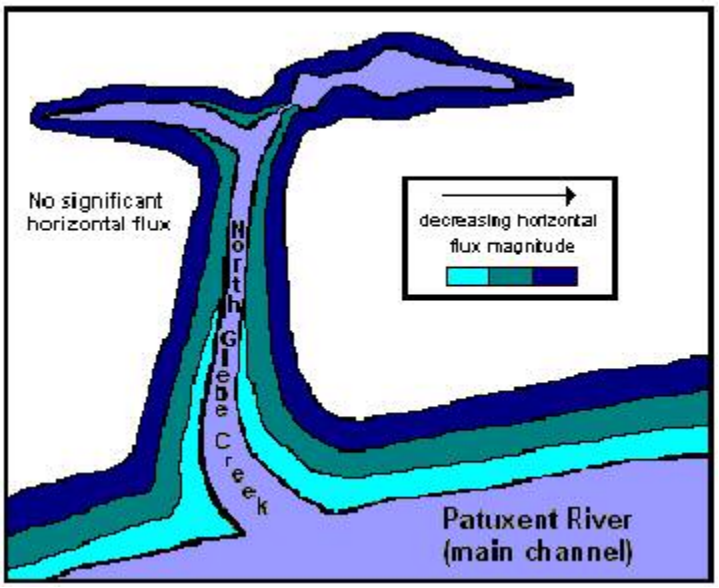

<u>Figure 7</u>: Cartoon illustrating hypothesis #3 (H3). With increasing distance from the main channel along the tidal network channel, both channel depth and K in the channel-adjacent sediments decreases. In addition, horizontal groundwater fluxes are only significant within the near-channel region of the tidal marsh. As a consequence of all of these factors, we expect that the magnitude of near-channel horizontal groundwater fluxes will decrease with increasing distance from the network channel creekbank and the rate of this decrease will increase with increasing distance from the main tidal channel. NOTE: The flux magnitude lines on this figure are for explanation purposes only and are not drawn to scale.

10^{-1} cm/s but were most frequently on the order of 10^{-3} cm/s. In a study conducted by Katyl (1995) in a forested freshwater wetland in Anne Arundel County, MD, measured hydraulic conductivities ranged from approximately 10^{-10} to 10^{-4} cm/s over the top 2.5 meters of sediment. Similarly, Muriceak (1996) measured K-values in a Calvert County, MD cypress swamp that ranged from 10^{-8} to $10^{-3.5}$ cm/s over the top 2 meters of sediment.

In all of the previously mentioned studies, the range of K-values measured at the shallowest depths overlapped with the range of values measured at the deepest depths. The highest K-values measured by Katyl and Muriceak were at the shallowest measurement depths, but no consistent change in K with depth was observed. So, in general, the hydraulic conductivity in wetland sediments varies greatly (up to 6 orders-of-magnitude over the top 2.5 meters) but demonstrates no consistent increase with increasing depth below the ground surface.

In this study, horizontal K-distributions with respect to proximity to a tidal channel will be examined. Previous studies of horizontal K-distributions have been scarce, but work done by Pasternack et al. (2000) on tidal freshwater channels showed that the grain-size distribution of floodplain sediments changes with distance from the main channel. Larger (sand-sized) particles are found near the juncture of the main channel and the tidal network channel. With increasing distance from the main channel, the average sediment size decreases. This can be explained by the observations of Leonard and Luther in 1995: stream-flow velocities decrease with increasing distance from the main channel. As flow velocity decreases, smaller and smaller particles are dropped out of suspension and onto the floodplain. As a result, we see the largest particles closest to the main channel and closest to the creekbank.

In 2002, Schultz and Ruppel examined hydraulic properties across the upland-estuary boundary in two Georgia salt marshes. They discovered a zone of reduced K (up to 2 orders-of-magnitude less) between the upland and the estuary. They speculated that this 'clogging layer' would drastically limit interaction between the upland groundwater and that found in the marsh. Schultz and Ruppel also observed this 'clogging layer' around tidal channels of low gradient. The lower K sediments around these channels tended to prevent horizontal tidal pumping to the groundwater adjacent to the channel, as was observed with steep-banked channels. Instead, the primary tidal response was from top-loading.

Assuming network channel creekbank gradient increases with increasing distance from the main tidal channel (H2), this latter finding by Schultz and Ruppel contradicts that of Pasternack et al. Their research observed a low-K 'clogging layer' around channel

banks of low gradient, which would be more descriptive of network channels closer to the main channel. However, their study was conducted in a salt marsh, whereas the work done by Pasternack et al. was in a freshwater marsh. This difference in results may be due to a difference in the average near-surface K between these two types of marshes. In their 1987 study, Knott et al. observed below average conductivities in near-surface sediments (with respect to deeper sediments) in the salt marsh in which they conducted their research. They noted that this result was contrary to studies conducted in freshwater marshes, where near-surface sediments tended to have lower conductivities than deeper sediments. This suggests that salt, left behind in near-surface sediments by evapotranspiration, can decrease the hydraulic conductivity within those sediments.

Tidal channel geomorphology

Studies of tidal channel morphology have consistently shown decreases in both channel width and depth with increasing distance from the channel mouth toward the channel head. In 1993, Leopold et al. measured a decrease in channel width from 47 to 0 ft over a 19,000 ft length of California natural estuarine tidal creek. Along this same stretch, an 'accompanying decrease in depth' was also observed. Work by Williams & Zedler in 1999 compared the channel morphology in 4 natural tidal marshes to that in 4 constructed tidal marshes. For the natural channels, they found a consistent decrease in F (width-to-depth ratio) with decreasing channel order. As discussed previously, a decrease in F would correspond to an increase in creekbank gradient. This F decrease was the result of a minor decrease in average channel depth (approximately 0.1 meters) accompanied by a much larger (approximately 8 meters) decrease in average channel width between 4^{th}- and 2^{nd}-order tidal channels.

Work done by Smith-Hall (2002) found strong correlations between stream frequency (based on stream order), channel length and contributing marsh drainage area for interior marsh tidal network channels. Examination of several freshwater tidal marshes approximately 2 ½ miles north of Jug Bay revealed that the frequency (stream density) of tidal network channels decreases exponentially with increasing stream order for 1st- through 3rd-order channels. It was also discovered that cumulative stream length (the length of a 3rd-order channel would include the length of the compared 1st- and 2nd-order channels that drain into it) increases exponentially with increasing channel order. When the amount of contributing marsh drainage area was compared to these network channel stream lengths, a very strong linear relationship was discovered. The equation for this relationship was:

$$A = 43.6(L) - 858$$

where A is the amount of contributing marsh area (in m^2) and L is the cumulative stream length (in meters). The correlation between these two parameters was $R^2 = 0.9886$.

A detailed comparison of changes in channel depth and width by Williams et al. (2002) found strong relationships ($R^2 = 0.84$ for channel depth and $R^2 = 0.88$ for channel width) between these factors and the amount of tidal salt marsh area contributing to the channel for three mature San Francisco Bay tidal creeks. Changes in channel depth were described by the equation:

$$d = 1.31A^{0.202}$$

where d is the channel depth in meters and A is the amount of contributing marsh area in hectares. Changes in channel width were described by the equation:

$$w = 3.44A^{0.552}$$

where w is the channel width in meters. A comparison of these trends with data collected for this study can be found in the Results section of this paper under 'H2 Results: Changes in creekbank gradient'.

Groundwater flux within tidal marshes

Harvey et al. (1987) characterized groundwater fluxes around tidal channels. (See Figure 8.) They focused on the area within approximately 5 meters of the creekbank and determined that, within this near-creek area, there is virtually no vertical component of groundwater flow during times of non-flooding. When the water level in the channel drops below the top of the creekbank, the largest pressure gradient is between the empty part of the channel and the saturated near-channel pore spaces. As a result, the pore water flows horizontally toward the channel. During times of flooding, top-loading pressures dominate and vertical infiltration fills empty pore spaces previously emptied by horizontal groundwater flux to the channel. According to Hughes et al. (1998), "…tidal forcing is a dominant mechanism of porewater movement in the saturated and intertidal zones, with the largest fluxes due to subsurface drainage to the creek."

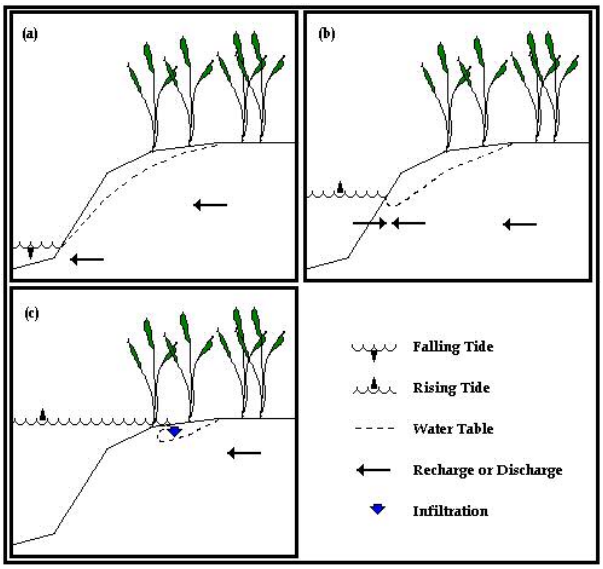

Figure 8: Diagram of the 3 stages of groundwater flow within 5 meters of a tidal channel. This figure, modified from Harvey et al. (1987), shows: a) discharge from the marsh during falling tide, b) simultaneous recharge and discharge in the early stages of a rising tide, and c) surface infiltration filling the remaining pore spaces once over-bank flooding has begun.

In 1988, Nuttle investigated horizontal groundwater flux adjacent to a tidal creek in a Boston, Massachusetts salt marsh. He determined that there are actually three distinct zones within the marsh. Within 2.5 meters of the tidal creekbank, horizontal groundwater flow oscillates tidally, flowing toward the channel at low tides and away from the channel at high tides. Between 2.5 and 15 meters from the channel is a transition zone where horizontal groundwater flow is driven by surface flooding. Beyond 15 meters from the creekbank, he found essentially no horizontal component of flow.

MATERIALS AND METHODS

Measurement of hydrologic properties

Minimization of response-time errors

Piezometers are the standard equipment used to measure pore pressures, or hydraulic head, within saturated sediments. The efficiency of a piezometer is a function of both the hydraulic conductivity of the sediments into which the piezometer is installed and the design of the piezometer. When sediment pore-pressure changes, the head within the piezometer changes in response. However, this response is not instantaneous. The hydraulic conductivity of the sediments around the piezometer intake affects the rate at which groundwater can flow into or out of the piezometer. Higher hydraulic conductivities will allow faster response times than lower hydraulic conductivities. In addition, a 2001 paper by Hanschke and Baird showed that the response-time of a piezometer can be minimized by minimizing the cross-sectional area of the standpipe and/or maximizing the size of the piezometer intake. A standpipe with a smaller cross-sectional area requires less water flow between the sediments and the piezometer to change the height of the water-column within the piezometer. A larger piezometer intake allows a larger volume of water to enter or exit the piezometer at a given time.

Hanschke & Baird produced a model using Hvorslev's (1951) empirical formula for 'basic hydrostatic time lag' (T):

$$T = \frac{A}{FK}$$

where A is the cross-sectional area within the standpipe (in units of length-squared), F is a piezometer intake shape factor (in units of length), and K is the hydraulic conductivity within the sediments around the intake (in units of distance/time). To calculate F, they

used the equation developed by Brand & Premchitt (1980) for a closed bottom, cylindrical intake:

$$F = \frac{2.4\pi L}{\ln\left(1.2\,L/d + \sqrt{1 + (1.2\,L/d)^2}\right)}$$

where L is the length of the intake and d is the outer diameter of the intake. Hanschke & Baird used the ratio F/A to calculate an 'efficiency' for two different piezometer designs. Higher efficiency is equated with faster piezometer response-time. The 'efficient' piezometer in their study had F/A = 39.3 cm^{-1}. The 'inefficient' piezometer had F/A = 0.8 cm^{-1}.

Three different sediment configurations were used by Hanschke & Baird: sand over silt, silt only and peat over silt. In the peat over silt simulation, which most closely matches the conditions at the Jug Bay site, head measured in the peat layer by the efficient piezometer very closely tracked actual changes in sediment pore-pressure, with both the time-lag and error magnitude being approximately zero. The inefficient piezometer, under the same conditions, had a maximum difference between actual and measured heads of 4 cm with duration of less than 1 hr. In the silt layer, the efficient piezometer had a maximum magnitude error of 1.3 cm with duration of approximately 2 hours. The inefficient piezometer registered errors greater than 14 cm that lasted over 6 hours.

Hydraulic conductivity measurement

Piezometers can also be used to measure hydraulic conductivity. In 1951, Hvorslev developed a method (called a slug-test) by which K could be measured in situ. For this test, the water height (or pressure head) within the piezometer is changed by inserting a slug into the piezometer. This produces a disequilibrium between the pressure

head in the piezometer and the pore-pressure in the sediments. As a result, the water in the piezometer will flow out of the intake and into the sediments until equilibrium is re-established. To determine K, the piezometer's rate of recovery is timed.

The original, or equilibrium, head (H_o) is measured before the slug is inserted. After the slug is inserted, an initial disequilibrium measurement (H) is made and timing of the recovery begins. Head measurements (H_t), along with the corresponding lapsed-time measurements (t), are ideally recorded until the head within the piezometer has returned to its original height. Then, h/h_o is plotted against t on a semi-logarithmic graph. (See Figure 10.) The h in the ratio h/h_o is equal to $H_o - H_t$. The h_o is equal to $H_o - H$. From this plot, a value for T_o (the time when $h/h_o = 0.37$) can be found. To calculate K, the equation:

$$K = \frac{r^2 \ln(L/R)}{2LT_o}$$

is used. In this equation, r is the radius of the well casing, R is the radius of the well

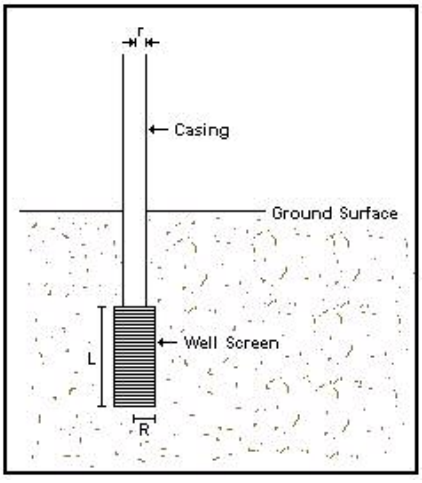

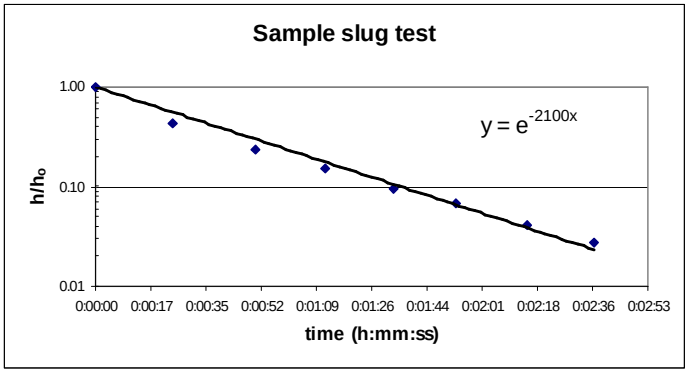

Figure 9 (left): Diagram showing the variables used by Hvorslev (1951). L is the length of the well screen, R is the radius of the well screen and r is the radius of the well casing. This image is from revised from Fetter, 1988.

Figure 10 (right): In situ hydraulic conductivity (K) can be measured using a slug-test. h/h_o vs. the amount of time that has lapsed since the beginning of the test is plotted on a semi-logarithmic graph. 'h' is the water height before displacement (H_o) minus the water height at time = t (H_t). 'h_o' is H_o minus the water height after displacement (H). 'T_o' is the time at which h/h_o equals 0.37, or when 63% recovery has been reached. T_o can be calculated from the equation for the regression line.

screen and L is the length of the well screen. (See Figure 9.) The K measured by this method is the average K over the length of the screened interval.

Sediment compressibility

One of the assumptions made by Hvorslev is that the medium in which a slug-test is being performed behaves in a rigid manner. This is never entirely true, but some soils match this assumption more closely than others. Wetland soils are particularly well known for their compressibility.

In his 1995 article, Baird showed how abruptly changing the head in a piezometer by inserting a slug will, in a compressible soil, cause the sediments around the piezometer intake to swell to accommodate the influx of water. As the head in the piezometer drops, the difference in pressure between the piezometer and the sediments reduces and the sediments begin to re-consolidate. (See Figure 11.) This change in piezometer response due to sediment swelling can be seen as an initially fast drop followed by a leveling out of the h/h_o vs. time data on a slug-test plot. (See Figure 12.) This response has been noted

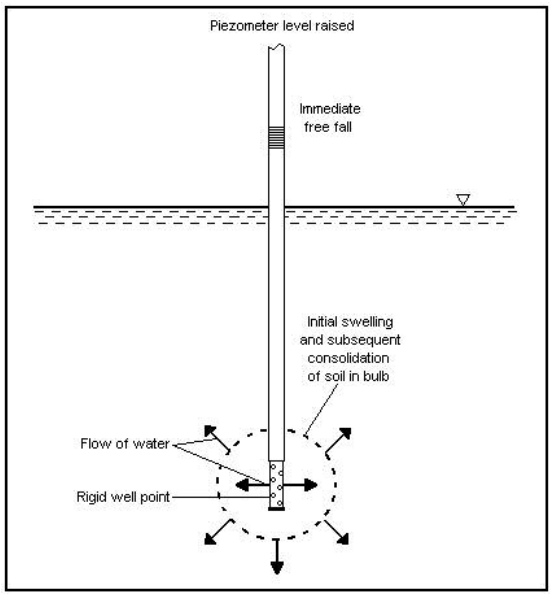

<u>Figure 11</u>: The effect of suddenly raising piezometric head in a compressible medium. The sediment around the intake will initially swell to accommodate the sudden influx of water, but will begin to re-compress as the pressure difference between the piezometer and the sediments drops. This figure is re-drawn from Baird, 1995.

in numerous articles, including Ingram et al. (1974), Hemond & Goldman (1985) and Baird & Gaffney (1994).

If there is relatively constant piezometer response after elevation of piezometric head for a slug test (i.e. early data fall along the same trend-line as later data), an unanchored trend-line through the h/h_o vs. time data will pass very close to the origin (0,1). For perfectly rigid sediments, this line would pass directly through the origin. If, on the other hand, there is an initial sediment swelling response, the trend-line will cross the axis well below the origin, as seen in Figure 12. Observing this fact, Baird (1995) used the ratio T_{90}/T_{50} as a measure of soil compressibility. T_{90} is the time during a slug-test when 90% recovery has occurred ($h/h_o = 0.10$) and T_{50} is the time when 50% recovery has occurred. If no initial fast (with respect to later data) decline occurs in the head ratio, the h/h_o vs. time trend-line will pass through the graph origin and the equation describing the trend-line will be:

$$h/h_o = e^{-C*(Ty)}$$

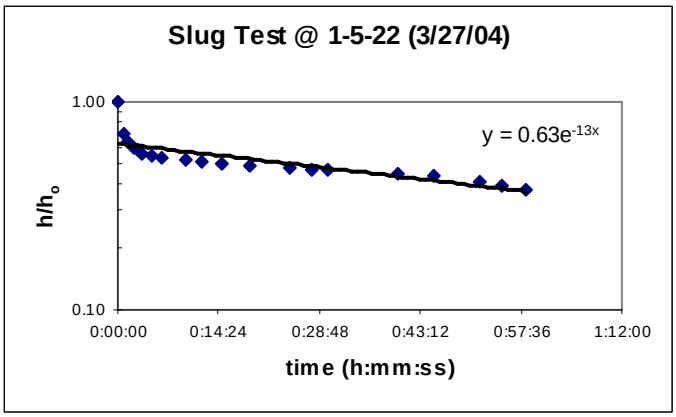

Figure 12: Piezometer response to a slug-test conducted in a compressible medium. Baird (1995) noted that, when a slug-test is performed in a compressible sediment, an h/h_o vs. time plot of the resultant data will show an initial fast drop followed by a leveling off in the rate of change of h/h_o.

where -C is a constant and T_y is the time corresponding to h/h_o read from the trend-line. Therefore:

$0.10 = e^{-C*(T90)}$ | $0.50 = e^{-C*(T50)}$

$\ln(0.10) = -C(T_{90})$ | $\ln(0.50) = -C(T_{50})$

$T_{90} = \ln(0.10) / -C$ | $T_{50} = \ln(0.50) / -C$

$$T_{90}/T_{50} = \ln(0.10) / \ln(0.50) = 3.322$$

So, if a soil is perfectly rigid, $T_{90}/T_{50} = 3.322$. If the soil is non-rigid, the trend-line will pass below the origin ($y < 1$) and the value of T_{90}/T_{50} will be greater than 3.322. The higher the value of T_{90}/T_{50}, the more compressible the soil. T_{90}/T_{50} values between 3.895 and 7.575 were recorded by Baird and Gaffney (1994) in fen peats and Premchitt and Brand (1981) measured T_{90}/T_{50} values between 5.87 and 13.25 in laboratory compression tests of tropical clays.

The study site

This study was conducted at the National Estuarine Research Reserve's Jug Bay, MD location. (See Figure 13.) The Jug Bay wetland is on Maryland's Western Shore and is located along the Patuxent River, a tributary to the Chesapeake Bay, at 38°46'53"N, 76°42'49"W. A large portion of the Patuxent's riparian zone is preserved as park-land for several miles upstream of Jug Bay. At the far north of the Jug Bay Reserve, the Western Branch, a second-order regional stream, meets the Patuxent. Vast freshwater tidal wetlands are supported by both of these rivers.

The Jug Bay wetland alone contains approximately 300 acres of freshwater, tidal marsh with an extensive structure of tidal network channels. The two main channels at this study site are the Patuxent River and Jug Bay itself. All of the tidal network channels connect with one of these two bodies. Jug Bay is bounded by three separate marshes:

South Glebe Marsh to the north, Black Walnut Creek Marsh to the west and Reed Marsh to the south. Research for this study was limited to South Glebe Marsh, North Glebe Marsh and Billingsley Marsh. North Glebe Marsh and Billingsley Marsh drain into the Patuxent. (For marsh locations, see Figure 14.)

All of the previously mentioned marshes flood semi-diurnally with the rising tide and drain back into the network channels at low tide. The tidal range in the low marshes is approximately 2 feet. The site's extensive mud flats are dominated by spatterdock (*Nuphar advena*). Wild rice (*Zizania aquatica*) is also present and attracts thousands of birds to the reserve.

Data collection

Ground-surface elevations

Because the sediments at the wetland are sub-solid (muddy), the ground does not support much surface pressure. This makes the use of traditional surveying equipment for

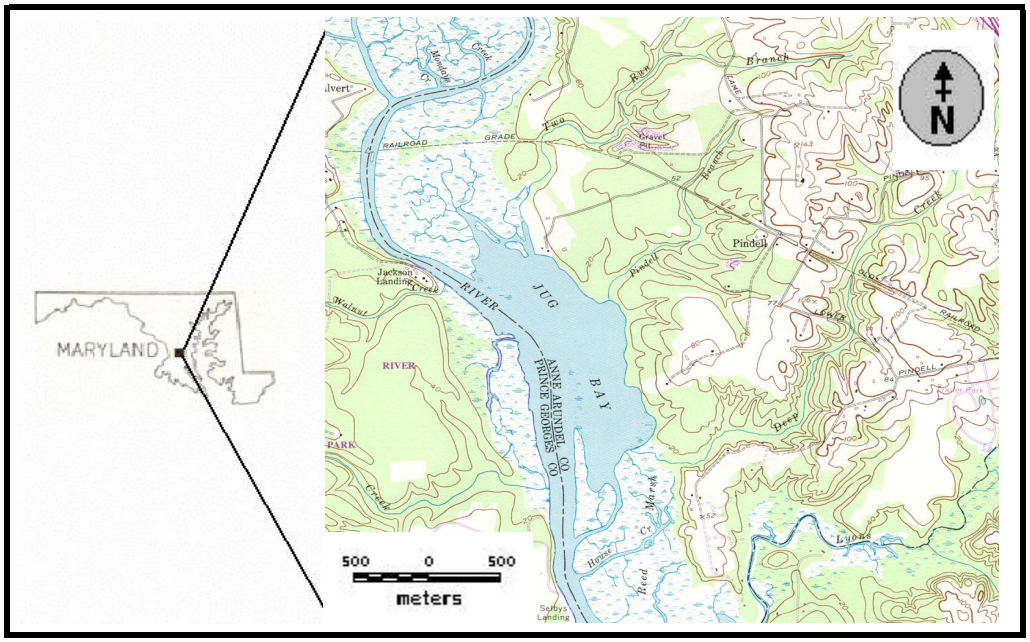

Figure 13: The Jug Bay study site. This freshwater tidal wetland is located along the Patuxent River, MD. Jug Bay is part of the National Estuarine Research Reserve. (Image taken from the USGS Bristol quadrangle map, photorevised 1979.)

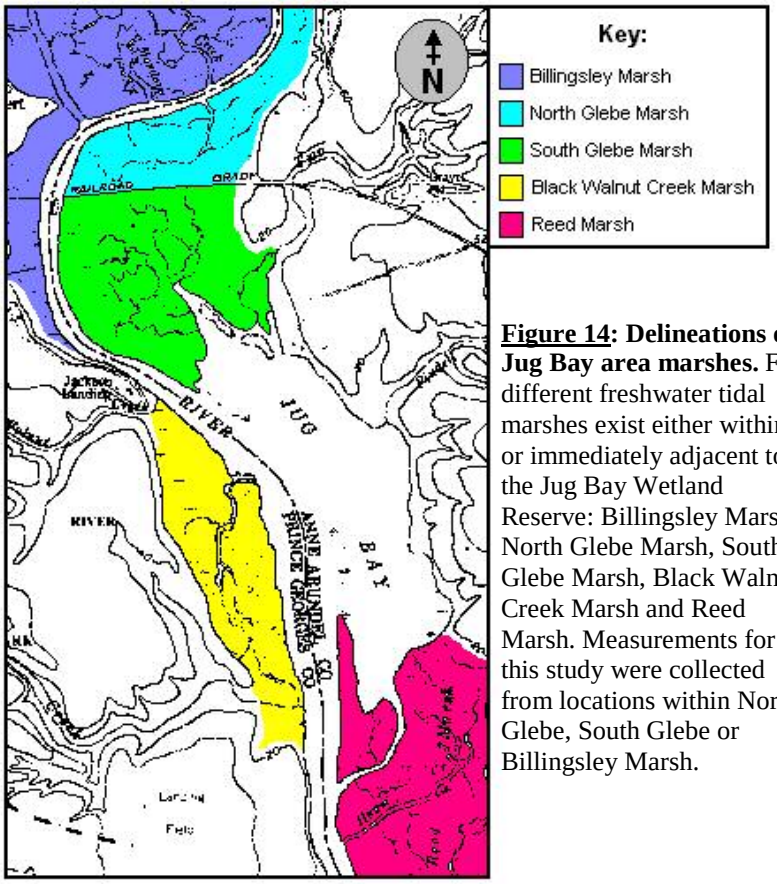

Figure 14: Delineations of Jug Bay area marshes. Five different freshwater tidal marshes exist either within or immediately adjacent to the Jug Bay Wetland Reserve: Billingsley Marsh, North Glebe Marsh, South Glebe Marsh, Black Walnut Creek Marsh and Reed Marsh. Measurements for this study were collected from locations within North Glebe, South Glebe or Billingsley Marsh.

the determination of ground-surface elevations extremely difficult. However, when calculating total piezometric head, it is necessary to know the relative surface elevations at the piezometer locations. For this reason, an alternative method for measuring relative elevations between piezometer locations was necessary. Fortunately, the National Estuarine Research Reserve has a YSI 6600 multi-parameter probe and data-logger installed approximately 700 meters from the location of the piezometers at the Railroad Bed Monitoring Station (RBMS). This instrument, among other things, records the water depth in the main channel running through the Jug Bay Wetland at 15 minute intervals. These data are collected, put through quality assurance / quality control checks, and published by the Maryland Department of Natural Resources.

To calculate ground-surface elevations, water depth measurements were made at each piezometer location, and the time of day that the measurement was made was recorded. Assuming that the surface of the flooding water made a perfectly horizontal plane, the depth of the water at the piezometer location was subtracted from the depth of the water at the monitoring station at the same time. (See Figure 15.) When water depth measurements at piezometer locations were made between actual measurement times at the monitoring station, a linear regression was used to approximate the water depth at the station. Multiple measurements were made at each piezometer location so that an average and standard deviation could be calculated for the ground-surface elevation estimations. (See Table 1.) All reported elevations are, therefore, relative to the ground-surface elevation at the monitoring station and assume that the elevation at the station is zero.

Piezometer design

Due to the large number of piezometers required for this study, the cost of each piezometer had to be minimized. For this reason, simple standpipe piezometers were

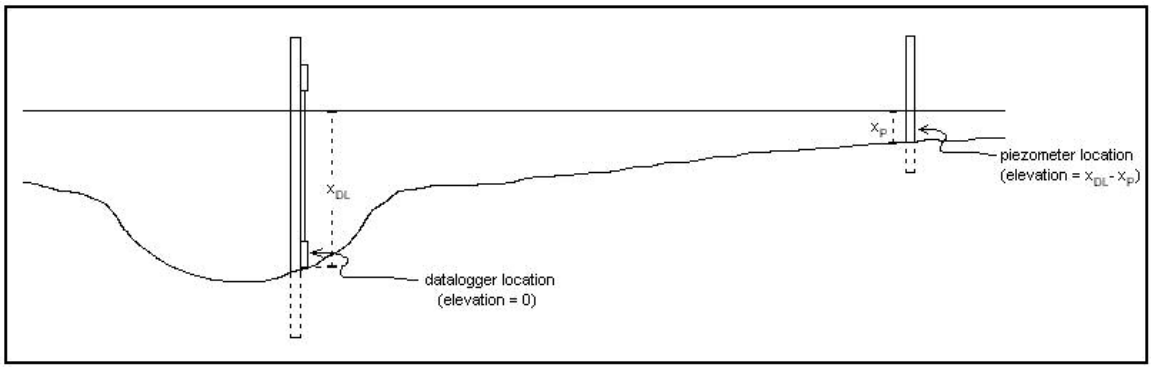

Figure 15: Calculation of relative ground-surface elevations. The ground surface elevation at each piezometer location was measured by relating the water depth at the piezometer to the water depth recorded by a datalogger at the Railroad Bed Monitoring Station. x_{DL} is the depth of the water at the monitoring station at a given time. x_P is the depth of the water at the piezometer location at the same time. Assuming the ground surface elevation at the monitoring station is zero, the elevation at the piezometer is $x_{DL} - x_P$.

Piezometer name	Elevation (m)	σ	n
1-0	1.02	0.03	7
1-5	1.12	0.03	7
1-15	1.17	0.02	6
1-25	1.48	0.01	3
2-0	0.84	0.03	6
2-5	0.98	0.02	6
2-15	1.03	0.02	7
2-25	1.06	0.01	4

Table 1: Calculated surface elevations. Surface elevations are measured relative to the bottom of the channel at the Railroad Bed Monitoring Station, where water-depth measurements are made. Piezometer names beginning with a '1' are located next to a first-order tidal network channel. Piezometer names beginning with a '2' are next to a second-order tidal network channel. Numbers following the dash in the piezometer name are the distance of the piezometer away from the network channel creekbank, measured in meters. 'n' is the number of data-points used to calculate the elevation.

used. This type of piezometer is usually (and in this case) made of PVC which is inserted vertically into the ground and has an opening at the depth where measurements are to be made. The simplest standpipe piezometers are unmodified pipe with the bottom of the pipe left open for flow of groundwater between the sediments and the pipe (piezometer). Most piezometers are capped at the bottom and slotted and screened over a specific interval (known as the 'screened interval' or 'intake') for flow of groundwater to and from the piezometer.

From Hanschke & Baird's 2001study, it is obvious that large, long-lived errors can occur in piezometers with a low F/A ratio. (See 'Minimization of response-time errors' subsection under 'Methods'.) In fact, even with a high F/A ratio, errors measured in silt overlain by peat, while small in magnitude, can last for a couple of hours. To minimize these time-lag errors in hydraulic head measurements, the piezometers for this study were designed to maximize the F/A ratio. PVC with an inner diameter of ½-inch was used. This is the minimum diameter recommended in order to avoid capillary effects within the piezometer. For ease of installation and to cause minimal disturbance to the surrounding sediments, the outer diameter of the intake was unaltered and equals the outer diameter of the PVC pipe. The length of the intake (L) was 15 cm.

The shallowest piezometer installed at the study site was 11 cm below the ground surface. Piezometer depth is measured from the center of the screened interval and is actually measuring the average head (or K) over the entire 15-cm range; so the 11cm deep piezometer is measuring an average head (or K) over the depth interval 3.5 to 18.5 cm. Increasing the length of the intake would bring the top of the screened interval even closer to the ground surface, which would be undesirable due to the possibility of direct seepage to the piezometer from surface water. This makes 15 cm the maximum practical length for the intake. All piezometers used in this study meet the same design specifications. The F/A ratio for this piezometer design is 22.5 cm^{-1}.

Besides being used for hydraulic head measurements, piezometers were also used to measure the hydraulic conductivity (K) within the marsh sediments. Hvorslev's (1951) method (also known as a 'slug-test') was used to calculate this parameter. This method is generally applicable when measuring K within a confined aquifer, but may be used in an unconfined aquifer if the length of the piezometer's screened interval (L) is greater than 8 times the radius of the well screen (R) (Fetter, 1988). In this case, L = 15 cm and R = 10.5 mm, so L/R = 14.3. (See Figure 16.)

Piezometers were made of ½-inch diameter PVC pipe with an actual measured inner diameter of 15mm and an actual measured outer diameter of 21mm. The length of PVC used varied depending on the depth to which the piezometer would be installed, but all piezometers stood approximately 1 meter above the ground surface after installation. The bottom of the pipe was capped, and holes were drilled into the pipe beginning approximately 1 cm above the base of the cap and continuing over an interval of 15 cm.

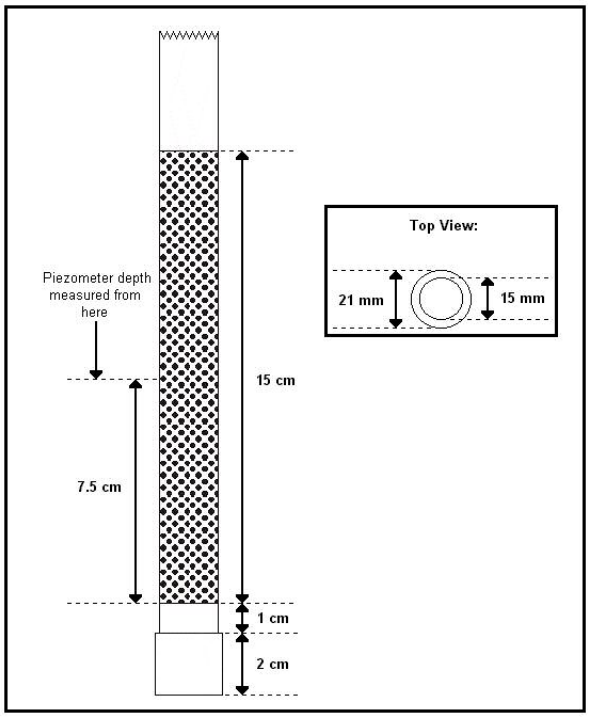

Figure 16: Piezometer design. Piezometers are constructed out of PVC pipe with an inside diameter of 15 mm and an outside diameter of 21 mm. The bottom of the PVC is capped . The screened interval is 15 cm and begins approximately 1 cm above the base of the cap. Piezometer depths are measured from the mid-point of the screened interval.

Holes were drilled completely around the circumference of the PVC to allow seepage of groundwater from all sides. The holes were then covered with a non-biodegradable mesh to prevent sediment from falling into and clogging the piezometer. The mesh was fastened to the PVC using duct tape. The piezometer depth was measured from the center of the screened interval or approximately 10.5 cm above the bottom of the pipe. The top of the piezometer was also capped to prevent debris from entering, but a 4mm hole was drilled just below the base of the cap to allow the pressure inside the piezometer to equilibrate with the atmospheric pressure.

Piezometer names

Piezometers were named according to their map location and depth below the ground surface. Two different systems were used when naming piezometers. Slug-test piezometers were all located 5 meters from the creekbank, so their names indicate which

channel they were adjacent to, how far they were from the main channel, and how deep they were installed below the ground surface. Piezometers used for horizontal groundwater flux calculations were located at different distances from the creekbank, but they were all located adjacent to North Glebe Creek. Their names indicate what order channel they were adjacent to, how far they were from the creekbank, and how deep they were installed below the ground surface.

Each name has 3 parts. For the slug-test piezometers, the first part is a two-letter abbreviation for the channel that the piezometer was installed next to. MC stands for Mondays Creek in Billingsley Marsh, OB stands for Observatory Creek in South Glebe Marsh and NG stands for North Glebe Creek in North Glebe Marsh. The second part of the name is a three-digit number that tells how many meters the location was from the main channel. The third part of the name is a twɵ digit number that tells how deep the piezometer was in centimeters. For example, Piezometer MC-100-30 is a slug-test piezometer that was located adjacent to Mondays Creek a distance of 100 meters from the main channel. It was installed to a depth of 30 cm below the ground surface.

For flux piezometers, the first part of the name is either a 1 or a 2 and designates the stream-order of the adjacent channel. The second part of the name tells how far in meters the piezometer was located from the network channel creekbank. The third part of the name tells how deep the piezometer was in centimeters. For example, Piezometer 2-15-39 was used for horizontal groundwater flux calculations. Therefore, it was located adjacent to North Glebe Creek. It was next to a second-order section of the stream, which was 100 meters from the main channel. (Flux piezometers installed adjacent to a first-order section of North Glebe Creek were 300 meters from the main channel.) Piezometer

2-15-39 was 15 meters from the network channel creekbank and was installed to a depth of 39 cm below the ground surface.

H1 Test: K decreases with increasing distance from the main channel

Piezometer locations

To determine whether K decreases with increasing distance from the main channel, piezometers nests were installed at varying distances from the main channel along three different network channels: Observatory Creek, Mondays Creek and North Glebe Creek. (See Figure 17.) Piezometer nests are sets of piezometers installed at the same location but at different depths. The nests located adjacent to Observatory Creek and Mondays Creek were 100 and 200 meters from the main channel. The nests located adjacent to North Glebe Creek were 100 and 300 meters from the main channel. Piezometers were installed 5 meters from the network channel creekbank and at two different depths. Nests along Observatory Creek and Mondays Creek were at 30 cm and 75 cm depths. Nests along North Glebe Creek were at 19 cm and 39 cm depths at the 100-meter location and 11 cm and 22 cm depths at the 300-meter location. The nests

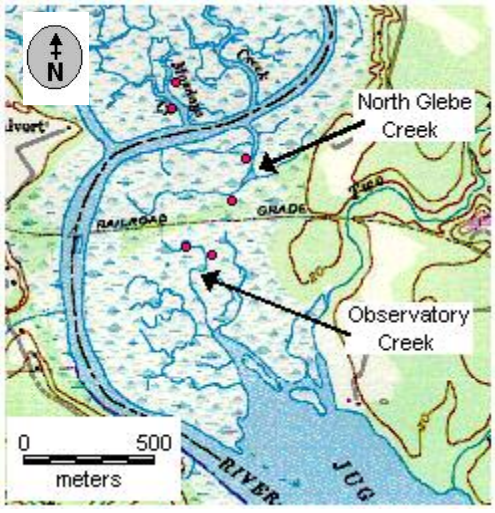

Figure 17: Hypothesis #1 test locations. Slug-test piezometers were installed at the locations marked by a red dot. They are all installed 5 meters from the creekbank. Locations along Mondays Creek are 100 and 200 meters from the main channel (the Patuxent River). Locations along North Glebe Creek are 100 and 300 meters from the main channel (the Patuxent River). Locations along Observatory Creek are 100 and 200 meters from the main channel (Jug Bay).

along North Glebe Creek are at different depths than those along the other two channels because they were also used for hypothesis #3. For Mondays Creek and North Glebe Creek, the Patuxent River serves as the main channel. For Observatory Creek, Jug Bay is the main channel.

Distances from the main channel are measured along the center of the network channel, so they are not straight line distances. Distances from the network channel are straight line distances and are measured perpendicular to the creekbank. All distances were measured in the field using a measuring tape.

Slug-tests

Hydraulic conductivities were measured using Hvorslev's slug-test method. In place of a slug, water was poured into the piezometers to elevate the head. Then the recovery rate was timed. A one-hour time limit was applied to each slug-test so, even if the head in the piezometer had not fully recovered within an hour, measurements were stopped and T_o was determined from the h/h_o vs. time regression line.

Due to the compressibility of the marsh sediments, data points on the h/h_o vs. time graphs did not always match well with the regression line. (See Figure 18A.) As pointed out by Baird (1995), Hvorslev's method assumes a rigid soil. If the soil behaves in a non-rigid manner, data-points on the h/h_o vs. time graph will not make an approximately straight line as described by Hvorslev. They will instead show an initial fast drop caused by swelling of sediments around the piezometer intake. Once swelling has ceased, data-points will show the characteristic straight line.

As described by Baird (see 'Sediment compressibility' subsection under 'Methods'), T_{90}/T_{50} ratios were calculated for each piezometer location used for this

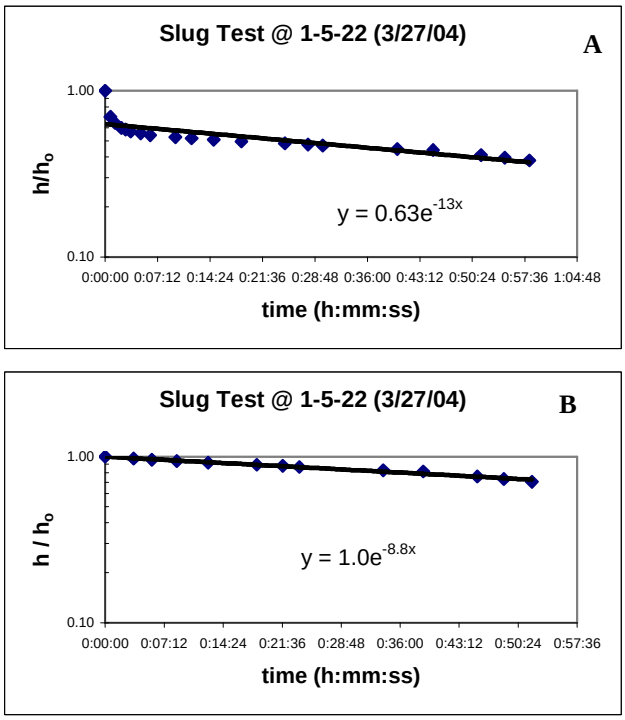

Figures 18A & B: Effects of a non-rigid soil on slug-tests. (A) At 3 locations, the compressibility of the sediment resulted in the data points not making a straight line on a semi-logarithmic h/h_o vs. time graph. When head is initially raised in the piezometer, the soil around the intake swells to accommodate the influx of new water. This produces a lower pore-pressure area around the intake and results in higher than average K measurements at the beginning of a slug-test (Baird, 1995). (B) To eliminate the effect of this initial pressure drop on the average K calculation, where this behavior was observed, the early data-points that did not fall on a straight line with the later data were eliminated from the graph. In allcases, this resulted in a one order-of-magnitude decrease in the calculated K.

study. (See Table 2.) Values ranged from 3.322 ('perfectly' rigid) to 8.291 (highly compressible) with a mean value of 4.340 (+/-1.647). As predicted by these calculated ratios, most h/h_o vs. time data from this study produced an approximately straight line on a semi-logarithmic graph. However, at three locations (Piezometer 1-5-22, Piezometer 2-5-19 and Piezometer 2-15-19) the initial drop in pore pressure around the intake was clearly observable in the quick initial drop in h/h_o per unit time followed by a leveling out of this rate. To eliminate the effect of this quick initial drop on the average calculated K at these locations, the first few data-points that did not fall on a straight line with the later data were eliminated from the h/h_o vs. time graphs. (See Figure 18B.) In all 3 cases, this resulted in a calculated K that was one order-of-magnitude slower than was calculated using all of the data points.

T_{90}/T_{50} at Each Piezometer Location:			
location	T_{90}/T_{50}	location	T_{90}/T_{50}
1-0-11	too fast	2-15-19	7.954
1-0-22	4.026	2-15-39	3.351
1-5-11	too fast	2-25-19	4.111
1-5-22	7.969	2-25-39	3.356
1-15-11	3.543	OB100-30	3.382
1-15-22	3.322	OB100-75	3.333
1-25-11	3.787	OB200-30	4.046
1-25-22	4.348	OB200-75	3.325
2-0-19	too fast	MC100-30	3.474
2-0-39	4.433	MC100-75	3.662
2-5-19	8.291	MC200-30	3.362
2-5-39	3.726		
	highest value:	8.291	
	lowest value:	3.322	
	mean value:	4.340	
	1σ:	1.647	

Table 2: Values of T_{90}/T_{50} for each piezometer location. Baird (1995) uses the ratio T_{90}/T_{50} as a measure of the rigidity of the medium (soil) at the location of a slug-test. No soil behaves in a perfectly rigid manner, but a value of this ratio close to 3.322 indicates nearly rigid behavior. As the value of the ratio increases, the compressibility of the medium increases. In this table, 'too fast' means that the piezometer recovered too quickly during the slug-test for a hydraulic conductivity measurement to be made.

In three cases, the hydraulic conductivity was too fast to be measured using the slug-test technique: at Piezometers 1-0-11, 1-5-11 and 2-0-19. For these locations, when a numerical value of K was required (for flux calculations), 5.00×10^{-3} cm/s was used. This value is just slightly higher than the highest measured K (4.99×10^{-3} cm/s).

Top-loading effects

Because it was believed that the state of compression of these wetland soils would also be affected by the top-loading pressure of standing water, K was measured at some locations multiple times at various stages during the tidal cycle. Along with head recovery data, surface-water height data was collected. Using this combination of data, changes in K with changes in surface-water height could be examined.

It was predicted that, with increasing surface-water height, the sediments would become increasingly compacted and the value of K within the sediments would decrease. However, two out of three plots of log K vs. surface-water height show K increasing with increasing surface-water height instead of decreasing as expected. (See Figure 19.) Only

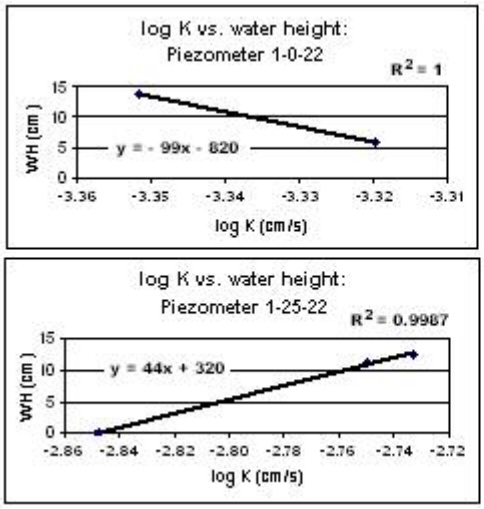

Figure 19: Changes in K associated with changes in surface-water height. At two out of three locations where multiple measurements of K were made, K increased with increasing surface-water height. Correlation between these two parameters at each piezometer locations was very good.

two K-values were measured at the location where the expected trend was observed, but at each of the other locations, K was measured four separate times. The correlation between surface-water height and log K was found to be extremely high: $R^2 = 0.9882$ and 0.9987. However, the rate of change varies greatly between locations.

At all three of these slug-test locations, measurements were made during a falling tide with a surface-water height drop rate of approximately 0.5 cm/min. In addition, there was no significant difference between the T_{90}/T_{50}-values measured at each of these locations (the value at 1-0-22 fell between the values at 1-25-11 and 1-25-22).

Differences between the piezometer showing the expected trend (1-0-22) and piezometers showing the opposite trend (1-25-11 and 1-25-22) are their distance from the network channel creekbank and the way the equilibrium head value changes with changing surface-water height. The piezometer that exhibited the expected behavior (decreasing K with increasing surface-water height) was located at the edge of the network channel creekbank. The other two piezometers were two parts of a single piezometer nest, installed to different depths below the ground surface 25 meters from the network channel creekbank.

As for changes in ‘equilibrium’ hydraulic head (meaning the head measured prior to slug insertion) over a changing tidal cycle, Piezometer 1-0-22 maintained a constant ‘equilibrium’ head throughout both slug-tests equal to approximately 35 cm above the ground surface. At the other two locations, ‘equilibrium’ head remained constant during non-flooding periods (approximately 2.5 cm above the ground surface at 1-25-11 and approximately 0.5 cm below the ground surface at 1-25-22) but changed during times of flooding. The ‘equilibrium’ head at Piezometer 1-25-11 fell at a rate of 20% the rate of surface-water height drop, and the ‘equilibrium’ head at Piezometer 1-25-22 fell at a rate of 32% of the rate of surface-water height drop, with the absolute value of measured head equaling approximately 1 cm higher (higher pressure) at 11cm depth than at 22cm depth.

Because of this difference in the rate of head drop at different depths below the ground surface, the vertical hydraulic gradient is increasing as the surface-water height decreases. (See Figure 20.) This would be consistent with decompression of sediments and an increasing rate of surface infiltration. This is contrary to the observed decrease in slug-test-measured K with decreasing surface-water height. However, the piezometer is measuring, primarily, the rate of horizontal groundwater flux. So vertical conductivities may be increasing at the same time that horizontal conductivities are

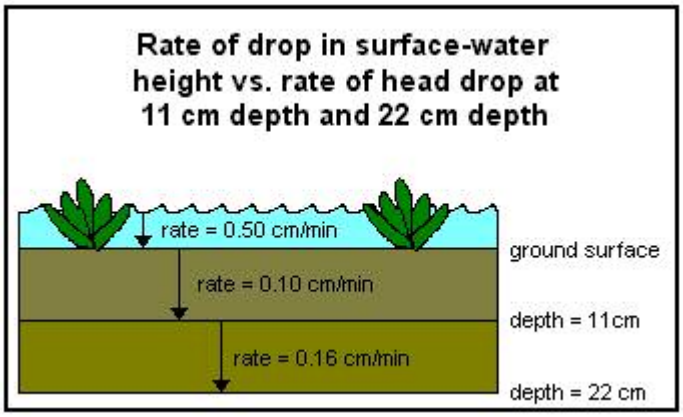

<u>Figure 20</u>: Comparison of drop rates for surface water and hydraulic head. At the same time that the surface-water height was dropping at a rate of 0.50 cm/min, a head drop of 0.10 cm/min was measured at a depth of 11 cm and a head drop of 0.16 cm/min was measured at a depth of 22 cm. Because pore pressure is decreasing more quickly with greater depth, the vertical hydraulic gradient in the downward direction is increasing.

decreasing. As surface-water height increases, platy organic particles compress under top-loading pressure into a horizontal orientation, making the 'path-of-least-resistance' a horizontal flow-path. But, as the surface-water height decreases and the sediments decompress, stretching in the vertical direction but not the horizontal direction, the organic particles are shifted to a more vertical orientation, favoring groundwater movement in the vertical direction. Of course, this is all just conjecture. Further study into the physics behind this changing hydraulic conductivity is needed.

In addition to K vs. surface-water height data, total hydraulic head vs. surface-water height data was collected. When hydraulic head was plotted against non-zero surface-water height, the correlation was poor. (See Figure 21.) But when the data were separated by the order of the adjacent network channel, the correlation with 1st-order data became even worse and the correlation with 2nd-order data became fairly good. The reason for this difference in head response adjacent to channels of different orders is that

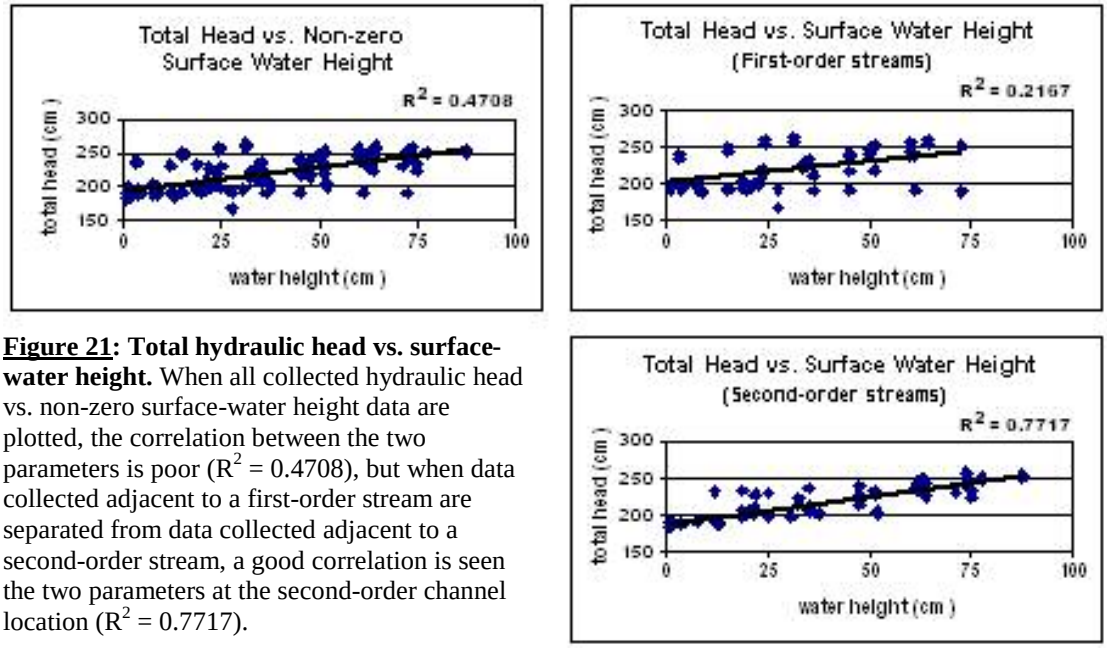

Figure 21: Total hydraulic head vs. surface-water height. When all collected hydraulic head vs. non-zero surface-water height data are plotted, the correlation between the two parameters is poor ($R^2 = 0.4708$), but when data collected adjacent to a first-order stream are separated from data collected adjacent to a second-order stream, a good correlation is seen the two parameters at the second-order channel location ($R^2 = 0.7717$).

flood waters get much deeper adjacent to 2nd-order channels. Because they are closer to the main channel and have a lower elevation than 1st-order channels, the tidal waters reach a greater height above the ground-surface near 2nd-order channels. This exerts a greater top-loading pressure on the sediments beneath the flood-water, resulting in a greater influence on hydraulic head.

For the purposes of this study, it suffices to say that 'top-loading effects' cause an uncertainty in the reproducibility of the measured K-values. Because multiple K measurements were not made at all locations, individual standard deviations cannot be used. So, to err on the side of larger than necessary uncertainties, the standard deviation calculated for the piezometer location with the largest spread of measured K-values will be applied to the measured K at all piezometer locations.

Where multiple K-measurements were made, the geometric mean value will be used instead of the arithmetic mean value. When the arithmetic mean of numbers with a large variability (like hydraulic conductivity measurements) is calculated, the result tends to be skewed toward larger values. The geometric mean uses the log of the numbers being averaged, thereby avoiding this bias. So, the geometric mean of the K-measurements made at each location will be used, but the uncertainties associated with each mean will be equal to the percentage error calculated for the piezometer with the largest range of measured K-values.

Sediment core analysis

Hypothesis #1 assumes that the marsh sediments will show spatial trends in their grain-size distributions. Hypothesis #1 is based on a study by Pasternack et al. (2000) which found that the silt-clay fraction increases with increasing distance from the main

channel. If this is not the case, then it does not follow that K would decrease with increasing distance from the main channel (assuming that K is primarily controlled by sediment grain-size). So, to determine whether there are spatial trends to various marsh sediment properties, four one-meter deep sediment cores were collected approximately 2 meters to the left (back to the stream) of slug-test piezometer locations MC100, MC200, OB100 and OB200. Cores were not drilled closer to the actual piezometer locations because the creation of such a large macropore changes the hydraulic conductivity within the sediments. A Russian peat borer with a 4-cm diameter semi- circular collection chamber was used to remove the sediment cores. Each core was divided into 10 10-cm long segments for analysis.

The volume of each core segment was calculated using the formula for the volume of a half-cylinder [$V = (\pi r^2 L)/2$; where r = half the diameter of the peat sampler = 2 cm and L = the actual measured length of the core segment]. Each segment was weighed, oven-dried at a temperature of 105^{o}C for 24 hours and weighed again so that the segment's bulk density and porosity could be calculated. The bulk density (P_b) of a sediment sample is its weight after drying divided by its original volume. The porosity (n) is reported as a percentage and is calculated using the equation:

$$n = [1 - (\text{bulk density}/\text{particle density})]*100$$

where the particle density is assumed to be 2.65 g/cm^3.

One core (the one from location OB100) was randomly selected for further analyses. Each segment from this core was analyzed for its organic matter (OM) content and grain-size distribution. The method of weight-loss upon combustion was used to determine organic matter content. Each segment was weighed, exposed to an open flame

for several minutes until there were no longer any visible fumes, cooled and re-weighed. The difference between the two weights divided by the original weight and multiplied by 100 gave the percentage of combustible OM in each segment.

After OM analysis was performed, the grain-size distribution of each core segment was measured using the sieving method. Sieves corresponding to the Udden-Wentworth grain-size scale were used. On this scale, grain-sizes are classified as follows:

grain diameter (mm)	description	ϕ - size
2 - 1	very course sand	-1 - 0
1 - 0.5	course sand	0 - 1
0.5 - 0.25	medium sand	1 - 2
0.25 - 0.125	fine sand	2 - 3
0.125 - 0.063	very fine sand	3 - 4
0.063 - 0.031	course silt	4 - 5
0.031 - 0.016	medium silt	5 - 6
0.016 - 0.008	fine silt	6 - 7
0.008 - 0.004	very fine silt	7 - 8
< 0.004	clay	> 8

where $\phi = - \log_2$(grain-size in mm) (Fetter, 1988). Sieves corresponding to ϕ-sizes -1 through 4 were used. Grains that passed through the $\phi = 4$ sieve were lumped together and classified as 'fines'. This classification is comprised of both silt and clay.

Time restrictions prevented grain-size analysis from being performed on more than one core. OM combustion must be performed first to remove any matter that is not a mineral particle, and OM combustion is quite time consuming. However, bulk density, which was calculated over the entire length of each core in 10-cm increments, can actually give a better idea of a sediment's K than grain-size. P_b is a measure of the amount of pore space in soil; a factor that more directly contributes to the K within that soil.

H2 Test: Creekbank gradient increases with increasing distance from the main channel

To determine whether network channel creekbank gradients tend to increase with increasing distance from the main channel, channel profiles were measured at 4 different locations along two network channels: North Glebe Creek and Observatory Creek. The channel profile locations correspond with the slug-test piezometer locations along these same channels. (See Figure 17.) Channel widths were measured using a measuring tape and are accurate to within 0.5 ft. The channels edge was considered to be the line along which vegetation began to grow. This method for determining the location of the channel's edge was used by Williams & Zedler (1999). Channel depth measurements were made at one-foot intervals across the channel width and are accurate to within 1 cm.

A channel's creekbank gradient at a given location is equal to d_{max} / w_e, where d_{max} is the depth of the channel at it deepest point along the measured cross-section, and w_e is the channel's effective width. Effective width is the horizontal distance measured from the deepest part of the channel to the channel's edge. (See Figure 22.) Because the channels are asymmetrical, creekbank gradient calculations were made for both sides of the channel.

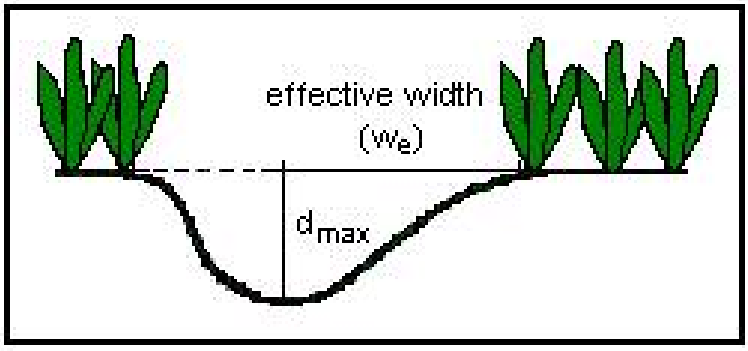

Figure 22: Measurement of creekbank gradient. The gradient of a network channel creekbank is equal to the rise / the run, or d_{max} / w_e.

So that network channel width and depth measurements made along North Glebe Creek could be compared to trends in these parameters observed by Williams et al. (2002) in three San Francisco Bay tidal salt marshes, these measurements were made at 50-meter intervals along the length of the creek. In addition, measurements of marsh watershed area for each 50-meter location were made using the measurement tool at Merlin Online (www.mdmerlin.net). This website publishes USGS 7.5 minute topographic maps. For this purpose, the Bristol Quadrangle map, photorevised in 1979, was used. Marsh watershed area for each channel location was measured three times. The reproducibility error in these area measurements was +/-0.05 ha.

H3 Test: The magnitude of horizontal groundwater flux will decrease with increasing distance from the network channel and the rate of this decrease will increase with increasing distance from the main channel.

Piezometer locations

Because multiple studies have concluded that horizontal groundwater flow in tidal marshes becomes negligible at a maximum of 15 meters from a tidal creekbank, piezometers were installed on both sides of this boundary, at 0, 5, 15, and 25 meters from the creekbank (Nuttle, 1986; Harvey et al., 1987; Nuttle, 1988). When choosing creekbank locations, one criterion was that the creekbank being examined had to be the only significant grade within a 25-meter radius around the 25-meter test location. This was to help avoid confounding effects of more than one significant gradient. A 'significant' gradient was considered to be either a marsh-bounding hillslope or a channel with a depth greater than 6 inches (15.24 cm).

Piezometer nests containing piezometers at two different depths were installed at the designated distances (0, 5, 15, and 25 meters from the creekbank) along a line

perpendicular to the creekbank at two different locations along North Glebe Creek. These locations correspond with the North Glebe Creek slug-test locations. (See Figure 17.) The piezometer line installed 100 meters from the main channel is adjacent to a second-order stretch of the creek. The piezometer line installed 300 meters from the main channel is adjacent to a first-order stretch of the creek. Piezometer depths are 1/3 and 2/3 of the maximum depth of the adjacent channel. In the case of the first-order channel piezometer line, depths are 11 and 22 cm. At the second-order channel locations, depths are 19 and 39 cm. Using this method, flux results from these two depths can be averaged to estimate total horizontal flux over the entire depth of the channel. The accuracy of this method depends on the reliability of the assumption that flux magnitude changes linearly with depth.

Data collection

In order to calculate groundwater flux between piezometer locations, hydraulic head measurements and K measurements had to be made at each piezometer location. K was measured using the slug-test method previously described. Hydraulic head measurements were made hourly over a seven-hour period so that changes over a tidal cycle could be observed. Data was not collected over a longer period because the measurements had to be made by hand during day-light hours.

Hydraulic head measurements were made by dropping a water level indicator into the piezometer and measuring the distance from the top of the piezometer to the water. Subtracting this distance from the piezometer length gave a value of piezometric head. To calculate total hydraulic head, piezometric head was added to the ground-surface elevation at the piezometer location minus the piezometer depth. In addition to head data,

measurement time and surface-water height data were collected so that head measurements could be compared to tidal stage data from the Railroad Bed Monitoring Station.

At the beginning of this data collection period, the tide was near its maximum stage. High tide was at approximately 8am and testing began at approximately 9am. The next low tide was at approximately 2pm, and testing continued past this point until approximately 3:30pm. So, measurements were made over most of a falling tide.

Tidal-cycle head measurements were actually made on two separate days. During the first set of measurements the maximum tide was only 1.18 m above the RBMS datum. During the second test period, the maximum tide was much higher (1.88 m above the datum). However, during the first test cycle, the piezometers located at 0 meters from the creekbank had not yet been installed, so this set of measurements will not be used when calculating flux to the channel. These measurements can be used, though, when looking at the effects of varying surface-water heights on various hydraulic parameters and when examining piezometer responses to changes in tidal stage.

Due to the height of the tide on the occasion of the second test cycle, some of the piezometers were flooded from the top so that head measurements could not be made. For those piezometer locations, piezometric head response data was examined and appropriate adjustments were made for differences in tidal height.

Flux calculations

Groundwater flux between piezometer locations was calculated using Dupuit's adaptation of the Darcy equation. Darcy's equation is written for confined aquifers of constant thickness, but the water-table aquifer found in a tidal marsh is unconfined.

Dupuit's equation accounts for the fact that the thickness of an unconfined aquifer changes. (See Figure 23.) The Dupuit equation for groundwater flux in an unconfined aquifer is:

$$q' = -\frac{1}{2} K \left(\frac{h_2^2 - h_1^2}{L} \right)$$

where q' is groundwater flux per unit width (in units of area/time), K is hydraulic conductivity (in units of distance/time), h is hydraulic head (in units of length) and L is the distance between hydraulic head measurements (in units of length) (Fetter, 1988). Flux is calculated from Piezometer 1 to Piezometer 2, so the negative sign in the equation insures that, if groundwater flux is from Piezometer 2 to Piezometer 1, the value of q' is negative.

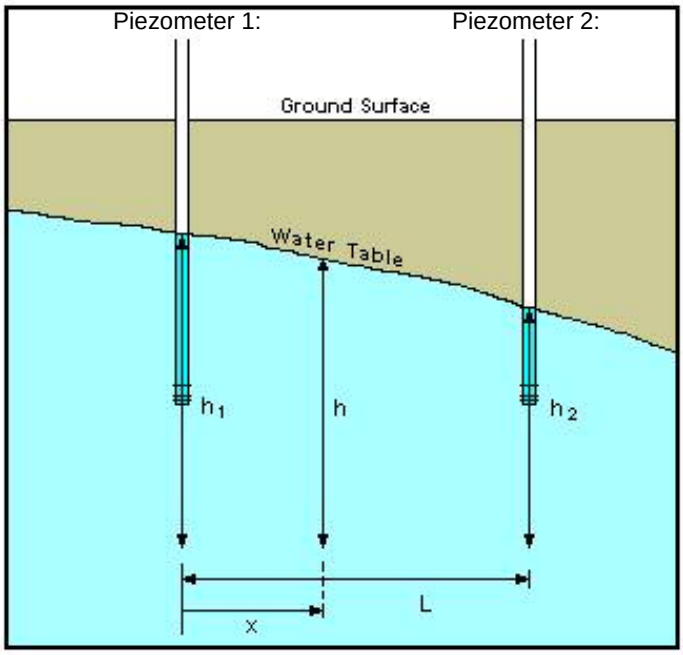

Figure 23: Explanation of Dupuit's variables. This figure, adapted from Fetter (1988), gives a visual explanation of the variables used in Dupuit's equation for groundwater flux per unit width. Unlike Darcy's flux equation, Dupuit's equation describes groundwater flow in an unconfined aquifer.

Calculated q'-values were used for comparison when determining differences in magnitude of flux between piezometers. Slug-tests were performed at all flux piezometer locations. The value of K used in the Dupuit equation was the geometric mean (GM) of the GM K-values calculated for each of the two piezometers between which flux was being calculated.

To get a volumetric value of horizontal flux (Q in units of volume/time) toward the network channel, hydraulic head is measured relative to the depth that corresponds to the maximum depth of the channel at the piezometer line location. To make this adjustment in the total hydraulic head measurements, which are based on the elevation at the monitoring station, the elevation of the adjacent channel bottom was subtracted from all hydraulic head values. The channel bottom elevation is equal to the elevation at the location of the piezometer 0 meters from the creekbank minus the channel depth.

Then, to estimate the volume of groundwater fluxing into the channel (Q), q’ is multiplied by the channel length over which flux is being calculated. By measuring changes in head over a tidal cycle, horizontal flux and the total amount of groundwater that enters the network channel can be calculated for this entire time period. Assuming the head response to changes in tide is always the same as during the test period, the amount of sediment-filtered groundwater thatenters the network channel can be calculated for any given time-period.

RESULTS

Hydrological characteristics of the marsh sediments

Bulk density, porosity and their spatial variations within the marsh

Bulk density (P_b) and porosity are properties of a soil that describe its degree of compactness. Porosity is a measure of the void space in a material and bulk density is a measure of the average sediment density when no water is present. The two terms are related to each other by the equation:

$$\text{Porosity} = [1 - (\text{bulk density}/\text{particle density})]*100\%$$

Typical upland bulk densities are 1.3 – 1.6 g/cm^3 (porosity = 39.6 to 50.9%) for compact surface soils and 1.0 – 1.2 g/cm^3 (porosity = 54.7 to 62.3%) for friable soils, but bulk densities measured in wetland soils tend to be much lower (Leeper & Uren, 1993). There are two basic reasons why wetland soil bulk densities tend to be lower: 1) a high occurrence of macropores created by plant roots and burrowing fauna, and/or 2) a high percentage of soil organic matter. Because organic matter has a much lower average density (approximately 0.224 g/cm^3 per Hughes et al., 1998) than mineral matter (2.65 g/cm^3), as OM% increases, the bulk density of the soil decreases. Hughes et al. (1998) measured bulk densities ranging from 0.68 to 1.24 g/cm^3 at depths between 0.8 and 1.4 meters in the lower inter-tidal zone of an Australian tidal salt marsh. Craft et al. (2002) measured even lower bulk densities in the upper 30 cm of a 2000 year old brackish marsh in North Carolina. Over this interval, they calculated an average bulk density of 0.13 g/cm^3.

P_b-values measured at the Jug Bay site were slightly higher than those measured by either Craft et al. or Hughes et al., ranging from 0.248 to 1.255 g/cm^3 within the top

meter of sediment. (See Table 3.) The highest and lowest mean bulk densities were both found along Mondays Creek. The mean at MC100 was 0.48 (+/-0.09) g/cm^3, while the mean at MC200 was 0.98 (+/-0.30) g/cm^3. The mean bulk densities for both Observatory Creek cores were very similar to each other: 0.65 (+/-0.16) g/cm^3 at OB100 and 0.67 (+/-0.14) g/cm^3 at OB200. Within the margin of error, there was no trend in average bulk density vs. distance from the main tidal channel. In addition, there was only a poor correlation between P_b and depth. (See Figure 24.) In fact, the highest measured bulk density was from 60-70 cm deep in core MC200. The lowest measured bulk density was at the top of core MC200, but the lowest value within core OB200 was not at the top but was instead from 10-20 cm deep. The average overall bulk density for all four cores was 0.70 (+/-0.26) g/cm^3.

Changes in organic matter content through a marsh sediment profile

Core OB100 was randomly selected for sediment organic matter content analysis. The average wt% OM for each 10-cm section is shown in Table 3. Measured OM% ranges from 8.4(+/-0.7)% to 15.1(+/-1.5)%, with an overall average of 10.6(+/-2.1)%. These results are slightly higher than surface sediment OM% measurements made by Kastler & Wiberg (1996) in two Chesapeake Bay, Virginia salt marshes. They measured organic matter contents ranging from 5 to 13%.

It was expected that the OM% would decrease with increasing depth below the ground surface because older OM, which would be deeper in the sediment profile, would be more decomposed. However, this trend was not observed. Pristine plant roots were found as deep as 1 meter below the ground surface and below sediment layers with more decomposed organic matter. Organic matter burial varies seasonally, but the resolution on

Analysis of Sediment Core Data:

OB100	length (cm)	σ	volume (cm^3)	σ	wet wt. (g)	σ	dry wt. (g)	σ	P_b (g/cm^3)	σ	porosity (%)	σ	pre-comb. wt (g)	σ	post-comb. wt (g)	σ	%OM	σ
0-10	7.00	0.13	44.0	4.5	58.1	0.1	16.4	0.1	0.37	0.04	85.9	8.6	16.9	0.1	14.8	0.1	12.4	0.8
10-20	9.50	0.13	59.7	6.0	101.0	0.1	37.8	0.1	0.63	0.06	76.1	7.6	17.2	0.1	15.6	0.1	9.3	0.8
20-30	11.00	0.13	69.1	7.0	105.4	0.1	39.7	0.1	0.57	0.06	78.3	7.8	14.1	0.1	12.3	0.1	12.8	1.0
30-40	10.00	0.13	62.8	6.3	98.6	0.1	33.9	0.1	0.54	0.05	79.6	8.0	10.9	0.1	9.7	0.1	11.0	1.3
40-50	10.00	0.13	62.8	6.3	98.0	0.1	30.6	0.1	0.49	0.05	81.6	8.2	9.3	0.1	7.9	0.1	15.1	1.5
50-60	11.00	0.13	69.1	7.0	111.2	0.1	47.9	0.1	0.69	0.07	73.8	7.4	20.3	0.1	18.3	0.1	9.9	0.7
60-70	10.00	0.13	62.8	6.3	113.9	0.1	52.9	0.1	0.84	0.08	68.2	6.8	22.8	0.1	20.7	0.1	9.2	0.6
70-80	10.00	0.13	62.8	6.3	116.9	0.1	52.1	0.1	0.83	0.08	68.7	6.9	21.4	0.1	19.6	0.1	8.4	0.7
80-90	9.50	0.13	59.7	6.0	112.5	0.1	49.6	0.1	0.83	0.08	68.6	6.9	20.0	0.1	18.1	0.1	9.5	0.7
90-100	10.00	0.13	62.8	6.3	107.7	0.1	46.6	0.1	0.74	0.07	72.0	7.2	16.7	0.1	15.2	0.1	9.0	0.8
OB200																		
0-10	9.00	0.13	56.5	5.7	85.5	0.1	31.0	0.1	0.55	0.06	79.3	7.9						
10-20	10.00	0.13	62.8	6.3	86.2	0.1	29.5	0.1	0.47	0.05	82.3	8.2						
20-30	10.00	0.13	62.8	6.3	107.8	0.1	42.1	0.1	0.67	0.07	74.7	7.5						
30-40	9.50	0.13	59.7	6.0	105.8	0.1	46.2	0.1	0.77	0.08	70.8	7.1						
40-50	12.00	0.13	75.4	7.6	111.6	0.1	42.2	0.1	0.56	0.06	78.9	7.9						
50-60	10.00	0.13	62.8	6.3	105.6	0.1	35.8	0.1	0.57	0.06	78.5	7.8						
60-70	11.50	0.13	72.3	7.3	113.1	0.1	44.6	0.1	0.62	0.06	76.7	7.7						
70-80	10.00	0.13	62.8	6.3	117.3	0.1	49.0	0.1	0.78	0.08	70.6	7.1						
80-90	11.00	0.13	69.1	7.0	128.6	0.1	60.2	0.1	0.87	0.09	67.1	6.7						
90-100	8.25	0.13	51.8	5.2	92.0	0.1	45.3	0.1	0.87	0.09	67.0	6.7						
MC100																		
0-10	10.00	0.13	62.8	6.3	74.6	0.1	17.7	0.1	0.28	0.03	89.4	8.9						
10-20	9.00	0.13	56.5	5.7	87.0	0.1	22.2	0.1	0.39	0.04	85.2	8.5						
20-30	11.00	0.13	69.1	7.0	108.7	0.1	32.0	0.1	0.46	0.05	82.5	8.3						
30-40	10.00	0.13	62.8	6.3	106.0	0.1	34.7	0.1	0.55	0.06	79.2	7.9						
40-50	9.00	0.13	56.5	5.7	77.1	0.1	24.4	0.1	0.43	0.04	83.7	8.4						
50-60	10.00	0.13	62.8	6.3	94.2	0.1	31.8	0.1	0.51	0.05	80.9	8.1						
60-70	10.00	0.13	62.8	6.3	106.7	0.1	34.2	0.1	0.54	0.05	79.5	7.9						
70-80	10.00	0.13	62.8	6.3	100.0	0.1	31.8	0.1	0.51	0.05	80.9	8.1						
80-90	10.00	0.13	62.8	6.3	103.1	0.1	29.9	0.1	0.48	0.05	82.0	8.2						
90-100	9.50	0.13	59.7	6.0	98.8	0.1	36.4	0.1	0.61	0.06	77.0	7.7						
MC200																		
0-10	10.00	0.13	62.8	6.3	60.8	0.1	15.6	0.1	0.25	0.03	90.6	9.1						
10-20	10.00	0.13	62.8	6.3	104.4	0.1	46.3	0.1	0.74	0.07	72.2	7.2						
20-30	9.50	0.13	59.7	6.0	119.2	0.1	58.6	0.1	0.98	0.10	63.0	6.3						
30-40	9.00	0.13	56.5	5.7	123.7	0.1	65.6	0.1	1.16	0.12	56.2	5.6						
40-50	9.50	0.13	59.7	6.0	114.8	0.1	65.3	0.1	1.09	0.11	58.7	5.9						
50-60	10.50	0.13	66.0	6.6	117.1	0.1	65.6	0.1	0.99	0.10	62.5	6.2						
60-70	9.50	0.13	59.7	6.0	132.7	0.1	74.9	0.1	1.25	0.13	52.6	5.3						
70-80	9.75	0.13	61.3	6.2	129.0	0.1	69.6	0.1	1.14	0.11	57.1	5.7						
80-90	10.00	0.13	62.8	6.3	136.3	0.1	74.4	0.1	1.18	0.12	55.3	5.5						
90-100	9.75	0.13	61.3	6.2	118.4	0.1	64.2	0.1	1.05	0.11	60.5	6.0						

Table 3: Results of sediment core analysis. Four 1-meter deep sediment cores were collected at the Jug Bay Reserve near the locations of the slug-test piezometers for which the cores are named. These cores were each divided into 10 segments, each approximately 10 cm long. Actual segment lengths are listed in this table under 'length'. In addition, results of bulk density (P_b) and porosity analyses for each core segment, and analysis for the percent organic matter (%OM) for core OB100 are given. In this table, σ is used as a general term for the uncertainty in a value. For more specific information on how values of σ were calculated, see 'Uncertainty calculations – Table 3' in Appendix A.

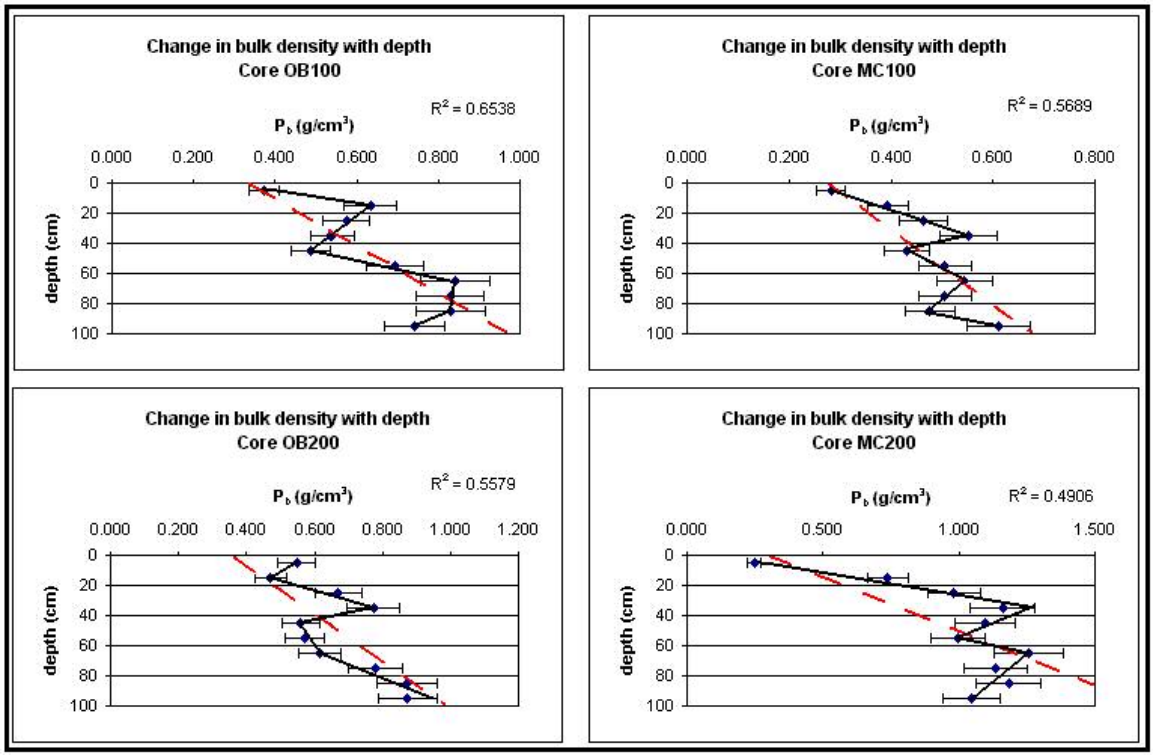

Figure 24: Change in bulk density (P_b) with depth at each core location. Bulk density does not increase linearly with depth, but does increase overall. The dashed red line is the regression line through the data.

these cores is not great enough for this trend to be visible. Sedimentation rates are on the order of a few millimeters per year. Observed OM content fluctuations could be due to changes in net primary production and/or changes in microbe populations on a centurial scale.

Although no spatial trend was observed in the sediment core OM content, they do correspond fairly well with OM-analyzed cores extracted by Ward et al. in 1998. (See Figure 25.) OM% measurements made by Ward et al. were much higher than those measured at Jug Bay, but they show the same initial decrease in the upper 10-20 cm followed by a peak around 40-50 cm deep and then a general leveling out of values. Core N13 from Ward et al. matches particularly well with core OB100.

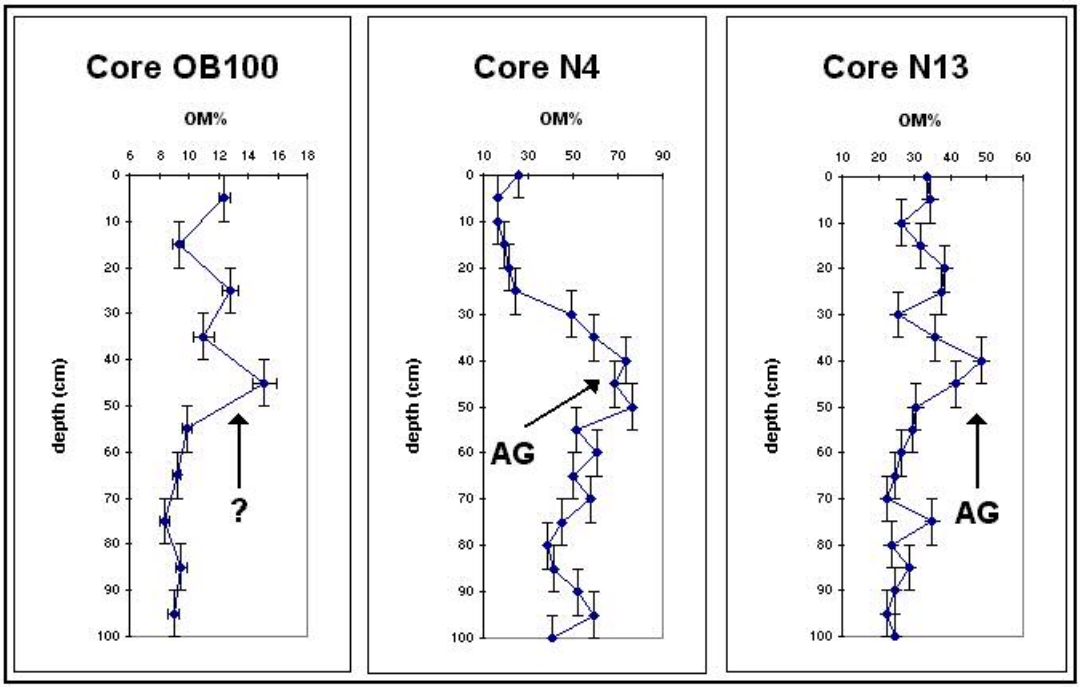

Figure 25: Comparison with organic matter content data collected by Ward et al., 1998. The first graph is the OM% data from Core OB100. The second and third graphs are modified from Ward et al. to match the scale in the first graph. Peaks labeled 'AG' were dated and attributed to a time when agricultural land was being cleared approximately 200 years BP. A peak is seen in the OB100 data at approximately the same depth but, since no dating was done on this core, a definite correlation cannot be made.

Cores N4 and N13 were collected from interior marsh locations along the Nanticoke River. Like the Patuxent River, the Nanticoke is an estuarine tributary to the Chesapeake Bay. It drains into the Bay at approximately the same latitude as the Patuxent, but on the Eastern Shore as opposed to the Western Shore. Cores done by Ward et al. were age dated using *Quercas* / *Ambrosia* pollen ratios, and they were able to attribute the 40-50 cm deep OM peaks to a period of extensive land clearing by European settlers, approximately 200 years BP (Kearney & Ward, 1986).

Although no vertical spatial trend was observed in the OM% data, there was, as expected, a fairly good correlation ($R^2 = 0.6311$) between OM% and bulk density. (See Figure 26.) Because of the low density of organic matter, its presence decreases the average density of sediments. However, since the correlation isn't stronger, there must be another factor affecting the soil's bulk density. Two facts support the hypothesis that this

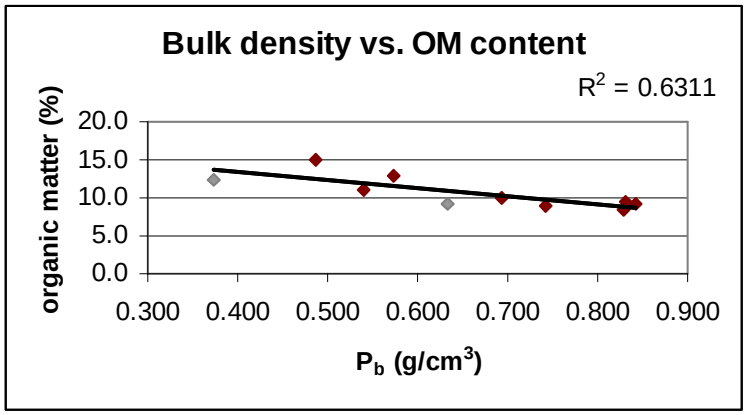

Figure 26: Bulk density (P_b) vs. organic matter content in Core OB100. Although the correlation is not strong, a soil's organic matter content does seem to have some effect on its bulk density. Data-points from less than 20 cm deep fall below the trend-line (in gray), suggesting that burrowing fauna may be creating macropores in the top-most sediments.

additional factor is loosening of sediments by burrowing fauna: 1) When data from the top 20 cm of sediment are removed, the correlation between bulk density and OM% improves to $R^2 = 0.7657$. Although some go deeper, most burrowing wetland fauna stay within the upper 20 cm of sediment (Williams, 1997). 2) The two P_b vs. OM% data-points from the upper 20 cm of sediment fell below the trend line. In other words, for the amount of OM that was measured in these samples, the trend line suggests that the bulk density should be higher. Burrowing creates macropores and loosens consolidated sediments, and both of these actions lower a soil's bulk density.

Changes in grain-size distributions with depth below the marsh surface

After OM combustion was performed, the segments of Core OB100 were further analyzed to determine their grain-size distributions. Grain-size separation was achieved using the sieving method. The silt and clay fractions were combined and classified as 'fines'. (See Table 4.) Three different grain-size distributions were observed among the core segments: 'approximately even' distribution, '$\phi = 2$ dominated' distribution and '$\phi = 2+3$ dominated' distribution. (See Figure 27.)

ϕ =	0	1	2	3	4	>4
GS =	1mm	0.5mm	0.25mm	0.125mm	0.063mm	<0.063mm
core segment	VC sand (wt%)	C sand (wt%)	M sand (wt%)	F sand (wt%)	VF sand (wt%)	"fines" (wt%)
0-10	0.0	13.9	23.6	22.2	13.2	27.1
10-20	0.5	14.8	54.1	24.9	3.3	2.4
20-30	0.0	10.0	38.0	41.3	8.0	2.7
30-40	0.9	9.3	55.6	25.9	6.5	1.9
40-50	0.0	8.0	38.6	37.5	12.5	3.4
50-60	0.0	9.2	42.2	36.7	10.1	1.8
60-70	0.0	12.5	56.5	22.3	7.1	1.6
70-80	0.0	12.9	60.1	20.2	5.1	1.7
80-90	0.0	15.6	61.1	18.6	3.6	1.2
90-100	0.7	15.9	61.4	17.9	3.4	0.7
total core	0.2	12.7	50.3	25.7	6.7	4.3

KEY:
VC: very course
C: course
M: medium
F: fine
VF: very fine
"fines": silt & clay
cum%: cumulative %

D_{10}: 10% of the grains are finer than this grain-size.
D_{50}: 50% of the grains are finer than this grain-size.
D_{60}: 60% of the grains are finer than this grain-size.

core segment	VC sand (cum%)	C sand (cum%)	M sand (cum%)	F sand (cum%)	VF sand (cum%)	"fines" (cum%)	D_{10}(mm)	D_{50}(mm)	D_{60}(mm)	C_u
0-10	100.0	100.0	86.1	62.5	40.3	27.1	0.006	0.090	0.118	20
10-20	100.0	99.5	84.7	30.6	5.7	2.4	0.074	0.170	0.193	3
20-30	100.0	100.0	90.0	52.0	10.7	2.7	0.062	0.122	0.151	2
30-40	100.0	99.1	89.8	34.3	8.3	1.9	0.067	0.160	0.183	3
40-50	100.0	100.0	92.0	53.4	15.9	3.4	0.053	0.119	0.146	3
50-60	100.0	100.0	90.8	48.6	11.9	1.8	0.060	0.129	0.159	3
60-70	100.0	100.0	87.5	31.0	8.7	1.6	0.067	0.167	0.189	3
70-80	100.0	100.0	87.1	27.0	6.7	1.7	0.073	0.173	0.194	3
80-90	100.0	100.0	84.4	23.4	4.8	1.2	0.080	0.180	0.200	2
90-100	100.0	99.3	83.4	22.1	4.1	0.7	0.083	0.182	0.202	2
total core	100.0	99.8	87.1	36.8	11.1	4.3	0.060	0.158	0.183	3

Table 4: Results from grain-size analysis of Core OB100. There were no measurable grains with a diameter larger than 2 mm ($\phi = -1$) in any of the core segments. D_{10}, D_{50} and D_{60} were calculated by using a linear regression between the next higher and next lower bin size. D_{10} for Segment 0-10 was calculated assuming the lower boundary size for fines is 0.016mm ($\phi = 6$). The ratio $D_{60}/D_{10} = C_u$ = the uniformity coefficient. $C_u < 4$ is well sorted. $C_u > 6$ is poorly sorted.

Only one core segment fell into the 'approximately even' distribution category: Segment 0-10. Within this uppermost segment, grain-sizes ranged from 1 to >4ϕ. This segment easily had the largest fraction of fines (27.1% of the grains by weight). The next largest fines fraction was 3.4% in Segment 40-50. This difference in the percentage of fines present could be because most of the fines are being transported tidally and are, therefore, not present long enough to become part of the deeper sediment profile. The medium and fine sand fractions in Segment 0-10 were only slightly smaller than the fines fraction (23.6 and 22.2%, respectively), and the course sand and very fine sand fractions were similar to each other in size: course sand = 13.9%, and very fine sand = 13.2%.

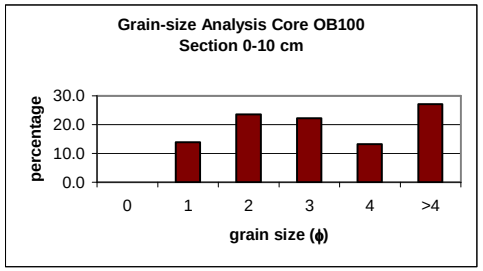

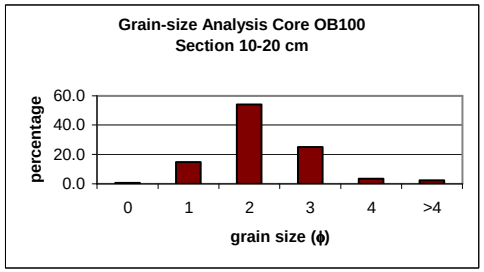

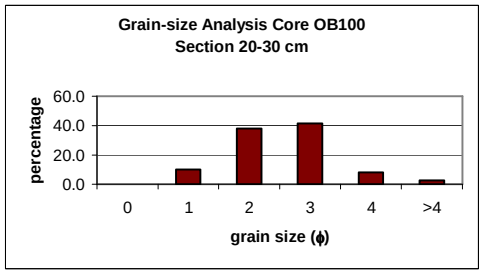

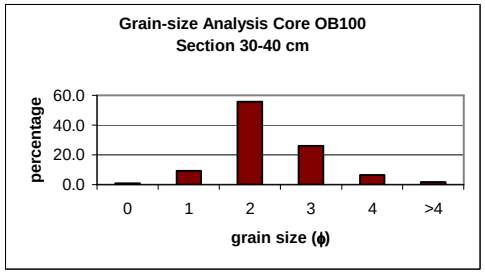

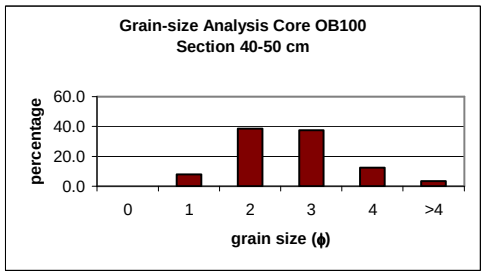

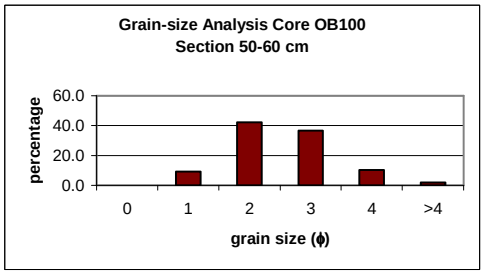

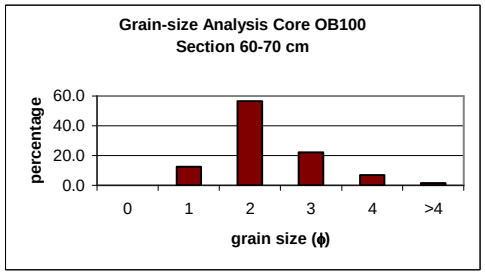

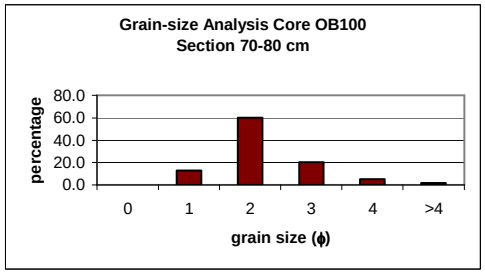

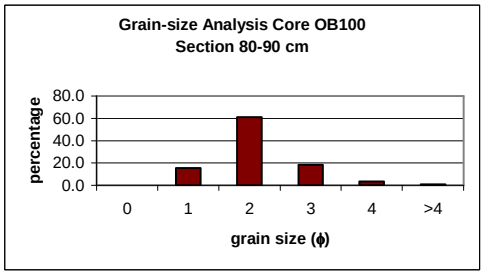

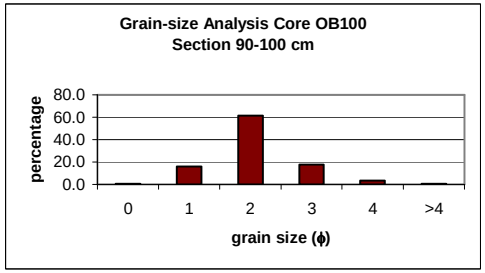

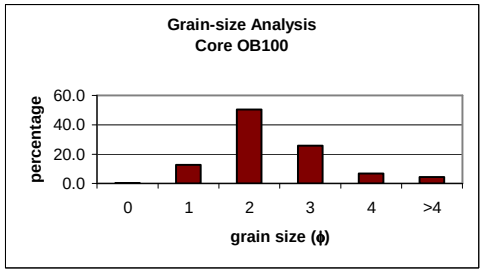

<u>Figure 27</u>: Grain-size distributions for Core OB100 and its segments. Segment 0-10 shows 'approximately even' distribution. Segment 10-20 is one example of a '$\phi = 2$ dominated' distribution and Segment 20-30 is one example of a '$\phi = 2+3$ dominated' distribution.

Three core segments (20-30, 40-50 and 50-60) had comparable medium and fine sand fractions so were classified as 'ϕ = 2+3 dominated' distributions. All of these segments had 39.45(+/-2.75)% of each of these grain-sizes. Six out of the ten core segments had 'ϕ = 2 (medium sand) dominated' distributions. All segments from below a depth of 60 cm were in this category, along with Segments 10-20 and 30-40. More than half of each of these segments was composed of medium sand-sized grains.

In addition, the uniformity coefficient (C_u) was calculated for each core segment. (See Table 4.) $C_u = D_{60}/D_{10}$ and is a measure of the degree of grain-size sorting in a sediment. $C_u < 4$ is considered to be well sorted. $C_u > 6$ is considered to be poorly sorted (Fetter, 1988). All core segments except for Segment 0-10 were well-sorted, and Segment 0-10, with a C_u-value of 20, was very poorly sorted.

Medium sand was the dominant grain-size for the total core, with 50.3% of the grains falling into this size category. Except for the top layer, the entire length of core could be described as well-sorted, medium-to-fine sand with negligible fines.

H1 Results: Spatial trends in hydraulic conductivity

K measurements used to determine whether K decreases with increasing distance from the main channel were all made 5 meters from the network channel creekbank but at different depths. Locations along North Glebe Marsh correspond with 5-meter flux piezometer locations and are at depths of 19, 22 and 39 cm. Flux at location 1-5-11 was too fast to be measured using the slug-test method. One piezometer at each of these depths was used. The average K at a depth of 19 cm was 2×10^{-3} cm/s. The average K at a depth of 22 cm was 5×10^{-6} cm/s. The average K at a depth of 39 cm was 1×10^{-3} cm/s.

The 19- and 39-cm deep piezometers were each 100 meters from the main channel and the 22-cm deep piezometer was located 300 meters from the main channel.

Four test locations were at a depth of 30 cm. At this depth, the average K was 2 x 10^{-5} cm/s (1σ range = 5 x 10^{-6} to 7 x 10^{-5} cm/s). Three test locations were at a depth of 75 cm. At this depth, the average K was 5 x 10^{-6} cm/s (1σ range = 5 x 10^{-7} to 6 x 10^{-5} cm/s). Overall, a poor correlation between K and depth was observed (R^2 = 0.4063), although a lower average K was measured in the deeper piezometer than in the shallower piezometer in 7 out of 8 piezometer nests. (See Figure 28.) Therefore, when calculating average K at various distances from the main channel, all depths were averaged together. (For a complete list of measured hydraulic conductivities and their associated uncertainties, see Table 6 at the end of this section.)

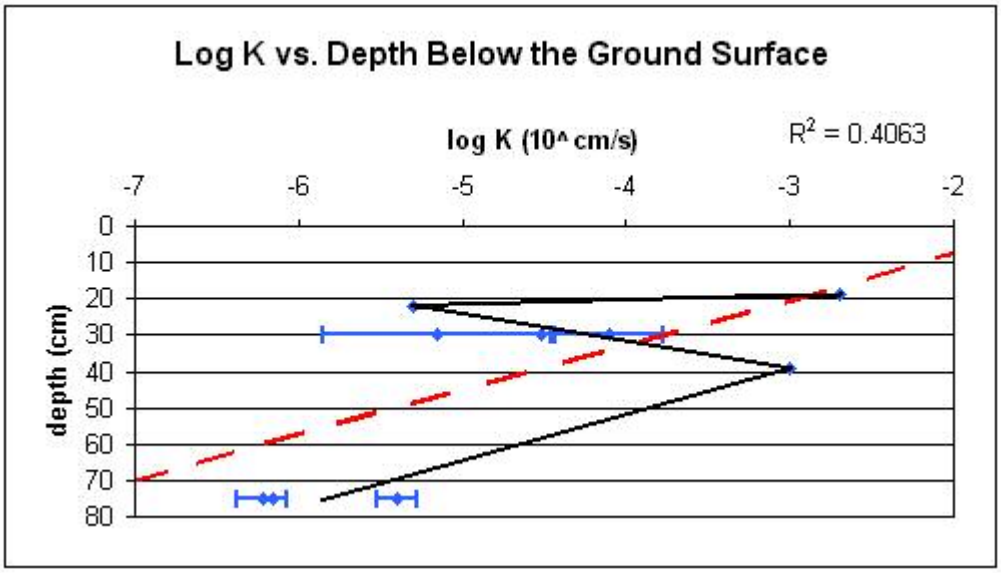

Figure 28: Change in K with increasing depth below the ground surface. This graphs shows all of the K measurements that were made 5 meters from a network channel creekbank. Correlation between depth and hydraulic conductivity is poor. The dashed, red line is the regression line through the data. Error bars are one standard deviation around the geometric mean. Where no error bars are shown, only one K-measurement was made.

On first observation, the back-and-forth, 'saw-tooth' changes in K with increasing depth below the ground surface, observed in Figure 28, appear similar to the 'saw-tooth' pattern of changes in bulk density with increasing depth below the ground surface, seen in Figures 24. However, further investigation reveals decreasing K between 19 and 22 cm below the surface, whereas all 4 sediment cores showed increasing P_b over this same interval. K and P_b do both increase through the depth interval 22 to 39 cm, except for in Core OB100 where P_b decreases but, between 39 and 75 cm deep, K decreases while 3-out-of-4 cores show increasing P_b. A graph of K vs. P_b showed virtually no correlation between these two parameters. (See Figure 29.)

Mean K-values measured along Mondays Creek and North Glebe Creek seem to indicate that K does decrease with increasing distance from the main channel, but data from Observatory Creek show the opposite trend. (See Table 5.) Differences between the means at 100 and 200 meters along Observatory Creek and Mondays Creek are both one

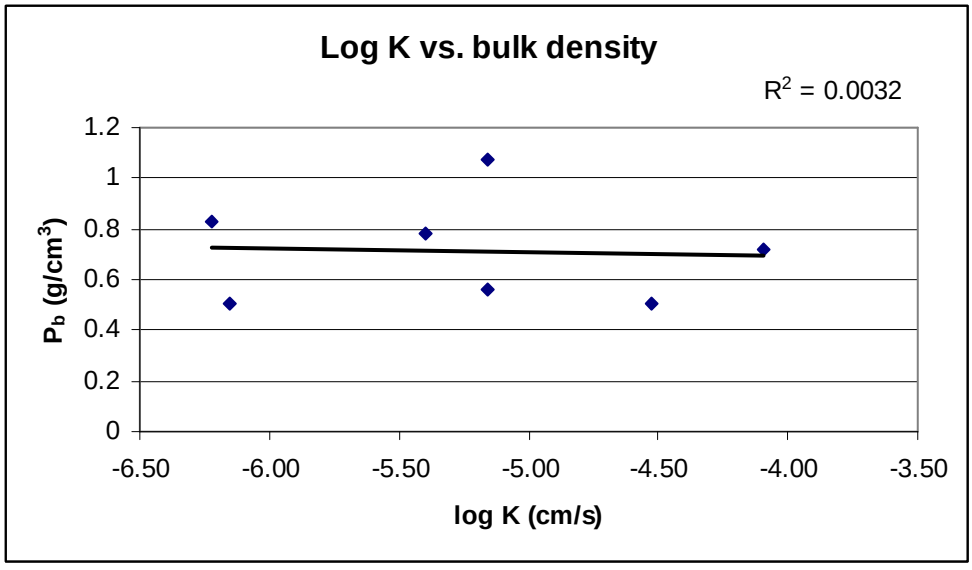

Figure 29: The correlation between hydraulic conductivity and bulk density. Data from locations where both K and P_b were measured are shown on this graph. Although both of these sediment properties show a back-and –forth pattern of change with increasing depth below the ground surface, there is virtually no correlation between them.

Location	distance (m)	GM K (cm/s)
OB-100	100	2.E-06
OB-200	200	2.E-05
MC-100	100	5.E-05
MC-200	200	7.E-06
2-5	100	2.E-03
1-5	300	5.E-06
Location	lower bound K (cm/s)	upper bound K (cm/s)
OB-100	3.E-07	1.E-05
OB-200	2.E-06	2.E-04
MC-100	3.E-05	8.E-05
MC-200		
2-5	1.E-03	2.E-03
1-5		

Table 5: Hydraulic conductivity and distance from the main channel data. The geometric mean K values shown in this table are averages of K measured at all depths at that location. Upper and lower bounds are 1 standard deviation around the mean. Where an upper and lower bound not given, only one measurement was made. The distance shown is from the main tidal channel to the test location measured along the network channel. Locations 2-5 and 1-5 are adjacent to N. Glebe Creek.

order-of-magnitude, but in opposite directions. Along North Glebe Creek the mean K-values show a decrease of 3 orders-of-magnitude over a stretch of 200 meters, but examination of individual measurements indicates that K can vary by as much as 4 orders-of-magnitude at a single location at different depths. Within the margin of error, a decrease in hydraulic conductivity with increasing distance from the main channel was not observed. (See Figure 30.)

Because piezometers had to be installed at various distances from the creekbank for the flux portion of this study and hydraulic conductivities had to be measured at those locations as well, measured values of K along North Glebe Marsh were used to determine whether a trend in changing K with increasing distance from the network channel creekbank was observable. At a 68% confidence level, the K at 0 meters from the tidal network channel creekbank was significantly higher than K at either 5 meters or 15 meters from the creekbank. (See Figure 31.) This was the only observed spatial trend in K. The geometric mean of all measured K values at all locations and depths was 5×10^{-5} (range = 2×10^{-6} to 1×10^{-3}) cm/s.

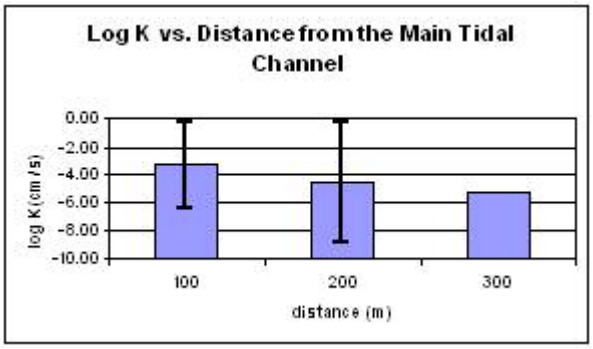

Figure 30: Mean values of hydraulic conductivity at varying distances from the main tidal channel. K measurements were made adjacent to 3 different network channels at 5 meters from the creekbank. Error bars shown are one standard deviation around all mean K-values measured at the given distance. No error bars are shown on the 300-meter column because only one measurement was made at that distance. At 100 meters, n = 6. At 200 meters, n = 3.

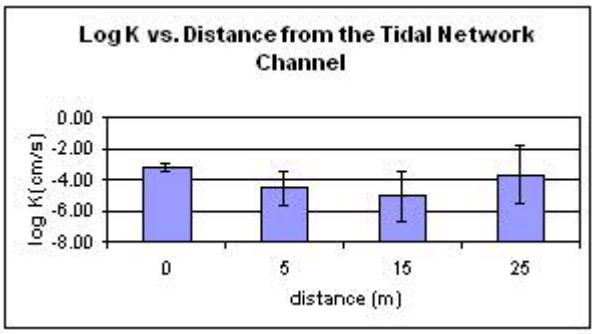

Figure 31: Mean values of hydraulic conductivity at varying distances from the tidal network channel. K was measured at 0, 5, 15 and 25 meters from the North Glebe Creek creekbank at two different locations. Error bars shown are one standard deviation around all mean K-values measured at the given distance. At 0 meters, n = 2. At 5 meters, n = 10. At 15 and 25 meters, n = 4. K at 0 meters from the creekbank is significantly higher than K measured at 5 and 15 meters from the creekbank, at a 68% confidence level.

Table 6: (next page) Measured hydraulic conductivities. K measurements from all piezometers, both slug-test and flux, are included in this table. All values of K are in cm/s. At locations where K was measured more than once, the geometric mean (GM) of all of the measured values was calculated and used as the average K at that location. At some locations, the head recovery rate was too fast to time, so a value of K for that location could not be measured. The average K for different depths (d) and different distances from the tidal network channel are listed in this table. These values are the geometric mean of the GM K-values that fall into the specified category. 'Range' is one standard deviation around the mean. 'Upper K boundary' and 'lower K boundary' are the upper and lower bounds around the GM K and are based on the spread of measured K-values at the location with the widest range of measurements (OB-100-30). Percent uncertainty on the high side is 505% of the GM K-value. Percent uncertainty on the low side is 20% of the GM K-value.

Location	K (cm/s)	log K	mean log K	GM K	upper K boundary	lower K boundary
OB-100-30	1.E-06	-6.00	-5.17	7.E-06	3.E-05	1.E-06
	1.E-05	-5.00				
	3.E-05	-4.52				
OB-100-75	4.E-07	-6.40	-6.24	6.E-07	3.E-06	5.E-07
	7.E-07	-6.15				
	7.E-07	-6.15				
OB-200-30	7.E-05	-4.15	-4.08	8.E-05	5.E-04	7.E-05
	4.E-05	-4.40				
	2.E-04	-3.70				
	1.E-04	-4.00				
OB-200-75	3.E-06	-5.52	-5.41	4.E-06	2.E-05	3.E-06
	5.E-06	-5.30				
	4.E-06	-5.40				
MC-100-30	3.E-05	-4.52	-4.52	3.E-05	2.E-04	2.E-05
MC-100-75	7.E-05	-4.15	-4.15	7.E-05	4.E-04	6.E-05
MC-200-30	7.E-06	-5.15	-5.15	7.E-06	4.E-05	5.E-06
1-0-22	4.E-04	-3.40	-3.35	4.E-04	3.E-03	4.E-04
	5.E-04	-3.30				
1-5-22	5.E-06	-5.30	-5.30	5.E-06	3.E-05	4.E-06
1-15-11	2.E-03	-2.70	-2.70	2.E-03	9.E-03	1.E-03
1-15-22	3.E-06	-5.52	-5.52	3.E-06	2.E-05	3.E-06
1-25-11	9.E-04	-3.05	-2.72	2.E-03	1.E-02	2.E-03
	7.E-04	-3.15				
	5.E-03	-2.30				
	4.E-03	-2.40				
1-25-22	1.E-03	-3.00	-2.85	1.E-03	1.E-02	1.E-03
	1.E-03	-3.00				
	2.E-03	-2.70				
	2.E-03	-2.70				
2-0-39	1.E-03	-3.00	-3.00	1.E-03	6.E-03	8.E-04
2-5-19	2.E-03	-2.70	-2.70	2.E-03	1.E-02	1.E-03
2-5-39	1.E-03	-3.00	-3.00	1.E-03	9.E-03	1.E-03
2-15-19	3.E-06	-5.52	-5.52	3.E-06	2.E-05	3.E-06
2-15-39	4.E-07	-6.40	-6.40	4.E-07	2.E-06	3.E-07
2-25-19	2.E-03	-2.70	-2.70	2.E-03	1.E-02	2.E-03
2-25-39	4.E-07	-6.40	-6.40	4.E-07	2.E-06	3.E-07

Locations where K was too fast to measure:

1-0-11
1-5-11
2-0-19

Overall average K:	5.E-05
range:	2E-6 to 1E-3
Avg. K for d=11 cm:	2.E-03
range:	1E-3 to 2E-3
Avg. K for d=19 cm:	2.E-04
range:	6E-6 to 9E-3
Avg. K for d=22 cm:	6.E-05
range:	3E-6 to 1E-3
Avg. K for d=30 cm:	2.E-05
range:	5E-6 to 7E-5
Avg. K for d=39 cm:	2.E-05
range:	2E-7 to 2E-3
Avg. K for d=75 cm:	5.E-06
range:	5E-7 to 6E-5

Note: Listed averages are calculated from the geometric mean K at each piezometer location.

Avg. K for distance=0 m:	7.E-04
range:	4E-4 to 1E-3
Avg. K for distance=5 m:	3.E-05
range:	2E-6 to 4E-4
Avg. K for distance=15 m:	9.E-06
range:	2E-7 to 3E-4
Avg. K for distance=25 m:	2.E-04
range:	3E-6 to 2E-2

H2 Results: Changes in creekbank gradient

When the gradient of the network channel creekbank is calculated using d_{max}/w_e, gradient does increase with increasing distance from the main channel in all but one case; along the Observatory Creek left side. (See Table 7.) However, when the depth of the channel half-way across the width is used in place of d_{max} and half of the channel width is used in place of w_e, the hypothesis holds for each individual channel.

There is no rate of gradient change with distance trend that is valid for both channels. Looking at the creekbank gradient on the left side of each channel, the rate of gradient change with distance from the main tidal channel (dg/dx_{left}) is directionally

Location	d_{max} (m)	$w_{e(left)}$ (m)	$w_{e(right)}$ (m)	$grad_{left}$	$grad_{right}$	$grad_{avg}$	% difference
OB100	1.28	4.88	3.75	0.26	0.34	0.30	24
OB200	0.90	3.66	1.52	0.25	0.59	0.42	58
NG100	0.58	6.86	7.41	0.08	0.08	0.08	0
NG300	0.33	2.44	0.79	0.14	0.42	0.28	67

Location	dg/dx_{left}	dg/dx_{right}	d_{center} (m)	width (m)	$grad_{center}$	dg/dx_{center}	distance (m)
OB100	-0.00017	0.0025	1.25	8.61	0.29	0.00050	100
OB200			0.88	5.18	0.34		200
NG100	0.00025	0.0017	0.58	14.28	0.08	0.00023	100
NG300			0.28	4.45	0.13		300

Table 7: Creekbank gradient data. 'd_{max}' is the maximum depth measured along the channel cross-section. 'w_e' is the effective width (as described in the 'H2 Test' subsection under 'Methods and Materials') and is given for each side of the channel. 'grad' is the gradient calculated for each side of the channel. '$grad_{avg}$' is the average of '$grad_{left}$' and '$grad_{right}$'. '% difference' is a measure of difference between the gradients measured on each side of the channel and equals: [(steep gradient – shallow gradient) / steep gradient]*100. '% difference' can be used as an indicator of channel symmetry. 'dg/dx' is the change in gradient / the change in distance from the main channel and is given for each side of the channel. 'd_{center}' is the depth of the channel measured half-way across the width of the channel. 'Width' is the width of the network channel where the cross-section was measured. '$grad_{center}$' is the creekbank gradient calculated by dividing d_{center} by ½ width.' dg/dx_{center}' is the change in gradient / the change in distance from the main channel calculated using $grad_{center}$. 'Distance' is the distance of the network channel cross-section from the main channel measured in meters.

opposite; gradient decreases with increasing distance along Observatory Creek and increases with increasing distance along North Glebe Creek. Looking at the creekbank gradient on the right side of each channel, the rate of gradient change with distance from the main tidal channel (dg/dx_{right}) is 32% faster along Observatory Creek than along N. Glebe Creek. When using [d_{center} / (½ x width)] to calculate gradient, the rate of gradient change with distance from the main tidal channel (dg/dx_{center})) is more than twice as fast along Observatory Creek as it is along N. Glebe Creek.

Different creekbank gradient results were obtained using the two different methods because the network channels are not symmetrical. (See Figures 32A- D.) Gradients measured on opposite sides of the same channel vary by as much as 67%. This gradient difference was found at NG300, where d_{max} was measured at two different locations. (See Figure 32D.) For this reason, the base of each bank is at a different

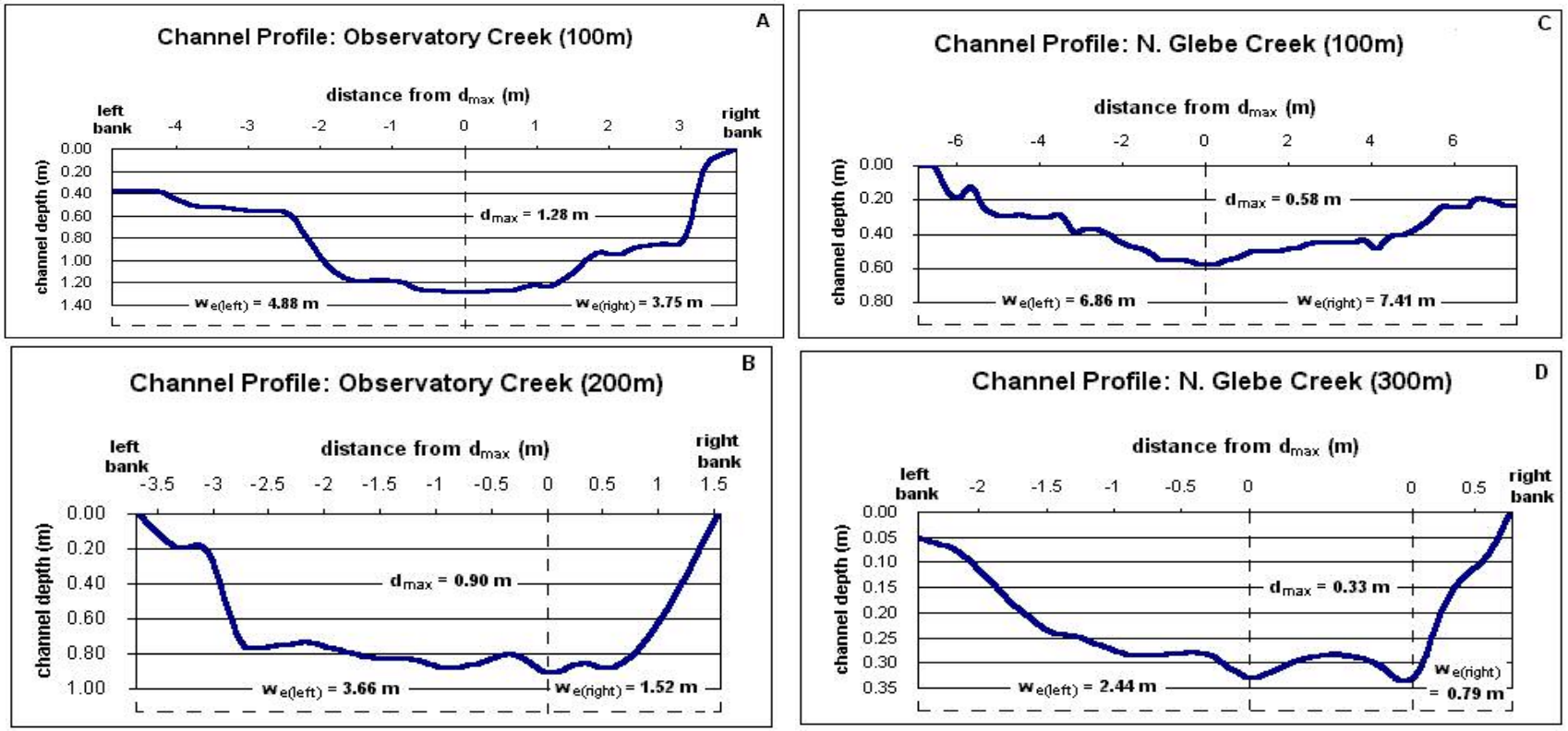

<u>Figures 32A-D</u>: Measured channel cross-sections. Network channel cross-sections were measured at 4 different locations: two along Observatory Creek and two along North Glebe Creek. Distances in parentheses in the graph titles are the distance of the cross-section from the main channel, measured along the network channel. The maximum channel depth (d_{max}) along the N. Glebe Creek 300 meter section was measured at two different locations (Graph 12D), so when calculating creekbank gradients at that location, the w_e for each side was measured from the d_{max} closest to that side. 'Left bank' and 'right bank' refer to the side of the channel looking toward the channel head (away from the main channel).

location. The smallest calculated % difference was a value of 0% at NG100. The creekbank gradient on both sides at this location is 0.08. If % difference is used as an approximation of channel symmetry (a lower value means the channel is more symmetrical), then it appears that network channels are more symmetrical closer to the main channel and become less so with increasing distance.

More detailed width and depth measurements were made along North Glebe Creek so that data from this location could be compared to that of Williams et al. (2002). Elevation calculations were made for the channel's left bank, channel bottom and right bank at 50-meter intervals. In addition, the area of the marsh watershed for each location was calculated. (See Table 8.)

Data collected at Jug Bay show poor correlation between channel depth and distance from the main channel. (See Figure 33A.) But this is because the depth is measured with respect to the top of the channel and not to a constant elevation. Looking at a 3-D map of channel bottom elevation, we see that, although the channel depth does not decrease over each 50-m interval and does not decrease at a steady rate, it does decrease overall. (See Figure 34.)

dist. from mouth (m)	elev left (cm)	elev middle (cm)	elev right (cm)	depth (m)	measurement uncertainty	width (m)	measurement uncertainty	marsh area (ha)	measurement uncertainty
0	95	75	95	0.20	+/-0.01 m	50.30	+/-0.15 m	19.40	+/-0.05 ha
50	116	88	116	0.28	+/-0.01 m	30.79	+/-0.15 m	14.55	+/-0.05 ha
100	123	65	101	0.58	+/-0.01 m	14.33	+/-0.15 m	10.67	+/-0.05 ha
150	101	74	125	0.51	+/-0.01 m	10.98	+/-0.15 m	8.73	+/-0.05 ha
200	146	83	141	0.64	+/-0.01 m	11.59	+/-0.15 m	4.85	+/-0.05 ha
250	154	138	154	0.17	+/-0.01 m	14.94	+/-0.15 m	3.88	+/-0.05 ha
300	158	135	163	0.28	+/-0.01 m	4.57	+/-0.15 m	2.91	+/-0.05 ha
350	149	142	154	0.11	+/-0.01 m	17.68	+/-0.15 m	1.94	+/-0.05 ha
400	152	147	152	0.05	+/-0.01 m	7.32	+/-0.15 m	0.49	+/-0.05 ha
408		133							
433(end)									

Table 8: Channel profile measurements made along North Glebe Creek. Channel width, depth and elevation measurements were made at 50-m intervals along N. Glebe Creek. 'Elev. left' and 'elev. right' are the elevations of the left and right creekbanks, respectively, with respect to the RBMS datum. 'Elev. middle' is the elevation of the creek bottom at the center of the channel. Contributing marsh area was also calculated for each channel location.

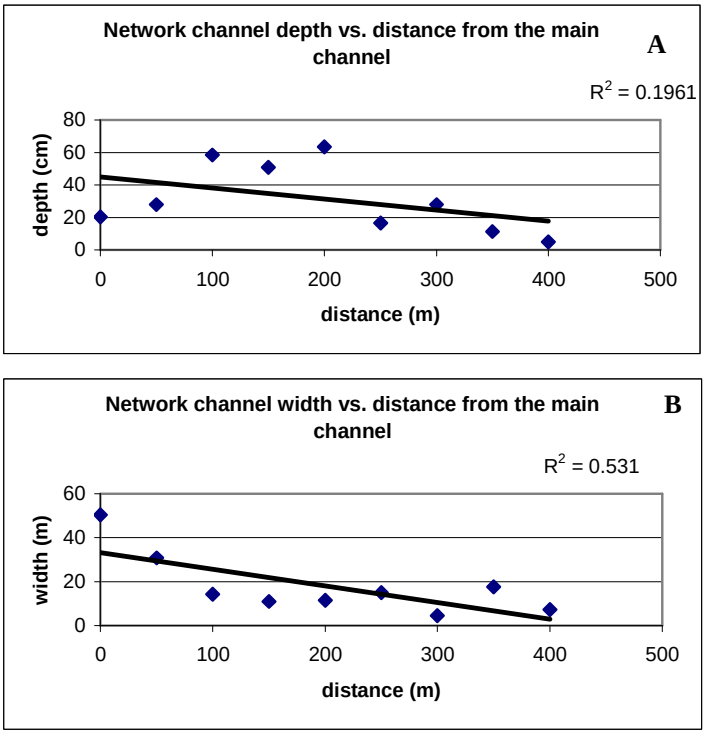

<u>Figures 33A & B</u>: Changes in channel depth and width with distance from the main tidal channel. Measurements are from North Glebe Creek. Graph A: Network channel depth, measured from the top of the creekbank, does not correlate well with distance from the main tidal channel. Over the first 50 meters, channel depth is around 10 inches. Between 100 to 200 meters, the depth increases to 20 to 25 inches. Then, depth again drops to around 10 inches and decreases toward the end of the channel. This lack of a good correlation between channel depth and distance from the main tidal channel may be due to sediment dropping out of suspension near the channel mouth when flow velocity decreases from that in the main channel. If depth data from the first 50 meters of channel is not used, the correlation between these two parameters goes up to $R^2 = 0.7825$. Graph B: Network channel width does not appear to decrease linearly with increasing distance from the main tidal channel. However, over the 2nd-order segment of channel (0 to 200 meters from the main channel) the width shows a fairly strong exponential decrease with increasing distance ($R^2 = 0.8733$).

Width data show a weak correlation with distance from the main tidal channel. (See Figure 33B.) This fact can also be observed in the inset of Figure 34. Beyond approximately 200 meters from the main channel (after the channel transitions from 2nd- to 1st-order), network channel width becomes extremely unpredictable; shrinking to less than 1 meter wide and then swelling to approximately 15-meter-wide pools over a less than 50-meter distance.

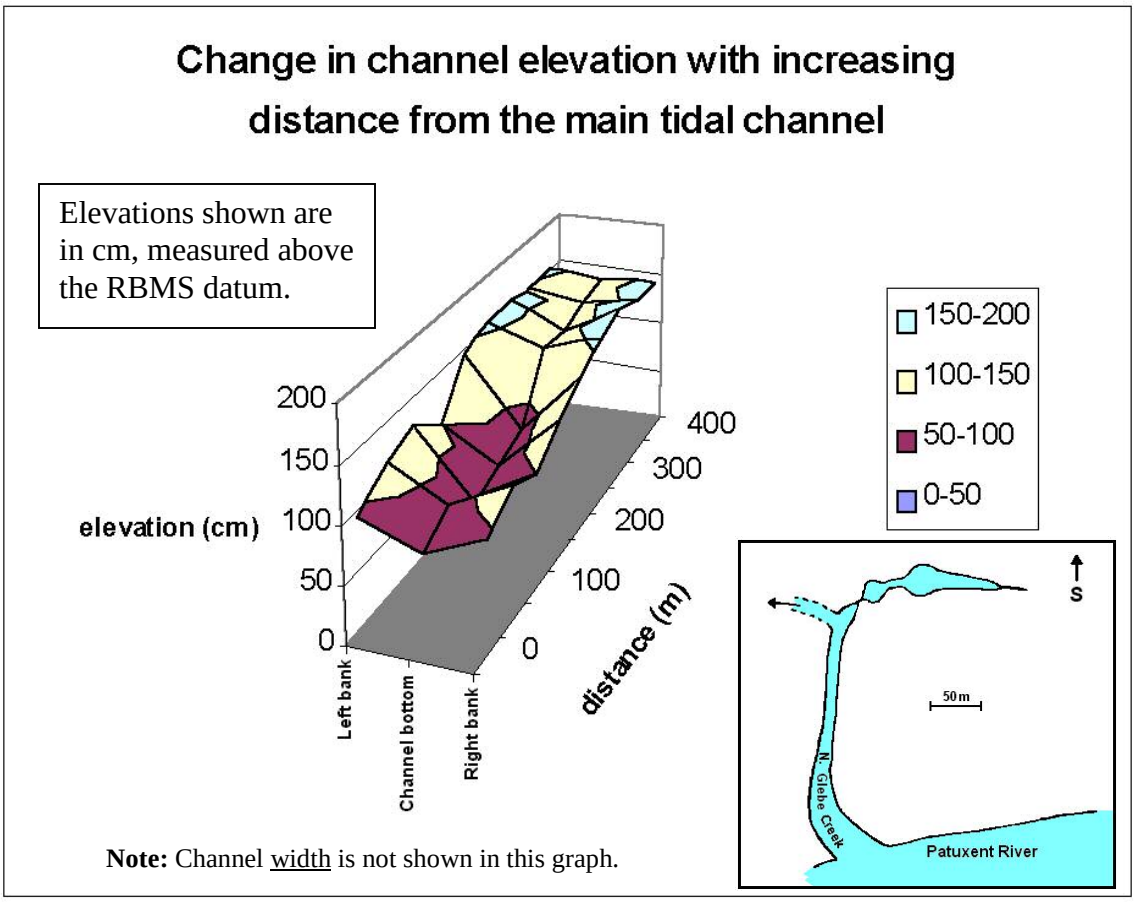

Figure 34: North Glebe Creek channel elevation. (Inset) North Glebe Creek drains into the Patuxent River. At approximately 250 meters from the main channel, it branches east and west. The westward bound channel is the first-order segment along which channel geomorphic, hydraulic head and K measurements have been made. (3-D graph) The elevation of the channel bottom and the creekbank tops increases overall with distance from the Patuxent, but not linearly.

When data from North Glebe Creek was compared with similar data collected by Williams et al. (2002), correlation with their exponential trends was fair to poor. (See Figure 35.) According to Williams et al., this is because the channel is not yet mature. It has not reached a dynamic equilibrium between deposition and erosion. This hypothesis is supported by the fact that the total channel length has decreased by approximately 300 meters over the past 25 years. This determination was made by comparing channel length measurements made in the field to the channel length shown on the 1979 photorevised version of the Bristol Quadrangle USGS topographic map.

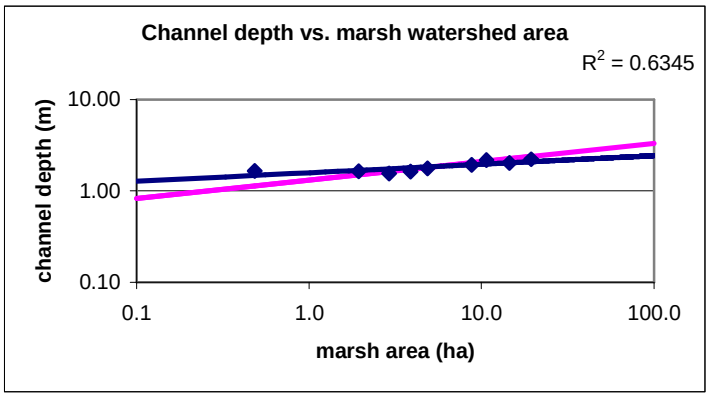

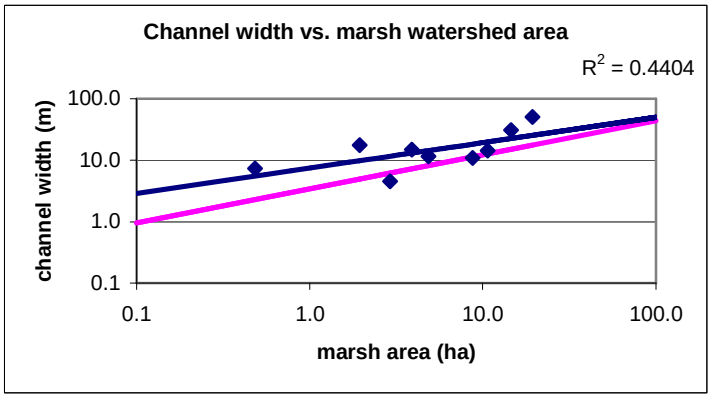

Figure 35: Comparison of depth and width data with trends from Williams et al., 2002. Williams et al. found that network channel depth and width increased exponentially with increasing amount of contributing marsh area. The pink lines in each graph are the regression lines obtained by Williams et al. Their data correlated strongly, with $R^2 = 0.84$ between channel depth and marsh area and $R^2 = 0.88$ between channel width and marsh area. Data collected along N. Glebe Marsh are shown in blue. Values on the depth vs. area graph were adjusted upward by 1.17 m to account for the difference in elevation datum between the two data sets.

H3 Results: Spatial trends in flux magnitude

Details for interpreting results

Calculated flux magnitudes from data collected over an approximately 7 hour falling tide period are shown in Figures 36A-D. In these graphs, Round 1 corresponds to measurements made around 9am, Round 2 corresponds to measurements made around 10am, etc. Hydraulic head measurements for a given round could not all be made simultaneously, but are within approximately 10 minutes of each other. Round 1 measurements were made about one hour after high tide, and Round 7 measurements were made about 1 to 1 ½ hours after low tide.

A negative value of q' indicates that horizontal groundwater flux is away from the channel. It was assumed that the direction of flux was correct, so in cases where

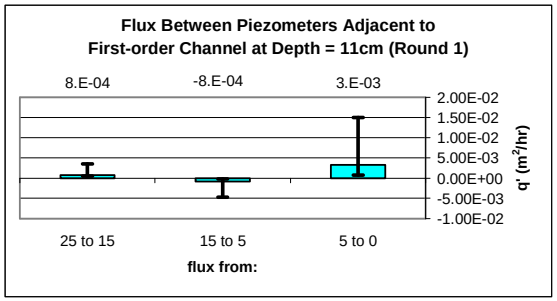

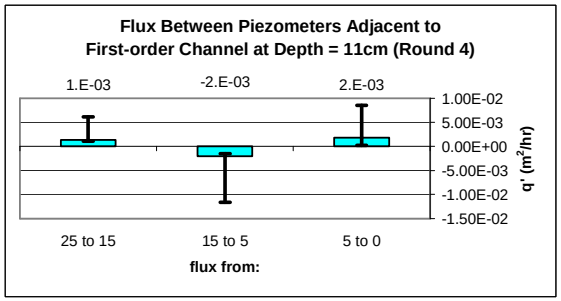

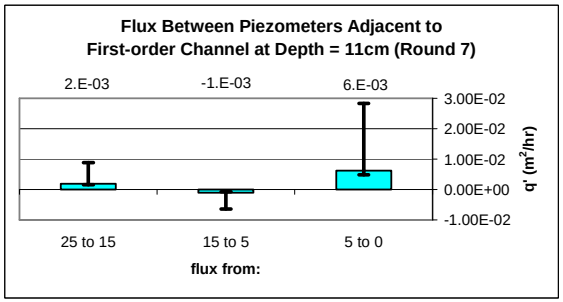

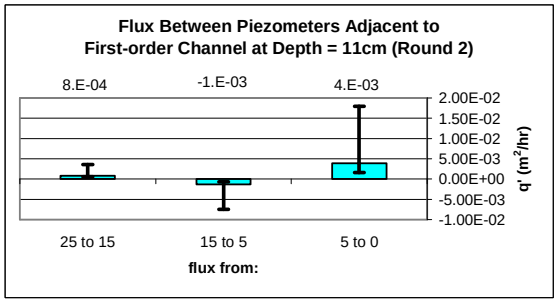

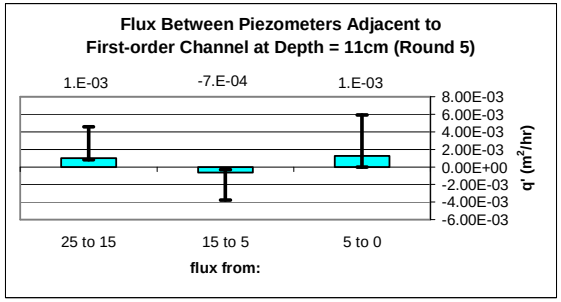

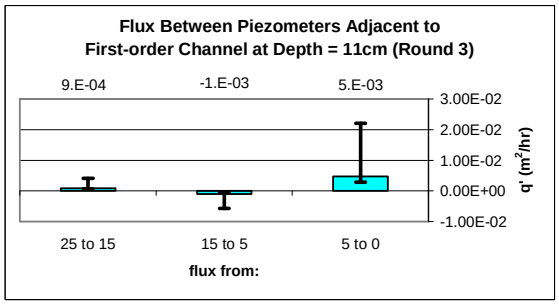

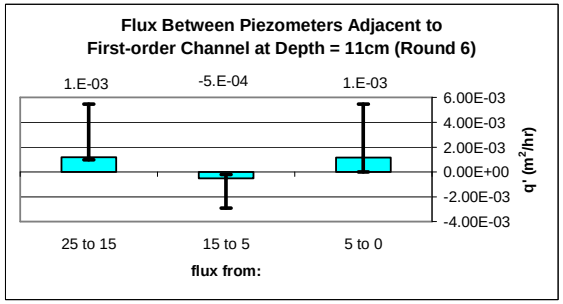

<u>Figure 36A</u>: Groundwater flux between first-order channel piezometer locations (depth = 11 cm). This set of graphs shows the magnitude of horizontal groundwater flux between piezometers located adjacent to a first-order section of N. Glebe Creek. These piezometers are all installed to a depth of 11 cm below the ground surface and are 0, 5, 15 and 25 meters from the network channel creekbank. '25 to 15' is flux from the 25-m piezometer toward the 15-m piezometer, '15 to 5' is flux from the 15-m piezometer toward the 5-m piezometer and '5 to 0' is flux from the 5-m piezometer toward the 0-m piezometer. Negative values of flux indicate that groundwater is moving away from the channel.

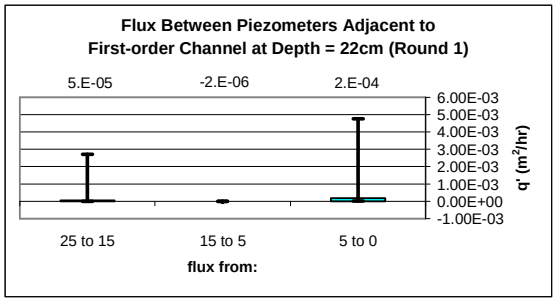

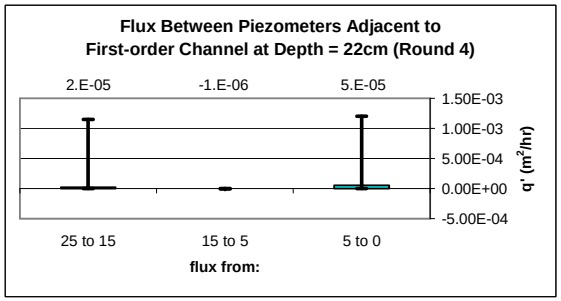

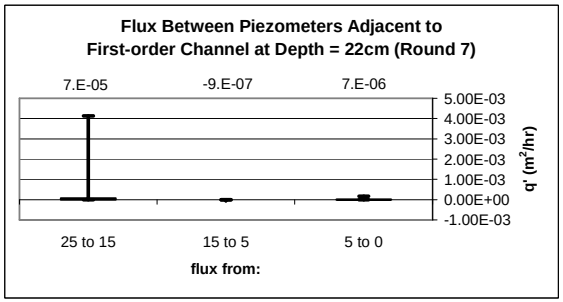

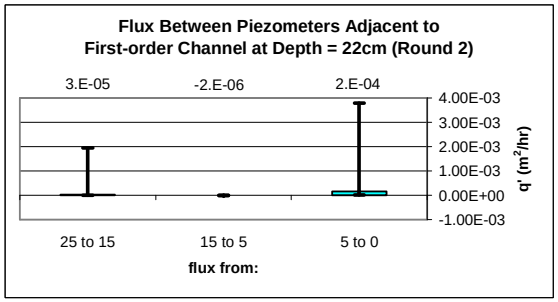

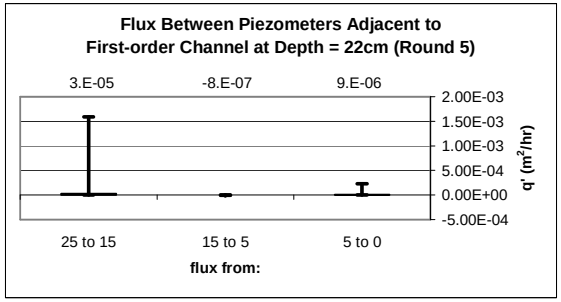

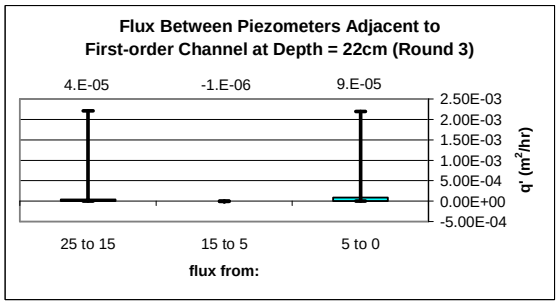

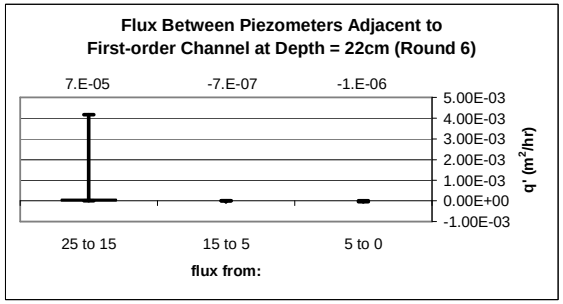

<u>Figure 36B</u>: Groundwater flux between first-order channel piezometer locations (depth = 22 cm). This set of graphs shows the magnitude of horizontal groundwater flux between piezometers located adjacent to a first-order section of N. Glebe Creek. These piezometers are all installed to a depth of 22 cm below the ground surface and are 0, 5, 15 and 25 meters from the network channel creekbank. '25 to 15' is flux from the 25-m piezometer toward the 15-m piezometer, '15 to 5' is flux from the 15-m piezometer toward the 5-m piezometer and '5 to 0' is flux from the 5-m piezometer toward the 0-m piezometer. Negative values of flux indicate that groundwater is moving away from the channel.

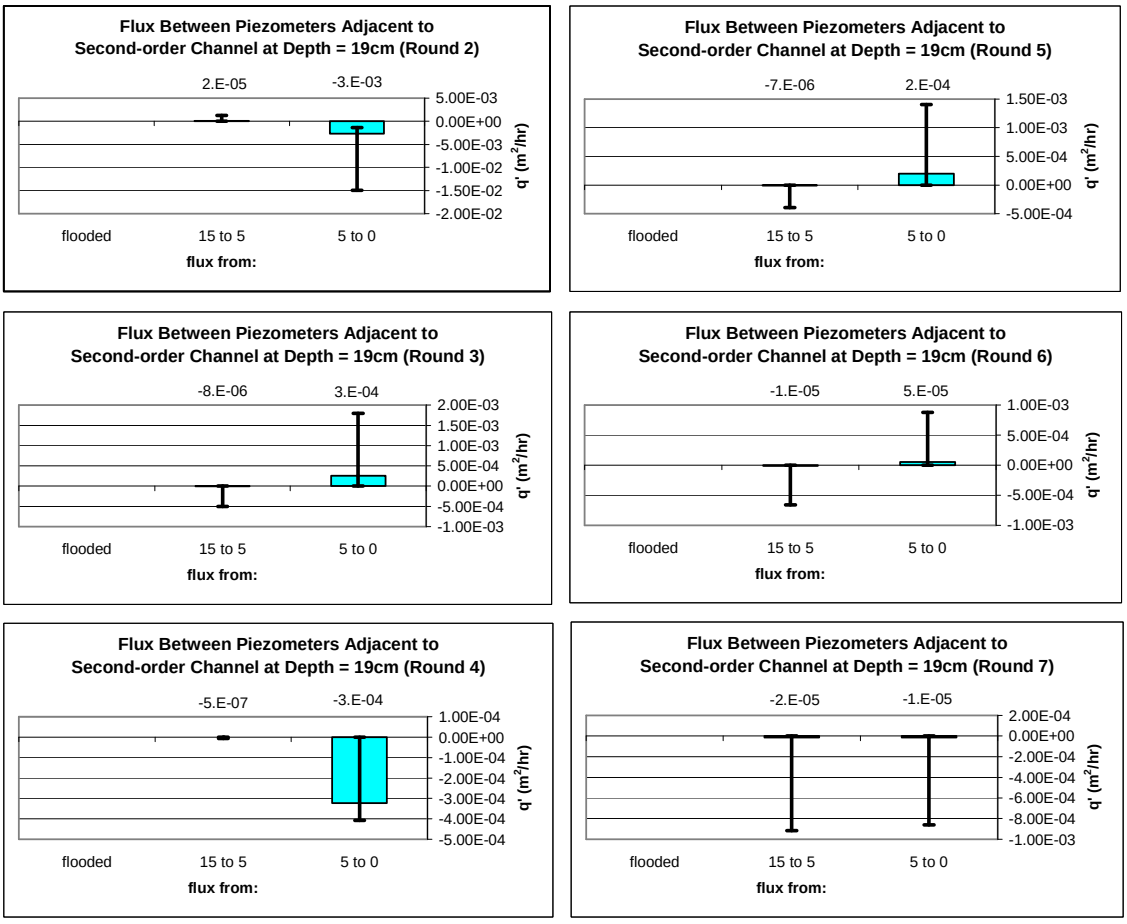

<u>Figure 36C</u>: Groundwater flux between second-order channel piezometer locations (depth = 19 cm). This set of graphs shows the magnitude of horizontal groundwater flux between piezometers located adjacent to a second-order section of N. Glebe Creek. These piezometers are all installed to a depth of 19 cm below the ground surface and are 0, 5, 15 and 25 meters from the network channel creekbank. '25 to 15' is flux from the 25-m piezometer toward the 15-m piezometer, '15 to 5' is flux from the 15-m piezometer toward the 5-m piezometer and '5 to 0' is flux from the 5-m piezometer toward the 0-m piezometer. Negative values of flux indicate that groundwater is moving away from the channel. 'Flooded' means that at least one of the two piezometers between which flux was being calculated was flooded by tidal water, so a head measurement could not be made at that time.

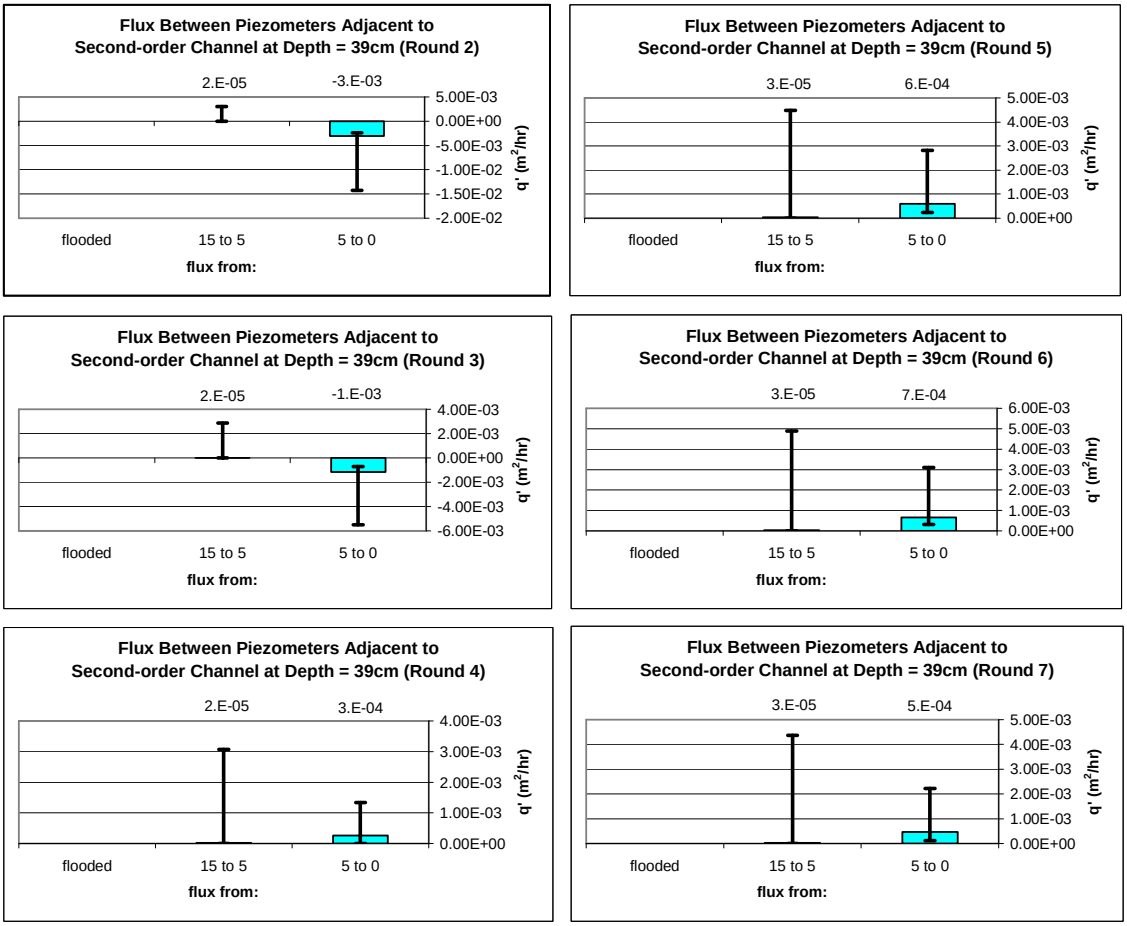

<u>Figure 36D</u>: Groundwater flux between second-order channel piezometer locations (depth = 39 cm). This set of graphs shows the magnitude of horizontal groundwater flux between piezometers located adjacent to a second-order section of N. Glebe Creek. These piezometers are all installed to a depth of 39 cm below the ground surface and are 0, 5, 15 and 25 meters from the network channel creekbank. '25 to 15' is flux from the 25-m piezometer toward the 15-m piezometer, '15 to 5' is flux from the 15-m piezometer toward the 5-m piezometer and '5 to 0' is flux from the 5-m piezometer toward the 0-m piezometer. Negative values of flux indicate that groundwater is moving away from the channel. 'Flooded' means that at least one of the two piezometers between which flux was being calculated was flooded by tidal water, so a head measurement could not be made at that time.

uncertainties suggested that the direction of flux could have been in either direction, the magnitude of the uncertainty was adjusted so that the range of possible q' values was only either positive or negative (uncertainties could not cause the range of values to cross zero). For a complete list of the exact calculated q' values and the associated uncertainties, see Appendix C.

First-order channel location

Figure 36A shows the magnitude and direction (either toward or away from the network channel) of horizontal groundwater flux calculated from data collected along the first-order channel piezometer line adjacent to N. Glebe Creek. Piezometer depths are 11 cm. Within the range of uncertainties, there is no flux magnitude difference between any of the piezometer locations during a single round. However, during every round, the mean calculated flux from 5 to 0 meters from the creekbank is either equal to or greater than the mean calculated flux between the other piezometer locations. During all seven rounds the calculated flux from 5 to 0 meters from the creekbank was between 1×10^{-3} and 5×10^{-3} m^2/hr (68% confidence level).

Although the magnitude of groundwater flux between 15 and 5 meters from the creekbank was not significantly different from the flux magnitudes between other piezometer locations, it was opposite in direction. During all seven measurement rounds, horizontal groundwater flux was toward the channel at distances between 25 and 15 meters and 5 and 0 meters from the network channel creekbank. But between 15 and 5 meters from the creekbank, groundwater flux was away from the channel. This suggests the possibility of a vertical to sub-vertical low-K zone somewhere around 15 meters from the creekbank (+/-10 meters) that allows faster tidal-water infiltration, resulting in a

lower water-table. This same directional trend is also observed at a depth of 22 cm during all measurement rounds except for Round 6, when flux between 5 and 0 meters is also away from the channel. (See Figure 36B.) Round 6 corresponds very closely with the low tide but, during this particular tidal cycle, flood water dropped no lower than 6 inches above the channel creekbank.

At a depth of 22 cm, the calculated mean flux magnitude was greatest between 5 and 0 meters from the creekbank and was smallest (and negative) between 15 and 5 meters from the creekbank during Rounds 1-4. During Rounds 5-7, the greatest mean flux magnitude was between 25 and 15 meters from the creekbank, with the smallest flux still between 15 and 5 meters. This change was not due to an increase in flux magnitude between 25 and 15 meters but was, instead, caused by a drop in magnitude between 5 and 0 meters. This probably signifies a draining of the near-channel sediment pores, resulting in a lowering of head (pore pressure) in the near-channel sediments. As the head in the sediments approaches the head in the channel, the magnitude of flux between the sediments and the channel decreases.

The flux between 5 and 0 meters from the channel at a depth of 22 cm was between 4×10^{-6} and 2×10^{-4} m^2/hr (68% confidence level) throughout the test period. This range is significantly lower than that calculated at 11 cm deep, indicating that most of the groundwater that flows into the network channel is from the near-surface sediments. Within the range of uncertainty, there was no difference in flux magnitude between any of the 22-cm deep piezometers during a single round.

Second-order channel location

At the second-order channel piezometer line location, the first round of measurements could not be made because the tidal flood stage was so high that removing the piezometer caps would present a risk of flooding the piezometers. In addition, the caps had been left off of the 25-m piezometers and they had flooded with tidal water. Therefore, measurements were not made at the 25-m location. The results of flux calculations made from head measurements at the 2nd-order locations are shown in Figures 36C-D.

During every round except for Round 7 at a depth of 19 cm (Figure 36C), the highest mean horizontal groundwater flux magnitude was between 5 and 0 meters. During Round 7, flux magnitude was highest between 15 and 5 meters from the network channel creekbank. But, within the range of uncertainty, there was no difference in flux magnitude between any two piezometers during a single round. The magnitude of flux between 5 and 0 meters from the channel ranged from 3×10^{-5} to 1×10^{-3} m^2/hr (68% confidence level) throughout the entire measurement period.

The direction of horizontal groundwater flux changed more at this location and depth than at any other. During Rounds 2 and 3, flux between 5 and 0 meters from the creekbank was away from the channel. Flux between 15 and 5 meters from the creekbank was toward the channel. During Round 4 of measurements, groundwater flux between all piezometer locations was away from the channel. During Rounds 5 and 6 flux directions were the opposite of Rounds 2 and 3 with groundwater between 5 and 0 meters from the creekbank flowing toward the channel and groundwater between 15 and 5 meters from

the creekbank flowing away from the channel. During Round 7, like Round 4, flux between all piezometer locations was away from the channel.

At a depth of 39 cm at the 2nd-order channel test location, the horizontal groundwater flux direction was away from the channel between 5 and 0 meters from the creekbank and toward the channel between 15 and 5 meters from the creekbank during Rounds 2 and 3. (See Figure 36D.) In all subsequent rounds, flux between all piezometer locations was toward the channel.

The highest calculated mean magnitude of flux was between 5 and 0 meters from the channel creekbank during all 7 rounds. However, within the range of uncertainty, there was no significant difference between any of the flux magnitudes within a single round. At 39 cm below the ground surface, the magnitude of flux between 5 and 0 meters from the channel ranged from 3×10^{-4} and 2×10^{-3} m^2/hr (68% confidence level) throughout the entire measurement period. This range overlaps with the corresponding range of measurements at a depth of 19 cm.

Spatial trends

As was previously mentioned, the magnitude of groundwater flux at a depth of 11 cm was significantly higher than the magnitude of flux at a depth of 22 cm between 5 and 0 meters from the creekbank at the first-order network channel location. (See Table 9.) This trend also held true at 15 to 5 and 25 to 15 meters from the creekbank. In addition, the overall range of flux magnitudes at 11 cm deep was greater than the overall range of flux magnitudes at 22 cm deep. However, this difference in flux magnitude with depth was not observed at the second-order channel location.

First-order location: (depth = 11cm)		Second-order location: (depth = 19 cm)	
distance from channel (m)	range of flux magnitudes (m^2/hr)	distance from channel (m)	range of flux magnitudes (m^2/hr)
5 to 0	1E-3 to 5E-3	5 to 0	3E-5 to 1E-3
15 to 5	6E-4 to 2E-3	15 to 5	2E-6 to 3E-5
25 to 15	8E-4 to 1E-3		
(depth = 22 cm)		**(depth = 39 cm)**	
distance from channel (m)	range of flux magnitudes (m^2/hr)	distance from channel (m)	range of flux magnitudes (m^2/hr)
5 to 0	4E-6 to 2E-4	5 to 0	3E-4 to 2E-3
15 to 5	7E-7 to 2E-6	15 to 5	2E-5 to 3E-5
25 to 15	3E-5 to 7E-5		

Table 9: Range of flux (q') magnitudes. In this table the range of calculated values of q' between each piezometer set are listed. Ranges are one standard deviation around the geometric mean q' value for all measurements made during the 7-round test period.

There was no significant difference (68% level) in horizontal groundwater flux magnitude with distance from the tidal network channel at a depth of 11 cm adjacent to the first-order section of channel but, at a depth of 22 cm, the flux magnitude from 5 to 0 meters and the flux magnitude from 25 to 15 meters were both significantly higher than the flux magnitude from 15 to 5 meters. There was no significant magnitude difference in the fluxes between 5 and 0 meters and between 25 and 15 meters from the creekbank.

At the second-order channel location, there was no significant difference in flux magnitude with distance from the channel at a depth of 19 cm but, at a depth of 39 cm, the magnitude of horizontal groundwater flux was greater between 5 and 0 meters from the creekbank than it was from 15 to 5 meters from the creekbank.

The range of flux magnitudes measured at the 1st-order channel location (one standard deviation around the geometric mean) was 7×10^{-7} to 5×10^{-3} m^2/hr. At the 2nd-order channel location, the range of measured flux magnitudes was 2×10^{-6} to 2×10^{-3} m^2/hr. So, there was no significant difference in the range of flux magnitudes measured adjacent to the 1st-order channel and the range measured adjacent to the 2nd-order

channel. However, examining flux direction at 5 to 0 meters from the creekbank, much more variability was observed adjacent to the 2nd-order channel. At the 1st-order location, flux at a depth of 11 cm was toward the channel during all seven rounds (100% of the time). At 22 cm depth, flux was toward the channel in all but one round (86% of the time). Next to the 2nd-order channel at a depth of 19 cm, flux was toward the channel only 50% of the time. At 39 cm deep, flux was toward the channel 67% of the time.

Head response to changes in tidal stage

In order to observe head response to the change in tidal stage, graphs were made showing the hydraulic head measurements that where used in the calculation of q', along with the tidal stage and ground surface elevation at each piezometer location. (See Appendix D.) (For measured total head values, see the table in Appendix B.) At most locations, during times of flooding, changes in hydraulic head seemed to roughly follow the change in tidal stage, rising as the top-loading pressure increased and falling when it decreased. During non-flooding times, head tended to remain within a few centimeters of the ground surface.

However, three piezometers did not show this tidal response: 1-0-22, 2-5-39 and 2-15-39. This is probably due to regions of low K within the sediments. At piezometer 2-15-39 the hydraulic conductivity was measured to be 4×10^{-7} cm/s. This is the lowest K of any of the piezometers where tidal-cycle head measurements were made. As pointed out by Hanschke and Baird (2001), low K sediments around the piezometer intake would affect the rate at which water can flow into or out of the piezometer. Therefore, pressure changes are most likely occurring in the sediments, but the piezometer cannot register them fast enough. At piezometers 1-0-22 and 2-5-39, the K is slightly above average for

the site (4×10^{-4} and 1×10^{-3} cm/s, respectively), so the lack of response to tidal stage changes must be due to another reason.

According to Hvorslev (1951), hydraulic head may not be equal to the water-table in an unconfined aquifer for the following reasons:

> "(a) perched ground-water tables or bodies of ground water isolated by impermeable soil strata; (b) downward seepage to more permeable and/or better drained strata; (c) upward seepage from strata under artesian pressure or by evaporation and transpiration; and (d) incomplete processes of consolidation or swelling caused by changes in loads and stresses."

T_{90}/T_{50} ratios are not particularly high at these two piezometer locations (see Table 2), so 'incomplete consolidation or swelling' is not a very likely explanation. The most likely explanation is that 'impermeable soil strata' or low-K layers are restricting flow to the piezometer location. Although K is not particularly low at the depth at which the piezometers are installed, there may very well be low K regions either above or below the piezometer depth restricting groundwater flow into the higher-K area. Sediment cores showed how heterogeneous these marsh soils are. Surrounding low-K areas are not only possible, but very likely.

If this were the case, the sediments below the low-K layer would be "protected" from pore pressure changes above and would tend to stay fairly constant. The low-K layer, by limiting the rate at which water could infiltrate, would cause lower pore pressure below the layer than exists above the layer during flooding and /or infiltration. Conversely, once pressures above the low-K layer dropped, the pressure below the layer would not be able to drop as quickly because the exfiltration rate would also be limited.

In general, a good estimate of hydraulic head at this site is tidal stage. At 57% of the piezometer locations, changes in head followed changes in tidal stage very closely ($R^2 > 0.9$). At 22% of the piezometer locations, changes in head followed changes in tidal

stage pretty well ($0.9 > R^2 > 0.75$) and at 14% of the piezometer locations, changes in head followed changes in tidal stage fairly well ($0.75 > R^2 > 0.6$). Changes in head followed changes in tidal stage poorly ($R^2 < 0.6$) at only 7% of the piezometer locations.

Volumetric flux calculations

The value of flux (q') that has previously been calculated in this paper is flux per unit width (in m^2/hr). To calculate a volumetric flux (Q in m^3/hr) to the tidal network channel, q' must be multiplied by the channel length into which flux is being measured. Channel lengths measured in the field were 233 meters for the 2nd-order segment of N. Glebe Creek and 200 meters for the 1st-order segment.

Because the value of hydraulic head used in the q' calculations is measured with respect to the bottom of the adjacent network channel bottom, just multiplying q' by the channel length gives a volume of horizontal groundwater flux into the channel *assuming that the channel depth is constant*. Obviously, this is not the case, but channel depth was measured at 50-m intervals over the entire channel. It was assumed that channel depth changes linearly between the measured points and the mean of the two end-points was used as an estimate of the average channel depth over each 50-m interval. (See Figure 37.) To calculate Q, two further assumptions had to be made: 1) Hydraulic head and K-values are the same all along the 1st- and 2nd-order segments of channel as theyare at the corresponding piezometer lines where measurements were made. 2) Head response to changes in tidal stage is the same on both sides of the channel.

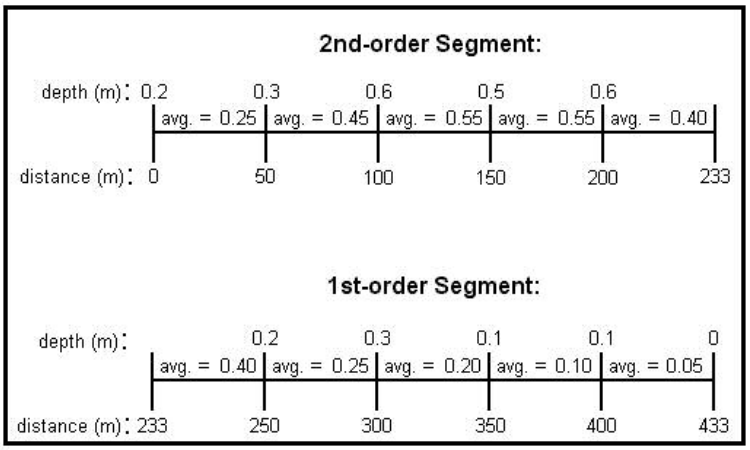

Figure 37: Average channel depths for each 50-m stream segment. Channel depth measurements were made at 50-m intervals along North Glebe Creek. 'Distance' is measured from the main channel toward the head of the tidal network channel. Assuming that the channel depth changes linearly between measured points, the mean of each two measured end-point depths is used as the average depth over the entire 50-m segment.

When calculating Q, hydraulic head values measured with respect to the channel bottom adjacent to each piezometer line were adjusted for differences in channel depth over each 50-m channel segment. (See Tables 10A &10C.) These adjusted head values were used to calculate q' in m^2/hr for each round of head measurements. Next, q' was multiplied by the channel length for each channel segment, giving values of Q over each segment for each round of measurements.

Because head measurements were made approximately every hour over ½ of a tidal cycle, values of Q (in m^3/hr) calculated over the entire measurement period were summed to estimate the total volume of groundwater (in m^3) fluxing toward the channel over ½ of a tidal cycle at both 1/3 and 2/3 the channel depth. Then the water volume at 1/3 the channel depth and the water volume at 2/3 the channel depth were averaged to determine the average amount of groundwater entering (or leaving) the channel on one

piez. #	head wrt channel (m) @ 300m	hydraulic head with respect to the channel bottom 233-250 m	250-300 m	300-350 m	350-400 m	400-433 m	avg. K (m/hr)
1-0-11	1.15	1.25	1.10	1.05	0.95	0.90	2.E-01
	1.03	1.13	0.98	0.93	0.83	0.78	2.E-01
	0.82	0.92	0.77	0.72	0.62	0.57	2.E-01
	0.76	0.86	0.71	0.66	0.56	0.51	2.E-01
	0.61	0.71	0.56	0.51	0.41	0.36	2.E-01
	0.56	0.66	0.51	0.46	0.36	0.31	2.E-01
	0.32	0.42	0.27	0.22	0.12	0.07	2.E-01
1-5-11	1.23	1.33	1.18	1.13	1.03	0.98	2.E-01
	1.13	1.23	1.08	1.03	0.93	0.88	2.E-01
	0.97	1.07	0.92	0.87	0.77	0.72	2.E-01
	0.83	0.93	0.78	0.73	0.63	0.58	2.E-01
	0.67	0.77	0.62	0.57	0.47	0.42	2.E-01
	0.62	0.72	0.57	0.52	0.42	0.37	2.E-01
	0.67	0.77	0.62	0.57	0.47	0.42	2.E-01
1-0-22	0.54	0.64	0.49	0.44	0.34	0.29	2.E-03
	0.56	0.66	0.51	0.46	0.36	0.31	2.E-03
	0.55	0.65	0.50	0.45	0.35	0.30	2.E-03
	0.55	0.65	0.50	0.45	0.35	0.30	2.E-03
	0.56	0.66	0.51	0.46	0.36	0.31	2.E-03
	0.56	0.66	0.51	0.46	0.36	0.31	2.E-03
	0.56	0.66	0.51	0.46	0.36	0.31	2.E-03
1-5-22	1.18	1.28	1.13	1.08	0.98	0.93	2.E-03
	1.09	1.19	1.04	0.99	0.89	0.84	2.E-03
	0.90	1.00	0.85	0.80	0.70	0.65	2.E-03
	0.76	0.86	0.71	0.66	0.56	0.51	2.E-03
	0.61	0.71	0.56	0.51	0.41	0.36	2.E-03
	0.56	0.66	0.51	0.46	0.36	0.31	2.E-03
	0.60	0.70	0.55	0.50	0.40	0.35	2.E-03

Q = q' x channel length

high 233-250m Q (m^3/hr)	low 233-250m Q (m^3/hr)	high 250-300m Q (m^3/hr)	low 250-300m Q (m^3/hr)	high 300-350m Q (m^3/hr)	low 300-350m Q (m^3/hr)	high 350-400m Q (m^3/hr)	low 350-400m Q (m^3/hr)	high 400-433m Q (m^3/hr)	low 400-433m Q (m^3/hr)
2.92E-01	2.27E-02	7.58E-01	5.90E-02	7.25E-01	5.64E-02	6.58E-01	5.12E-02	4.13E-01	3.21E-02
3.48E-01	3.98E-02	8.94E-01	1.02E-01	8.51E-01	9.71E-02	7.64E-01	8.71E-02	4.75E-01	5.42E-02
4.31E-01	6.51E-02	1.08E+00	1.62E-01	1.01E+00	1.53E-01	8.85E-01	1.33E-01	5.42E-01	8.17E-02
1.72E-01	8.52E-03	4.21E-01	2.08E-02	3.93E-01	1.94E-02	3.36E-01	1.66E-02	2.03E-01	1.00E-02
1.24E-01	2.53E-03	2.90E-01	5.91E-03	2.65E-01	5.40E-03	2.16E-01	4.37E-03	1.27E-01	2.54E-03
1.15E-01	2.36E-03	2.66E-01	5.41E-03	2.41E-01	4.90E-03	1.92E-01	3.87E-03	1.11E-01	2.21E-03
5.96E-01	1.13E-01	1.31E+00	2.48E-01	1.16E+00	2.20E-01	8.69E-01	1.62E-01	4.77E-01	8.81E-02

Sum of fluxes over 1/2 tidal cycle (m^3):

high	low	high	low	high	low	high	low	high	low
2.08	0.25	5.02	0.60	4.65	0.56	3.92	0.46	2.35	0.27

high 233-250m Q (m^3/hr)	low 233-250m Q (m^3/hr)	high 250-300m Q (m^3/hr)	low 250-300m Q (m^3/hr)	high 300-350m Q (m^3/hr)	low 300-350m Q (m^3/hr)	high 350-400m Q (m^3/hr)	low 350-400m Q (m^3/hr)	high 400-433m Q (m^3/hr)	low 400-433m Q (m^3/hr)
9.13E-02	6.85E-04	2.27E-01	1.70E-03	2.13E-01	1.59E-03	1.85E-01	1.38E-03	1.13E-01	8.42E-04
7.29E-02	5.42E-04	1.80E-01	1.33E-03	1.68E-01	1.25E-03	1.45E-01	1.07E-03	8.79E-02	6.50E-04
4.28E-02	3.04E-04	1.03E-01	7.32E-04	9.56E-02	6.77E-04	8.03E-02	5.68E-04	4.80E-02	3.39E-04
2.39E-02	1.48E-04	5.64E-02	3.48E-04	5.17E-02	3.19E-04	4.24E-02	2.60E-04	2.49E-02	1.52E-04
4.83E-03	0.00E+00	1.11E-02	0.00E+00	1.00E-02	0.00E+00	7.95E-03	0.00E+00	4.56E-03	0.00E+00
0.00E+00	-2.42E-04	0.00E+00	-5.51E-04	0.00E+00	-4.97E-04	0.00E+00	-3.88E-04	0.00E+00	-2.21E-04
3.59E-03	0.00E+00	8.23E-03	0.00E+00	7.46E-03	0.00E+00	5.91E-03	0.00E+00	3.39E-03	0.00E+00

Sum of fluxes over 1/2 tidal cycle (m^3):

high	low	high	low	high	low	high	low	high	low
0.24	0.00	0.59	0.00	0.55	0.00	0.47	0.00	0.28	0.00

Average of flux at depth =11cm and depth = 22cm (m^3):

high	low	high	low	high	low	high	low	high	low
1.16	0.13	2.80	0.30	2.60	0.28	2.19	0.23	1.31	0.14

q' between 5 and 0 meters from the creekbank

233-250m q' (m^2/hr)	+	-	250-300m q' (m^2/hr)	+	-	300-350m q' (m^2/hr)	+	-	350-400m q' (m^2/hr)	+	-	400-433m q' (m^2/hr)	+	-
4.01E-03	1.32E-02	2.67E-03	3.54E-03	1.16E-02	2.36E-03	3.39E-03	1.11E-02	2.26E-03	3.08E-03	1.01E-02	2.05E-03	2.92E-03	9.58E-03	1.95E-03
4.82E-03	1.57E-02	2.48E-03	4.21E-03	1.37E-02	2.16E-03	4.00E-03	1.30E-02	2.06E-03	3.59E-03	1.17E-02	1.85E-03	3.39E-03	1.10E-02	1.75E-03
6.00E-03	1.94E-02	2.17E-03	5.09E-03	1.64E-02	1.84E-03	4.79E-03	1.55E-02	1.73E-03	4.18E-03	1.35E-02	1.52E-03	3.88E-03	1.25E-02	1.41E-03
2.35E-03	7.77E-03	1.85E-03	1.96E-03	6.47E-03	1.54E-03	1.83E-03	6.03E-03	1.44E-03	1.56E-03	5.17E-03	1.23E-03	1.43E-03	4.73E-03	1.13E-03
1.67E-03	5.59E-03	1.53E-03	1.34E-03	4.46E-03	1.22E-03	1.22E-03	4.08E-03	1.12E-03	9.97E-04	3.33E-03	9.10E-04	8.84E-04	2.95E-03	8.07E-04
1.56E-03	5.22E-03	1.43E-03	1.23E-03	4.09E-03	1.12E-03	1.11E-03	3.72E-03	1.01E-03	8.87E-04	2.96E-03	8.10E-04	7.74E-04	2.58E-03	7.07E-04
8.31E-03	2.67E-02	1.65E-03	6.22E-03	2.00E-02	1.25E-03	5.52E-03	1.78E-02	1.13E-03	4.12E-03	1.33E-02	8.73E-04	3.42E-03	1.10E-02	7.52E-04
2.44E-04	5.12E-03	2.04E-04	2.06E-04	4.32E-03	1.72E-04	1.93E-04	4.06E-03	1.62E-04	1.68E-04	3.52E-03	1.40E-04	1.55E-04	3.26E-03	1.30E-04
1.95E-04	4.10E-03	1.63E-04	1.63E-04	3.43E-03	1.37E-04	1.53E-04	3.21E-03	1.28E-04	1.32E-04	2.76E-03	1.10E-04	1.21E-04	2.54E-03	1.01E-04
1.15E-04	2.41E-03	9.67E-05	9.38E-05	1.97E-03	7.92E-05	8.69E-05	1.82E-03	7.34E-05	7.31E-05	1.53E-03	6.17E-05	6.62E-05	1.39E-03	5.59E-05
6.40E-05	1.34E-03	5.53E-05	5.13E-05	1.08E-03	4.43E-05	4.70E-05	9.87E-04	4.07E-05	3.86E-05	8.09E-04	3.34E-05	3.43E-05	7.20E-04	2.97E-05
1.29E-05	2.71E-04	1.29E-05	1.01E-05	2.11E-04	1.01E-05	9.12E-06	1.92E-04	9.12E-06	7.23E-06	1.52E-04	7.23E-06	6.28E-06	1.32E-04	6.28E-06
-1.18E-06	1.18E-06	1.31E-05	-9.13E-07	9.13E-07	1.01E-05	-8.24E-07	8.24E-07	9.11E-06	-6.44E-07	6.44E-07	7.12E-06	-5.54E-07	5.54E-07	6.13E-06
9.58E-06	2.02E-04	9.58E-06	7.47E-06	1.57E-04	7.47E-06	6.77E-06	1.42E-04	6.77E-06	5.36E-06	1.13E-04	5.36E-06	4.66E-06	9.80E-05	4.66E-06

Sum of fluxes over 1st-order segment: (for 1/2 tidal cycle)

(This is the sum of Q over each depth interval multiplied by 2 to account for both sides of the channel.)

high = 10.06 m^3

low = 1.08 m^3

Total flux over 1st-order segment: (for one full tidal cycle)

high = 20.12 m^3

low = 2.16 m^3

Table 10A: The volume range of groundwater flowing toward the 1st-order section of N. Glebe Creek, calculated using specific K-values. In this table, the upper and lower bounds of Q are calculated from the q' values which have been adjusted for differences in channel depth over the length of the channel. Negative values of Q are away from the tidal network channel. Uncertainties in q' were calculated using the methods described in Appendix C. 'Avg. K' values are the average of the 2 GM K values at the piezometers between which flux is being measured.

piez. #	head wrt channel (m) @ 300m	hydraulic head with respect to the channel bottom 233-250 m	250-300 m	300-350 m	350-400 m	400-433 m	avg. K (m/hr)	Q = q' x channel length: high 233-250m Q (m^3/hr)	low 233-250m Q (m^3/hr)	high 250-300m Q (m^3/hr)	low 250-300m Q (m^3/hr)	high 300-350m Q (m^3/hr)	low 300-350m Q (m^3/hr)	high 350-400m Q (m^3/hr)	low 350-400m Q (m^3/hr)	high 400-433m Q (m^3/hr)	low 400-433m Q (m^3/hr)
1-0-11	1.15	1.25	1.10	1.05	0.95	0.90	2.E-03	1.23E-02	0.00E+00	3.19E-02	0.00E+00	3.05E-02	0.00E+00	2.77E-02	0.00E+00	1.74E-02	0.00E+00
	1.03	1.13	0.98	0.93	0.83	0.78	2.E-03	1.48E-02	0.00E+00	3.79E-02	0.00E+00	3.60E-02	0.00E+00	3.23E-02	0.00E+00	2.01E-02	0.00E+00
	0.82	0.92	0.77	0.72	0.62	0.57	2.E-03	1.84E-02	0.00E+00	4.58E-02	0.00E+00	4.31E-02	0.00E+00	3.77E-02	0.00E+00	2.31E-02	0.00E+00
	0.76	0.86	0.71	0.66	0.56	0.51	2.E-03	7.20E-03	0.00E+00	1.76E-02	0.00E+00	1.64E-02	0.00E+00	1.41E-02	0.00E+00	8.51E-03	0.00E+00
	0.61	0.71	0.56	0.51	0.41	0.36	2.E-03	5.13E-03	0.00E+00	1.20E-02	0.00E+00	1.10E-02	0.00E+00	8.99E-03	0.00E+00	5.26E-03	0.00E+00
	0.56	0.66	0.51	0.46	0.36	0.31	2.E-03	4.80E-03	0.00E+00	1.11E-02	0.00E+00	1.00E-02	0.00E+00	8.00E-03	0.00E+00	4.61E-03	0.00E+00
	0.32	0.42	0.27	0.22	0.12	0.07	2.E-03	2.54E-02	2.87E-05	5.59E-02	6.04E-05	4.97E-02	5.21E-05	3.71E-02	3.46E-05	2.03E-02	1.66E-05
1-5-11	1.23	1.33	1.18	1.13	1.03	0.98	2.E-03										
	1.13	1.23	1.08	1.03	0.93	0.88	2.E-03										
	0.97	1.07	0.92	0.87	0.77	0.72	2.E-03										
	0.83	0.93	0.78	0.73	0.63	0.58	2.E-03										
	0.67	0.77	0.62	0.57	0.47	0.42	2.E-03										
	0.62	0.72	0.57	0.52	0.42	0.37	2.E-03										
	0.67	0.77	0.62	0.57	0.47	0.42	2.E-03										
1-0-22	0.54	0.64	0.49	0.44	0.34	0.29	2.E-03	7.47E-02	1.26E-04	1.85E-01	3.12E-04	1.74E-01	2.92E-04	1.51E-01	2.52E-04	9.22E-02	1.53E-04
	0.56	0.66	0.51	0.46	0.36	0.31	2.E-03	5.97E-02	9.49E-05	1.47E-01	2.32E-04	1.38E-01	2.16E-04	1.19E-01	1.85E-04	7.19E-02	1.11E-04
	0.55	0.65	0.50	0.45	0.35	0.30	2.E-03	3.51E-02	4.02E-05	8.45E-02	9.55E-05	7.82E-02	8.79E-05	6.58E-02	7.23E-05	3.93E-02	4.25E-05
	0.55	0.65	0.50	0.45	0.35	0.30	2.E-03	1.96E-02	0.00E+00	4.62E-02	0.00E+00	4.23E-02	0.00E+00	3.47E-02	0.00E+00	2.04E-02	0.00E+00
	0.56	0.66	0.51	0.46	0.36	0.31	2.E-03	3.96E-03	0.00E+00	9.08E-03	0.00E+00	8.23E-03	0.00E+00	6.52E-03	0.00E+00	3.74E-03	0.00E+00
	0.56	0.66	0.51	0.46	0.36	0.31	2.E-03	0.00E+00	-2.74E-04	0.00E+00	-6.23E-04	0.00E+00	-5.62E-04	0.00E+00	-4.39E-04	0.00E+00	-2.50E-04
	0.56	0.66	0.51	0.46	0.36	0.31	2.E-03	2.94E-03	0.00E+00	6.75E-03	0.00E+00	6.12E-03	0.00E+00	4.85E-03	0.00E+00	2.78E-03	0.00E+00
1-5-22	1.18	1.28	1.13	1.08	0.98	0.93	2.E-03										
	1.09	1.19	1.04	0.99	0.89	0.84	2.E-03										
	0.90	1.00	0.85	0.80	0.70	0.65	2.E-03										
	0.76	0.86	0.71	0.66	0.56	0.51	2.E-03										
	0.61	0.71	0.56	0.51	0.41	0.36	2.E-03										
	0.56	0.66	0.51	0.46	0.36	0.31	2.E-03										
	0.60	0.70	0.55	0.50	0.40	0.35	2.E-03										

Sum of fluxes over 1/2 tidal cycle (m^3):

high 233-250m	low 233-250m	high 250-300m	low 250-300m	high 300-350m	low 300-350m	high 350-400m	low 350-400m	high 400-433m	low 400-433m
0.09	0.00	0.21	0.00	0.20	0.00	0.17	0.00	0.10	0.00

Sum of fluxes over 1/2 tidal cycle (m^3):

high 233-250m	low 233-250m	high 250-300m	low 250-300m	high 300-350m	low 300-350m	high 350-400m	low 350-400m	high 400-433m	low 400-433m
0.20	0.00	0.48	0.00	0.45	0.00	0.38	0.00	0.23	0.00

Average of flux at depth =11cm and depth = 22cm (m^3):

high 233-250m	low 233-250m	high 250-300m	low 250-300m	high 300-350m	low 300-350m	high 350-400m	low 350-400m	high 400-433m	low 400-433m
0.14	0.00	0.35	0.00	0.32	0.00	0.27	0.00	0.16	0.00

q' between 5 and 0 meters from the creekbank

233-250m q' (m^2/hr)	+	-	250-300m q' (m^2/hr)	+	-	300-350m q' (m^2/hr)	+	-	350-400m q' (m^2/hr)	+	-	400-433m q' (m^2/hr)	+	-
4.01E-05	6.82E-04	4.01E-05	3.54E-05	6.03E-04	3.54E-05	3.39E-05	5.76E-04	3.39E-05	3.08E-05	5.24E-04	3.08E-05	2.92E-05	4.97E-04	2.92E-05
4.82E-05	8.20E-04	4.82E-05	4.21E-05	7.15E-04	4.21E-05	4.00E-05	6.81E-04	4.00E-05	3.59E-05	6.11E-04	3.59E-05	3.39E-05	5.76E-04	3.39E-05
6.00E-05	1.02E-03	6.00E-05	5.09E-05	8.65E-04	5.09E-05	4.79E-05	8.14E-04	4.79E-05	4.18E-05	7.11E-04	4.18E-05	3.88E-05	6.60E-04	3.88E-05
2.35E-05	4.00E-04	2.35E-05	1.96E-05	3.33E-04	1.96E-05	1.83E-05	3.11E-04	1.83E-05	1.56E-05	2.66E-04	1.56E-05	1.43E-05	2.44E-04	1.43E-05
1.67E-05	2.85E-04	1.67E-05	1.34E-05	2.28E-04	1.34E-05	1.22E-05	2.08E-04	1.22E-05	9.97E-06	1.70E-04	9.97E-06	8.84E-06	1.51E-04	8.84E-06
1.56E-05	2.66E-04	1.56E-05	1.23E-05	2.09E-04	1.23E-05	1.11E-05	1.90E-04	1.11E-05	8.87E-06	1.51E-04	8.87E-06	7.74E-06	1.32E-04	7.74E-06
8.31E-05	1.41E-03	8.14E-05	6.22E-05	1.06E-03	6.09E-05	5.52E-05	9.38E-04	5.41E-05	4.12E-05	7.01E-04	4.05E-05	3.42E-05	5.82E-04	3.37E-05
2.44E-04	4.15E-03	2.37E-04	2.06E-04	3.50E-03	2.00E-04	1.93E-04	3.29E-03	1.88E-04	1.68E-04	2.86E-03	1.63E-04	1.55E-04	2.64E-03	1.51E-04
1.95E-04	3.32E-03	1.90E-04	1.63E-04	2.78E-03	1.59E-04	1.53E-04	2.60E-03	1.49E-04	1.32E-04	2.24E-03	1.28E-04	1.21E-04	2.06E-03	1.18E-04
1.15E-04	1.95E-03	1.12E-04	9.38E-05	1.60E-03	9.19E-05	8.69E-05	1.48E-03	8.52E-05	7.31E-05	1.24E-03	7.16E-05	6.62E-05	1.12E-03	6.49E-05
6.40E-05	1.09E-03	6.40E-05	5.13E-05	8.72E-04	5.13E-05	4.70E-05	8.00E-04	4.70E-05	3.86E-05	6.56E-04	3.86E-05	3.43E-05	5.83E-04	3.43E-05
1.29E-05	2.20E-04	1.29E-05	1.01E-05	1.72E-04	1.01E-05	9.12E-06	1.55E-04	9.12E-06	7.23E-06	1.23E-04	7.23E-06	6.28E-06	1.07E-04	6.28E-06
-1.18E-06	1.18E-06	1.50E-05	-9.13E-07	9.13E-07	1.15E-05	-8.24E-07	8.24E-07	1.04E-05	-6.44E-07	6.44E-07	8.14E-06	-5.54E-07	5.54E-07	7.01E-06
9.58E-06	1.64E-04	9.58E-06	7.47E-06	1.28E-04	7.47E-06	6.77E-06	1.16E-04	6.77E-06	5.36E-06	9.16E-05	5.36E-06	4.66E-06	7.96E-05	4.66E-06

Sum of fluxes over 1st-order segment: (for 1/2 tidal cycle)

(This is the sum of Q over each depth interval multiplied by 2 to account for both sides of the channel.)

high = 1.24 m^3
low = 0.00 m^3

Total flux over 1st-order segment: (for one full tidal cycle)

high = 2.48 m^3
low = 0.00 m^3

Table 10B: The volume range of groundwater flowing toward the 1st-order section of N. Glebe Creek, calculated using the overall average K. In this table, the upper and lower bounds of Q are calculated from the q' values which have been adjusted for differences in channel depth over the length of the channel. Negative values of Q are away from the tidal network channel. Uncertainties in q' were calculated using the methods described in Appendix C. The value of 'avg. K' is the geometric mean of all measured K-values at the Jug Bay study site.

piez. #	head wrt channel (m) @ 100m	hydraulic head with respect to the channel bottom 0-50 m	50-100 m	100-150 m	150-200 m	200-233 m	avg. K (m/hr)
2-0-19	1.60	1.25	1.45	1.55	1.55	1.40	1.E-01
	1.57	1.22	1.42	1.52	1.52	1.37	1.E-01
	1.37	1.02	1.22	1.32	1.32	1.17	1.E-01
	1.20	0.85	1.05	1.15	1.15	1.00	1.E-01
	1.07	0.72	0.92	1.02	1.02	0.87	1.E-01
	1.03	0.68	0.88	0.98	0.98	0.83	1.E-01
	1.11	0.76	0.96	1.06	1.06	0.91	1.E-01
2-5-19	1.59	1.24	1.44	1.54	1.54	1.39	1.E-01
	1.49	1.14	1.34	1.44	1.44	1.29	1.E-01
	1.38	1.03	1.23	1.33	1.33	1.18	1.E-01
	1.19	0.84	1.04	1.14	1.14	0.99	1.E-01
	1.08	0.73	0.93	1.03	1.03	0.88	1.E-01
	1.03	0.68	0.88	0.98	0.98	0.83	1.E-01
	1.11	0.76	0.96	1.06	1.06	0.91	1.E-01
2-0-39	1.56	1.21	1.41	1.51	1.51	1.36	4.E-02
	1.55	1.20	1.40	1.50	1.50	1.35	4.E-02
	1.42	1.07	1.27	1.37	1.37	1.22	4.E-02
	1.25	0.90	1.10	1.20	1.20	1.05	4.E-02
	1.09	0.74	0.94	1.04	1.04	0.89	4.E-02
	1.03	0.68	0.88	0.98	0.98	0.83	4.E-02
	1.07	0.72	0.92	1.02	1.02	0.87	4.E-02
2-5-39	1.30	0.95	1.15	1.25	1.25	1.10	4.E-02
	1.30	0.95	1.15	1.25	1.25	1.10	4.E-02
	1.32	0.97	1.17	1.27	1.27	1.12	4.E-02
	1.27	0.92	1.12	1.22	1.22	1.07	4.E-02
	1.15	0.80	1.00	1.10	1.10	0.95	4.E-02
	1.11	0.76	0.96	1.06	1.06	0.91	4.E-02
	1.12	0.77	0.97	1.07	1.07	0.92	4.E-02

Q = q' x channel length

high 0-50m Q (m^3/hr)	low 0-50m Q (m^3/hr)	high 50-100m Q (m^3/hr)	low 50-100m Q (m^3/hr)	high 100-150m Q (m^3/hr)	low 100-150m Q (m^3/hr)	high 150-200m Q (m^3/hr)	low 150-200m Q (m^3/hr)	high 200-233m Q (m^3/hr)	low 200-233m Q (m^3/hr)
0.00E+00	-6.01E-02	0.00E+00	-6.97E-02	0.00E+00	-7.45E-02	0.00E+00	-7.45E-02	0.00E+00	-4.44E-02
0.00E+00	-1.44E-01	0.00E+00	-1.69E-01	0.00E+00	-1.81E-01	0.00E+00	-1.81E-01	0.00E+00	-1.07E-01
7.62E-02	0.00E+00	9.11E-02	0.00E+00	9.85E-02	0.00E+00	9.85E-02	0.00E+00	5.77E-02	0.00E+00
0.00E+00	-4.17E-02	0.00E+00	-5.15E-02	0.00E+00	-5.64E-02	0.00E+00	-5.64E-02	0.00E+00	-3.23E-02
5.36E-02	0.00E+00	6.84E-02	0.00E+00	7.59E-02	0.00E+00	7.59E-02	0.00E+00	4.27E-02	0.00E+00
3.29E-02	0.00E+00	4.25E-02	0.00E+00	4.74E-02	0.00E+00	4.74E-02	0.00E+00	2.65E-02	0.00E+00
3.05E-02	0.00E+00	3.86E-02	0.00E+00	4.26E-02	0.00E+00	4.26E-02	0.00E+00	2.41E-02	0.00E+00

Sum of fluxes over 1/2 tidal cycle (m^3):

high	low	high	low	high	low	high	low	high	low
0.19	-0.25	0.24	-0.29	0.26	-0.31	0.26	-0.31	0.15	-0.18

0.00E+00	-1.40E-01	0.00E+00	-1.66E-01	0.00E+00	-1.79E-01	0.00E+00	-1.79E-01	0.00E+00	-1.05E-01
0.00E+00	-1.28E-01	0.00E+00	-1.52E-01	0.00E+00	-1.64E-01	0.00E+00	-1.64E-01	0.00E+00	-9.64E-02
0.00E+00	-5.63E-02	0.00E+00	-6.73E-02	0.00E+00	-7.28E-02	0.00E+00	-7.28E-02	0.00E+00	-4.26E-02
5.09E-02	0.00E+00	6.21E-02	0.00E+00	6.77E-02	0.00E+00	6.77E-02	0.00E+00	3.91E-02	0.00E+00
9.86E-02	7.07E-03	1.24E-01	8.86E-03	1.37E-01	9.75E-03	1.37E-01	9.75E-03	7.77E-02	5.55E-03
1.05E-01	9.16E-03	1.35E-01	1.17E-02	1.49E-01	1.29E-02	1.49E-01	1.29E-02	8.40E-02	7.28E-03
7.73E-02	3.31E-03	9.81E-02	4.16E-03	1.08E-01	4.59E-03	1.08E-01	4.59E-03	6.13E-02	2.61E-03

Sum of fluxes over 1/2 tidal cycle (m^3):

high	low	high	low	high	low	high	low	high	low
0.33	-0.31	0.42	-0.36	0.46	-0.39	0.46	-0.39	0.26	-0.23

Average of flux at depth =19cm and depth = 39cm (m^3):

high	low	high	low	high	low	high	low	high	low
0.26	-0.28	0.33	-0.33	0.36	-0.35	0.36	-0.35	0.21	-0.21

q' between 5 and 0 meters from the creekbank

0-50m q' (m^2/hr)	+	-	50-100m q' (m^2/hr)	+	-	100-150m q' (m^2/hr)	+	-	150-200m q' (m^2/hr)	+	-	200-233m q' (m^2/hr)	+	-
-2.47E-04	2.47E-04	9.54E-04	-2.87E-04	2.87E-04	1.11E-03	-3.07E-04	3.07E-04	1.18E-03	-3.07E-04	3.07E-04	1.18E-03	-2.77E-04	2.77E-04	1.07E-03
-1.91E-03	1.91E-03	9.83E-04	-2.23E-03	2.23E-03	1.15E-03	-2.39E-03	2.39E-03	1.23E-03	-2.39E-03	2.39E-03	1.23E-03	-2.15E-03	2.15E-03	1.11E-03
2.18E-04	1.31E-03	2.18E-04	2.60E-04	1.56E-03	2.60E-04	2.81E-04	1.69E-03	2.81E-04	2.81E-04	1.69E-03	2.81E-04	2.49E-04	1.50E-03	2.49E-04
-1.82E-04	1.82E-04	6.51E-04	-2.25E-04	2.25E-04	8.04E-04	-2.47E-04	2.47E-04	8.81E-04	-2.47E-04	2.47E-04	8.81E-04	-2.14E-04	2.14E-04	7.66E-04
1.53E-04	9.19E-04	1.53E-04	1.95E-04	1.17E-03	1.95E-04	2.17E-04	1.30E-03	2.17E-04	2.17E-04	1.30E-03	2.17E-04	1.85E-04	1.11E-03	1.85E-04
6.12E-05	5.96E-04	6.12E-05	7.92E-05	7.72E-04	7.92E-05	8.82E-05	8.60E-04	8.82E-05	8.82E-05	8.60E-04	8.82E-05	7.47E-05	7.28E-04	7.47E-05
2.20E-05	5.88E-04	2.20E-05	2.79E-05	7.43E-04	2.79E-05	3.08E-05	8.21E-04	3.08E-05	3.08E-05	8.21E-04	3.08E-05	2.64E-05	7.05E-04	2.64E-05
-2.29E-03	2.29E-03	5.12E-04	-2.71E-03	2.71E-03	6.04E-04	-2.92E-03	2.92E-03	6.50E-04	-2.92E-03	2.92E-03	6.50E-04	-2.61E-03	2.61E-03	5.81E-04
-2.08E-03	2.08E-03	4.86E-04	-2.47E-03	2.47E-03	5.74E-04	-2.66E-03	2.66E-03	6.18E-04	-2.66E-03	2.66E-03	6.18E-04	-2.37E-03	2.37E-03	5.52E-04
-7.78E-04	7.78E-04	3.49E-04	-9.31E-04	9.31E-04	4.16E-04	-1.01E-03	1.01E-03	4.50E-04	-1.01E-03	1.01E-03	4.50E-04	-8.92E-04	8.92E-04	3.99E-04
1.92E-04	8.26E-04	1.92E-04	2.34E-04	1.01E-03	2.34E-04	2.55E-04	1.10E-03	2.55E-04	2.55E-04	1.10E-03	2.55E-04	2.24E-04	9.62E-04	2.24E-04
3.88E-04	1.58E-03	2.46E-04	4.89E-04	1.99E-03	3.11E-04	5.39E-04	2.20E-03	3.44E-04	5.39E-04	2.20E-03	3.44E-04	4.63E-04	1.89E-03	2.95E-04
4.15E-04	1.69E-03	2.32E-04	5.31E-04	2.16E-03	2.97E-04	5.88E-04	2.40E-03	3.30E-04	5.88E-04	2.40E-03	3.30E-04	5.02E-04	2.04E-03	2.81E-04
3.03E-04	1.24E-03	2.37E-04	3.84E-04	1.58E-03	3.01E-04	4.25E-04	1.74E-03	3.33E-04	4.25E-04	1.74E-03	3.33E-04	3.64E-04	1.49E-03	2.85E-04

Sum of fluxes over 2nd-order segment: (for 1/2 tidal cycle)

(This is the sum of Q over each depth interval multiplied by 2 to account for both sides of the channel.)

high = 1.52 m^3

low = -1.52 m^3

Total flux over 2nd-order segment: (for one full tidal cycle)

high = 3.04 m^3

low = -3.04 m^3

Table 10C: The volume range of groundwater flowing toward the 2nd-order section of N. Glebe Creek, calculated using specific K-values. In this table, the upper and lower bounds of Q are calculated from the q' values which have been adjusted for differences in channel depth over the length of the channel. Negative values of Q are away from the tidal network channel. Uncertainties in q' were calculated using the methods described in Appendix C. 'Avg. K' values are the average of the 2 GM K values at the piezometers between which flux is being measured.

piez. #	head wrt channel (m) @ 100m	hydraulic head with respect to the channel bottom 0-50 m	50-100 m	100-150 m	150-200 m	200-233 m	avg. K (m/hr)
2-0-19	1.60	1.25	1.45	1.55	1.55	1.40	2.E-03
	1.57	1.22	1.42	1.52	1.52	1.37	2.E-03
	1.37	1.02	1.22	1.32	1.32	1.17	2.E-03
	1.20	0.85	1.05	1.15	1.15	1.00	2.E-03
	1.07	0.72	0.92	1.02	1.02	0.87	2.E-03
	1.03	0.68	0.88	0.98	0.98	0.83	2.E-03
	1.11	0.76	0.96	1.06	1.06	0.91	2.E-03
2-5-19	1.59	1.24	1.44	1.54	1.54	1.39	2.E-03
	1.49	1.14	1.34	1.44	1.44	1.29	2.E-03
	1.38	1.03	1.23	1.33	1.33	1.18	2.E-03
	1.19	0.84	1.04	1.14	1.14	0.99	2.E-03
	1.08	0.73	0.93	1.03	1.03	0.88	2.E-03
	1.03	0.68	0.88	0.98	0.98	0.83	2.E-03
	1.11	0.76	0.96	1.06	1.06	0.91	2.E-03
2-0-39	1.56	1.21	1.41	1.51	1.51	1.36	2.E-03
	1.55	1.20	1.40	1.50	1.50	1.35	2.E-03
	1.42	1.07	1.27	1.37	1.37	1.22	2.E-03
	1.25	0.90	1.10	1.20	1.20	1.05	2.E-03
	1.09	0.74	0.94	1.04	1.04	0.89	2.E-03
	1.03	0.68	0.88	0.98	0.98	0.83	2.E-03
	1.07	0.72	0.92	1.02	1.02	0.87	2.E-03
2-5-39	1.30	0.95	1.15	1.25	1.25	1.10	2.E-03
	1.30	0.95	1.15	1.25	1.25	1.10	2.E-03
	1.32	0.97	1.17	1.27	1.27	1.12	2.E-03
	1.27	0.92	1.12	1.22	1.22	1.07	2.E-03
	1.15	0.80	1.00	1.10	1.10	0.95	2.E-03
	1.11	0.76	0.96	1.06	1.06	0.91	2.E-03
	1.12	0.77	0.97	1.07	1.07	0.92	2.E-03

Q = q' x channel length

high 0-50m Q (m^3/hr)	low 0-50m Q (m^3/hr)	high 50-100m Q (m^3/hr)	low 50-100m Q (m^3/hr)	high 100-150m Q (m^3/hr)	low 100-150m Q (m^3/hr)	high 150-200m Q (m^3/hr)	low 150-200m Q (m^3/hr)	high 200-233m Q (m^3/hr)	low 200-233m Q (m^3/hr)
0.00E+00	-1.68E-03	0.00E+00	-1.94E-03	0.00E+00	-2.08E-03	0.00E+00	-2.08E-03	0.00E+00	-1.24E-03
0.00E+00	-4.18E-03	0.00E+00	-4.89E-03	0.00E+00	-5.24E-03	0.00E+00	-5.24E-03	0.00E+00	-3.11E-03
4.10E-03	0.00E+00	4.89E-03	0.00E+00	5.29E-03	0.00E+00	5.29E-03	0.00E+00	3.10E-03	0.00E+00
0.00E+00	-1.16E-03	0.00E+00	-1.43E-03	0.00E+00	-1.57E-03	0.00E+00	-1.57E-03	0.00E+00	-8.99E-04
2.88E-03	0.00E+00	3.68E-03	0.00E+00	4.08E-03	0.00E+00	4.08E-03	0.00E+00	2.30E-03	0.00E+00
1.35E-03	0.00E+00	1.75E-03	0.00E+00	1.95E-03	0.00E+00	1.95E-03	0.00E+00	1.09E-03	0.00E+00
9.57E-04	0.00E+00	1.21E-03	0.00E+00	1.34E-03	0.00E+00	1.34E-03	0.00E+00	7.57E-04	0.00E+00

Sum of fluxes over 1/2 tidal cycle (m^3):

high	low	high	low	high	low	high	low	high	low
0.01	-0.01	0.01	-0.01	0.01	-0.01	0.01	-0.01	0.01	-0.01

0.00E+00	-1.14E-02	0.00E+00	-1.35E-02	0.00E+00	-1.45E-02	0.00E+00	-1.45E-02	0.00E+00	-8.55E-03
0.00E+00	-1.04E-02	0.00E+00	-1.23E-02	0.00E+00	-1.33E-02	0.00E+00	-1.33E-02	0.00E+00	-7.80E-03
0.00E+00	-4.15E-03	0.00E+00	-4.96E-03	0.00E+00	-5.37E-03	0.00E+00	-5.37E-03	0.00E+00	-3.14E-03
8.71E-03	0.00E+00	1.06E-02	0.00E+00	1.16E-02	0.00E+00	1.16E-02	0.00E+00	6.69E-03	0.00E+00
1.75E-02	0.00E+00	2.20E-02	0.00E+00	2.43E-02	0.00E+00	2.43E-02	0.00E+00	1.38E-02	0.00E+00
1.87E-02	0.00E+00	2.39E-02	0.00E+00	2.65E-02	0.00E+00	2.65E-02	0.00E+00	1.49E-02	0.00E+00
1.37E-02	0.00E+00	1.73E-02	0.00E+00	1.91E-02	0.00E+00	1.91E-02	0.00E+00	1.08E-02	0.00E+00

Sum of fluxes over 1/2 tidal cycle (m^3):

high	low	high	low	high	low	high	low	high	low
0.06	-0.03	0.07	-0.03	0.08	-0.03	0.08	-0.03	0.05	-0.02

Average of flux at depth =19cm and depth = 39cm (m^3):

high	low	high	low	high	low	high	low	high	low
0.03	-0.02	0.04	-0.02	0.05	-0.02	0.05	-0.02	0.03	-0.01

q' between 5 and 0 meters from the creekbank

0-50m q' (m^2/hr)	+	-	50-100m q' (m^2/hr)	+	-	100-150m q' (m^2/hr)	+	-	150-200m q' (m^2/hr)	+	-	200-233m q' (m^2/hr)	+	-
-4.94E-06	4.94E-06	2.86E-05	-5.73E-06	5.73E-06	3.32E-05	-6.13E-06	6.13E-06	3.55E-05	-6.13E-06	6.13E-06	3.55E-05	-5.54E-06	5.54E-06	3.20E-05
-3.81E-05	3.81E-05	4.55E-05	-4.46E-05	4.46E-05	5.32E-05	-4.78E-05	4.78E-05	5.70E-05	-4.78E-05	4.78E-05	5.70E-05	-4.30E-05	4.30E-05	5.12E-05
4.35E-06	7.76E-05	4.35E-06	5.20E-06	9.27E-05	5.20E-06	5.62E-06	1.00E-04	5.62E-06	5.62E-06	1.00E-04	5.62E-06	4.99E-06	8.89E-05	4.99E-06
-3.64E-06	3.64E-06	1.95E-05	-4.50E-06	4.50E-06	2.41E-05	-4.93E-06	4.93E-06	2.64E-05	-4.93E-06	4.93E-06	2.64E-05	-4.29E-06	4.29E-06	2.30E-05
3.06E-06	5.45E-05	3.06E-06	3.91E-06	6.96E-05	3.91E-06	4.33E-06	7.72E-05	4.33E-06	4.33E-06	7.72E-05	4.33E-06	3.70E-06	6.59E-05	3.70E-06
1.22E-06	2.59E-05	1.22E-06	1.58E-06	3.35E-05	1.58E-06	1.76E-06	3.73E-05	1.76E-06	1.76E-06	3.73E-05	1.76E-06	1.49E-06	3.16E-05	1.49E-06
4.41E-07	1.87E-05	4.41E-07	5.57E-07	2.36E-05	5.57E-07	6.16E-07	2.61E-05	6.16E-07	6.16E-07	2.61E-05	6.16E-07	5.28E-07	2.24E-05	5.28E-07
-1.14E-04	1.14E-04	1.13E-04	-1.36E-04	1.36E-04	1.34E-04	-1.46E-04	1.46E-04	1.44E-04	-1.46E-04	1.46E-04	1.44E-04	-1.30E-04	1.30E-04	1.29E-04
-1.04E-04	1.04E-04	1.03E-04	-1.23E-04	1.23E-04	1.23E-04	-1.33E-04	1.33E-04	1.32E-04	-1.33E-04	1.33E-04	1.32E-04	-1.19E-04	1.19E-04	1.18E-04
-3.89E-05	3.89E-05	4.40E-05	-4.65E-05	4.65E-05	5.27E-05	-5.03E-05	5.03E-05	5.70E-05	-5.03E-05	5.03E-05	5.70E-05	-4.46E-05	4.46E-05	5.05E-05
9.60E-06	1.65E-04	9.60E-06	1.17E-05	2.01E-04	1.17E-05	1.28E-05	2.19E-04	1.28E-05	1.28E-05	2.19E-04	1.28E-05	1.12E-05	1.92E-04	1.12E-05
1.94E-05	3.30E-04	1.94E-05	2.44E-05	4.16E-04	2.44E-05	2.69E-05	4.59E-04	2.69E-05	2.69E-05	4.59E-04	2.69E-05	2.32E-05	3.94E-04	2.32E-05
2.08E-05	3.53E-04	2.08E-05	2.65E-05	4.51E-04	2.65E-05	2.94E-05	5.00E-04	2.94E-05	2.94E-05	5.00E-04	2.94E-05	2.51E-05	4.27E-04	2.51E-05
1.51E-05	2.58E-04	1.51E-05	1.92E-05	3.27E-04	1.92E-05	2.12E-05	3.62E-04	2.12E-05	2.12E-05	3.62E-04	2.12E-05	1.82E-05	3.10E-04	1.82E-05

Sum of fluxes over 2nd-order segment: (for 1/2 tidal cycle)

(This is the sum of Q over each depth interval multiplied by 2 to account for both sides of the channel.)

high = 0.20 m^3

low = -0.09 m^3

Total flux over 2nd-order segment: (for one full tidal cycle)

high = 0.40 m^3

low = -0.18 m^3

Table 10D: The volume range of groundwater flowing toward the 2nd-order section of N. Glebe Creek, calculated using the overall average K. In this table, the upper and lower bounds of Q are calculated from the q' values which have been adjusted for differences in channel depth over the length of the channel. Negative values of Q are away from the tidal network channel. Uncertainties in q' were calculated using the methods described in Appendix C. The value of 'avg. K' is the geometric mean of all measured K-values at the Jug Bay study site.

side for each stream segment. These results were then summed for the entire length of channel, multiplied by 2 once to account for groundwater flux on the other side of the channel, and multiplied by 2 again to calculate the total volume of groundwater fluxing horizontally toward (or away from) the channel over a full tidal cycle. The same calculation techniques were used for Tables10B & 10D but, instead of using specific average values of K for each location, the average of all K measurements made at the site was used.

Both high and low estimates are given in Tables 10A-D. High estimates are calculated from the upper bound values of q' and low estimates are calculated from the lower bound values of q'. Total flux over a tidal cycle along the 1st-order part of North Glebe Creek was determined to be between 2.16 and 20.12 m^3 when specific values of K were used and between 0.00 and 2.48 m^3 when the overall K was used. Over the 2nd-order section of channel, the total flux over a tidal cycle was determined to be -3.04 to 3.04 m^3 when specific values of K were used and between -0.18 and 0.40 m^3 when the overall K was used. So, groundwater flux over the entire length of N. Glebe Creek over one full tidal cycle was calculated to be either -0.88 to 23.16 m^3 (using specific values of K) or -0.18 to 2.88 m^3 (using the overall average value of K).

Large ranges of uncertainty in Q are a result of large ranges of uncertainty in K-values. When the overall value of K is used to calculate Q, the calculated flux range falls within the range of values calculated when specific values of K were used. However, the range median is approximately one order-of-magnitude less than the range median calculated using specific K-values.

DISCUSSION

Spatial distribution of K

Although K was not found to decrease with increasing distance from the main tidal channel, the average K at 0 meters from the creekbank was significantly higher than the average K at both 5 and 15 meters from the creekbank. This fact counters observations by Schultz & Ruppel (2002) that fine particles dropping out of suspension around channels of low gradient produce a 'clogging layer', limiting flux between the channel and near-channel marsh sediments.

Unexpectedly, K did not seem to increase with depth below the ground surface. This was due to the overall heterogeneity in the marsh sediments. Sediment cores indicated that well-packed fine sediment layers and more friable layers with pristine root matter can be directly adjacent to each other and mixed in any order in a marsh sediment depth profile.

Changes in creekbank gradient

Creekbank gradient does seem to increase with increasing distance from the main channel and some data indicate that channel width-to-depth ratio (F), which is inversely related to creekbank gradient, correlates well with K. (See Figure 38.) When K at 5 meters from the network channel creekbank is plotted against w/d_{max}, $R^2 = 0.8569$. When the same K-values are plotted against w/d_{center}, the R^2 drops only slightly to 0.8329. At zero meters from the creekbank, both K and F data were only collected at two locations, so determination of a relationship between these two parameters at that distance could not be made. However, when K- and F values at 15 and 25 meters from the creekbank were

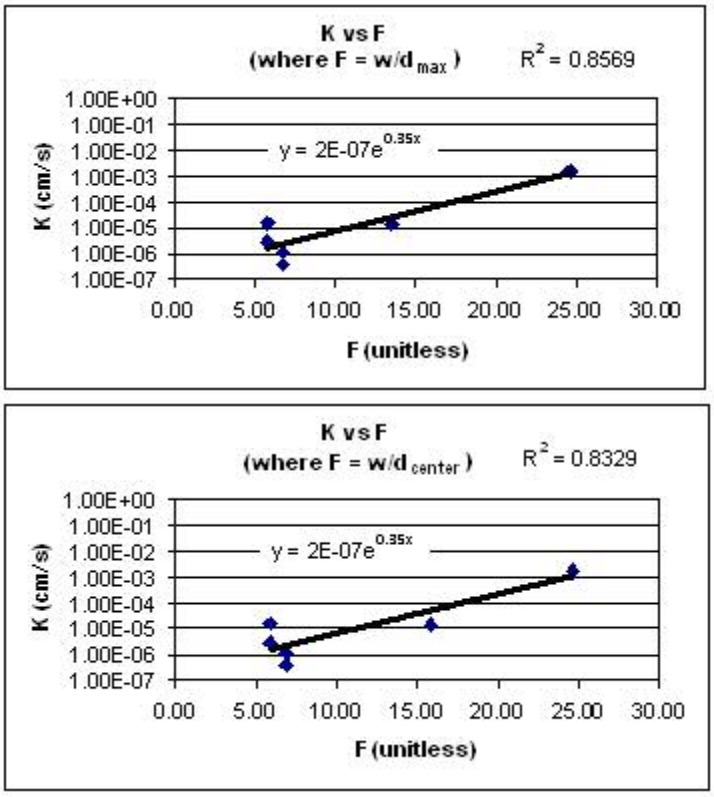

Figure 38: Correlation between K and F. A strong correlation was found between hydraulic conductivity (K) measurements made 5 meters from three different network channels and the width-depth-ratio (F) of the adjacent channel. The graph on top shows K vs. F calculated using the maximum channel depth measured along the channel cross-section. The graph on the bottom shows K vs. F calculated using the depth at the center of the channel cross-section.

compared, the correlation was very poor (R^2 = 0.3312 to 0.3104, respectively). These facts suggest that a strong relationship between K and F exists up to 10(+/-5) meters from the tidal network channel creekbank.

In addition, plotting the 0- and 5-meter K vs. F regression lines on the same graph reveals that K at both of these distances from the network channel creekbank increases with increasing F. (See Figure 39.) Because F is inversely related to gradient, and because data from this study demonstrate that gradient does tend to increase with increasing distance up the network channel from the main tidal channel, these K vs. F data indirectly support Hypothesis #1.

Also from Figure 39, we see that the largest ΔK from 0 to 5 meters from the network channel creekbank is at F = 0 (the stream-head, where both width and depth go

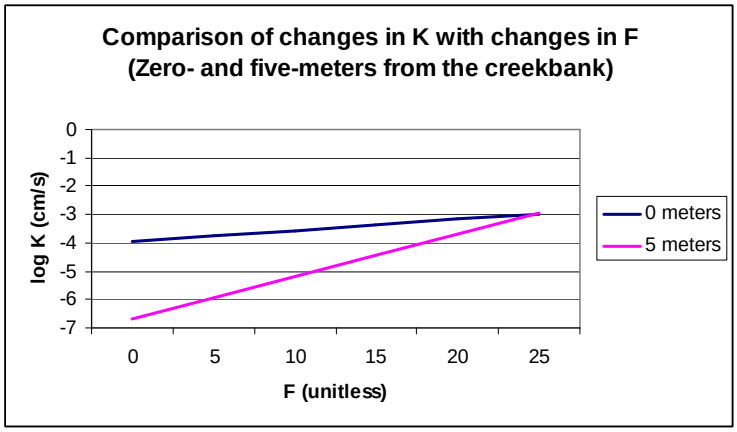

Figure 39: Changes in K and F at zero and five meters from the network channel creekbank. On this graph, the best-fit lines for K vs. F data collected at 0 and 5 meters from the network channel creekbank are plotted. These data were collected along both North Glebe and Observatory Creeks. The equation for the 0-meter line is: log K = 0.038F – 3.9. The equation for the 5-meter line is: log K = 0.15F – 6.7.

to zero). As F increases (approaching the main tidal channel), the values of K at 0 and 5 meters from the creekbank approach each other and converge at F = 25. (See Figure 40.) No values of F > 25 were used in this data-set, even though higher values were measured, because there were no corresponding K-values. However, if the regression lines are extrapolated beyond F = 25, K at 5 meters from the creekbank becomes higher than at 0 meters from the creekbank, and the ΔK between these two distances increases with increasing F.

Spatial trends in groundwater flux magnitude

Horizontal groundwater flux magnitude was not observed to decrease with increasing distance from the main channel. It was hypothesized that this would be the case because the K measured in sediments adjacent to the tidal network channel would decrease with increasing distance from the main tidal channel. As mentioned previously, this trend in K-distributions was not observed.

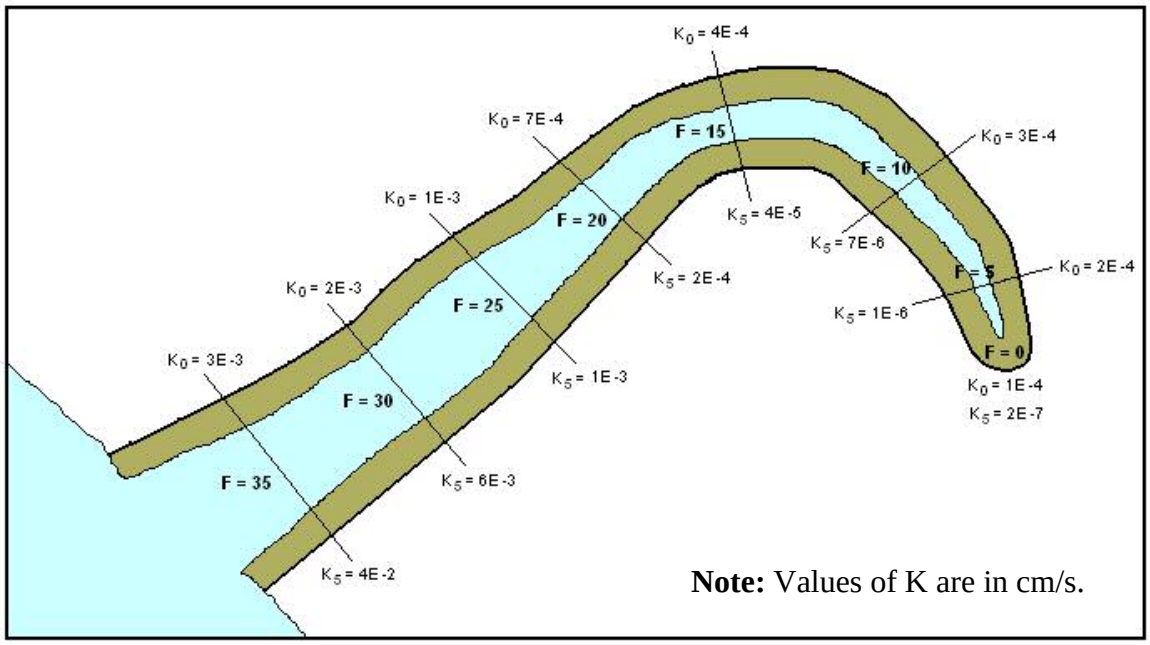

Figure 40: Hypothetical tidal network channel showing results of K vs. F trend-lines. Data collected in this study supported the hypothesis that network channel creekbank gradients would increase with increasing distance from the main tidal channel. F is inversely related to gradient, so F is at a minimum at the furthest distance from the main channel; the head of the network channel. Values of K shown in this cartoon are calculated from the regression lines shown in Figure 39. K_0 is hydraulic conductivity at zero meters from the creekbank and K_5 is hydraulic conductivity at 5 meters from the creekbank. The olive-colored area around the channel shows the zone within 5 meters of the creekbank (NOT DRAWN TO SCALE).

However, at the 2nd-order channel location at a depth of 39 cm, the magnitude of horizontal flux from 5 to 0 meters from the creekbank was significantly higher than the magnitude of flux from 15 to 5 meters from the creekbank. At the first-order channel location, the magnitude of flux from 5 to 0 meters and 25 to 15 meters were both significantly higher than the magnitude of flux from 15 to 5 meters from the creekbank. This suggests that horizontal groundwater flux magnitude does decrease with increasing distance from the network channel, but this trend does not hold beyond 15 meters from the creekbank. In contrast to studies by Nuttle (1986), Harvey et al. (1987) and Nuttle (1988), significant horizontal fluxes, as high as 1×10^{-3} m^2/hr, were observed beyond 15 meters from the creekbank. These trends in changing flux magnitude with distance from

the tidal network channel correspond well with trends in K-distribution at the first-order channel location, but not as well at the 2nd-order location. (See Figure 41.)

Several flux magnitude vs. depth trends were observed adjacent to the 1st-order channel location. The average flux magnitude at a depth of 11 cm was significantly greater than the average flux magnitude at 22 cm below the ground-surface. The average flux magnitude between all piezometer locations was significantly greater at 11 cm deep than at 22 cm deep. In addition, the range of flux magnitudes at 11 cm deep was significantly higher than the range of flux magnitudes at 22 cm deep. Unlike the previously discussed trend, (flux magnitude decreasing with increasing distance from the network channel),

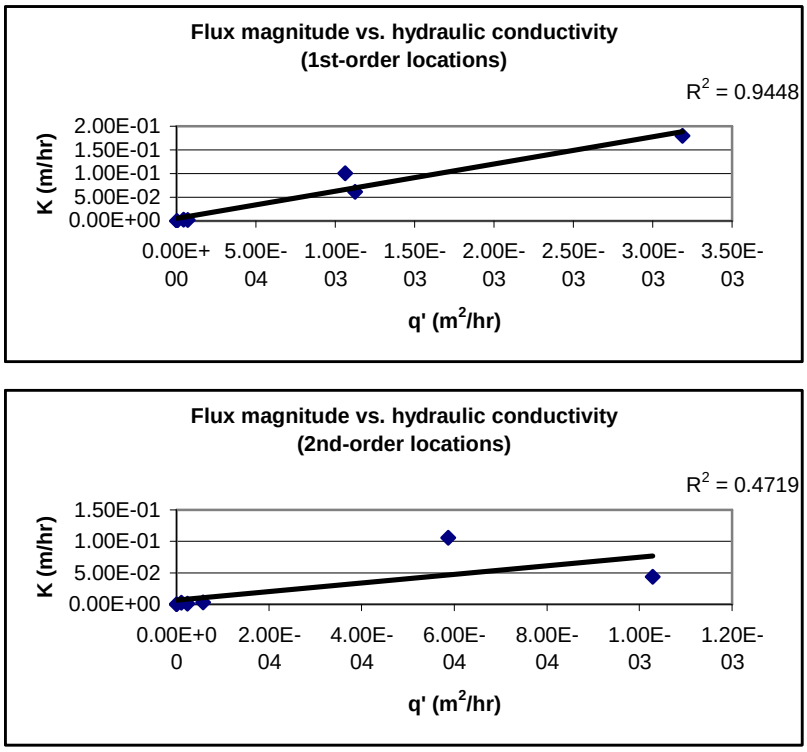

Figure 41: The correlation between flux magnitude (q') and hydraulic conductivity (K). The average flux magnitude between successive piezometer locations was plotted against the average of the K-values measured at these same locations. It was found that K was a strong predictor of q' at the first-order channel location but not at the 2nd-order channel location. This suggests that some other factor, perhaps top-loading pressure from tidal flooding, is more dominant at the 2nd-order channel location.

this apparent decrease in q’ with depth below the ground surface is not directly related to changes in K.

CONCLUSIONS

One consequence of this decreasing q' with increasing depth could be that most of the groundwater that drains into the first-order channel is from near the ground surface and is newly-infiltrated tidal water. Newer water may have lower concentrations of constituents such as nutrients and heavy metals that can become concentrated in tidal marsh groundwater. Also, near the surface is where live plant roots are found. These plant roots remove nutrients from the newly infiltrated tidal water and use them for sustenance. This finding suggests that the higher the density of first-order network channels in a tidal marsh, the better that marsh will be at filtering tidal waters. Even though the 2nd-order stretch of channel on North Glebe Creek was longer and deeper on average (0.44 m deep vs. 0.20 m deep) than the 1st-order stretch, the total amount of groundwater entering the 1st-order stretch over a tidal cycle was considerably higher than the total amount of groundwater entering (or possibly leaving) the 2nd-order stretch. This could be due to greater top-loading effects closer to the main tidal channel. Further research should be conducted to determine the accuracy of this conclusion.

Overall, flux magnitudes were more predictable around the 1st-order network channel than around the 2nd-order network channel. q' was observed to decrease with increasing distance (up to 15 meters) from the network channel creekbank at both locations. However, at the 1st-order location, q' corresponded very strongly with measured average K-values and decreased with increasing depth below the ground surface.

Observed high-K zones directly adjacent to the network channel creekbank are likely causes for higher groundwater flux magnitudes in this region. But, sediment K-

values showed a lack of predictability with depth below the ground surface or distance from the main tidal channel, making use of these parameters for estimating groundwater flux unreliable.

Because q' correlated well with K at the 1st-order channel location, use of location-specific K-values when calculating Q distal from the main tidal channel would be indicated. Conversely, use of the site-general K-value to calculate Q resulted in a less than 1 m^3 difference in the calculated median volumetric flux to the 2nd-order section of channel over one full tidal cycle, suggesting that this method could be fairly reliably employed when estimating flux proximal to the main tidal channel.

In addition, a strong correlation between F and K data collected within approximately 10 meters of two separate tidal network channels demonstrates that network channel geomorphic characteristics could, potentially, be used to make estimations of groundwater flux habits around these channels. Work done by Schumm (1960 and subsequent) on alluvial channel forms and their relation to the silt-clay fraction within the channel-bounding sediments is, at least partially, applicable to tidal network channels and may be key in the search for these relationships.

Appendix A: Uncertainty calculations - Table 3

Core segment **lengths** (L) were measured to the nearest ¼ cm, so the measurements are precise to within 0.13 cm. The uncertainty in the core **radius** (r) is a function of the design of the peat borer. Inspection of this instrument indicates that the diameter is 4.0 (+/-0.2) cm, therefore, the radius is 2.0 (+/-0.1) cm. Core segment **weights** were measured to the nearest 0.1 g, so these values are precise to within 0.1 g.

To calculate volume, the radius must be square, so the uncertainty in the **radius^2** = $nA^{(n-1)}E_A$ where n is the power (2), A is the radius and E_A is the uncertainty in the radius (Taylor, 1997). So, the uncertainty in $r^2 = 2*2^{(1)}*0.1 = 0.4$ cm. **Volume** = $(\pi/2)*r^2*L$, so the uncertainty in the volume is $(\pi/2)*\text{sqrt}[(E_AB)^2 + (E_BA)^2]$ where B is the length of the core segment and E_B is the uncertainty in the length of the core segment. Therefore, the uncertainty in the volume is $(\pi/2)*\text{sqrt}[(0.4*L)^2 + (0.13*r^2)^2]$.

Bulk density (P_b) = dry wt / volume, so the uncertainty in P_b is $(1/D^2)*\text{sqrt}[(E_CD)^2+(E_DC)^2]$ where C is the dry weight and D is the volume. So, the uncertainty in P_b = $(1/\text{volume}^2)*\text{sqrt}[(0.1*\text{volume})^2 + (\text{uncertainty in volume}*\text{dry wt})^2]$. In each case, the uncertainty in P_b is approximately 10%. So, since **porosity** = $[1 - (P_b/2.65)]*100$, the uncertainty in porosity was estimated to be 10%.

The **percent organic matter** (%OM) for each segment of core OB100 was calculated using the formula:

$$\%OM = [(W_B - W_A)/W_B]*100$$

where W_B is the weight before combustion and W_A is the weight after combustion. The uncertainty in the value $W_B - W_A$ is $\text{sqrt}[0.1^2 + 0.1^2] = 0.1414$, so the uncertainty in the %OM calculation is $\{(1/W_B^2)*\text{sqrt}[(0.1414*W_B)^2 + (0.1*(W_B-W_A))^2]\}*100$. Results fall in the range of +/-0.6 to 1.5%, but 3 separate portions from segment 50-60 of core OB100 were analyzed for %OM and the reproducibility error (1σ) was only +/-0.1%.

Appendix B: Methods for converting hydraulic head with respect to elevation at the Railroad Bed Monitoring Station to hydraulic head with respect to the bottom of the channel

The following table shows the conversion from hydraulic head measured with respect to the elevation at the Railroad Bed Monitoring Station to hydraulic head measured with respect to the bottom of the adjacent network channel. The deepest part of the channel adjacent to each piezometer line is used. At the first-order channel location, the channel is 33 cm deep and at the second-order channel location the channel is 58 cm deep. h_T is the hydraulic head measured with respect to the monitoring station and surface elevation is the elevation of the ground at each piezometer location, also measured with respect to the monitoring station. e_{ch} is the elevation at the bottom of the channel with respect to the monitoring station and was calculated by subtracting the channel depth from the ground surface elevation at the location of the piezometer 0 meters from the creekbank. Hydraulic head measured with respect to the channel bottom (h_T wrt ch) is then calculated by subtracting the elevation of the channel bottom from the original head measurement. The σ-values associated with these measurements are the uncertainty in the elevation estimation (from Table 1 in the Methods section) plus a measurement error of +/- 0.005 m, which includes the uncertainty in the measurement of the channel depth and the uncertainty in the head measurement.

Appendix B: Methods for converting hydraulic head with respect to elevation at the Railroad Bed Monitoring Station to hydraulic head with respect to the bottom of the channel

Calculations of hydraulic head with respect to the elevation at the bottom of the adjacent channel:

Location	time	h_T (m)	surf. elev. (e_s) (m)	$e_{ch} = e_s$@0 - ch. Depth	h_T wrt ch = $h_T - e_{ch}$	σ
1-0-11	9:01	1.84	1.02	0.69	1.15	0.04
1-0-11	10:05	1.72	1.02	0.69	1.03	0.04
1-0-11	11:21	1.51	1.02	0.69	0.82	0.04
1-0-11	12:03	1.45	1.02	0.69	0.76	0.04
1-0-11	13:20	1.30	1.02	0.69	0.61	0.04
1-0-11	14:25	1.25	1.02	0.69	0.56	0.04
1-0-11	15:19	1.01	1.02	0.69	0.32	0.04
1-5-11	9:05	1.92	1.12	0.69	1.23	0.04
1-5-11	10:11	1.82	1.12	0.69	1.13	0.04
1-5-11	11:15	1.66	1.12	0.69	0.97	0.04
1-5-11	12:08	1.52	1.12	0.69	0.83	0.04
1-5-11	13:16	1.36	1.12	0.69	0.67	0.04
1-5-11	14:28	1.31	1.12	0.69	0.62	0.04
1-5-11	15:14	1.36	1.12	0.69	0.67	0.04
1-15-11	9:09	1.85	1.17	0.69	1.16	0.03
1-15-11	10:15	1.70	1.17	0.69	1.01	0.03
1-15-11	11:10	1.55	1.17	0.69	0.86	0.03
1-15-11	12:12	1.22	1.17	0.69	0.53	0.03
1-15-11	13:11	1.25	1.17	0.69	0.56	0.03
1-15-11	14:31	1.22	1.17	0.69	0.53	0.03
1-15-11	15:09	1.16	1.17	0.69	0.47	0.03
1-25-11	9:11	1.95	1.48	0.69	1.26	0.01
1-25-11	10:20	1.82	1.48	0.69	1.13	0.01
1-25-11	11:03	1.70	1.48	0.69	1.01	0.01
1-25-11	12:19	1.53	1.48	0.69	0.84	0.01
1-25-11	13:05	1.49	1.48	0.69	0.80	0.01
1-25-11	14:34	1.51	1.48	0.69	0.82	0.01
1-25-11	15:05	1.61	1.48	0.69	0.92	0.01

Location	time	h_T (m)	surf. elev. (e_s) (m)	$e_{ch} = e_s$@0 - ch. Depth	h_T wrt ch = $h_T - e_{ch}$	σ
2-0-19						
2-0-19	10:15	1.83	0.84	0.26	1.57	0.03
2-0-19	11:20	1.63	0.84	0.26	1.37	0.03
2-0-19	12:25	1.46	0.84	0.26	1.20	0.03
2-0-19	13:30	1.33	0.84	0.26	1.07	0.03
2-0-19	14:50	1.29	0.84	0.26	1.03	0.03
2-0-19	15:40	1.37	0.84	0.26	1.11	0.03
2-5-19						
2-5-19	10:30	1.75	0.98	0.26	1.49	0.02
2-5-19	11:15	1.64	0.98	0.26	1.38	0.02
2-5-19	12:20	1.45	0.98	0.26	1.19	0.02
2-5-19	13:20	1.34	0.98	0.26	1.08	0.02
2-5-19	14:45	1.29	0.98	0.26	1.03	0.02
2-5-19	15:30	1.37	0.98	0.26	1.11	0.02
2-15-19						
2-15-19	10:02	1.80	1.03	0.26	1.54	0.03
2-15-19	11:10	1.62	1.03	0.26	1.36	0.03
2-15-19	12:10	1.45	1.03	0.26	1.19	0.03
2-15-19	13:02	1.31	1.03	0.26	1.05	0.03
2-15-19	14:30	1.25	1.03	0.26	0.99	0.03
2-15-19	15:20	1.31	1.03	0.26	1.05	0.03
2-25-19	flooded		1.06	0.26		
2-25-19	flooded		1.06	0.26		
2-25-19	flooded		1.06	0.26		
2-25-19	flooded		1.06	0.26		
2-25-19	flooded		1.06	0.26		
2-25-19	flooded		1.06	0.26		
2-25-19	flooded		1.06	0.26		

Location	time	h_T (m)	surf. elev. (e_s) (m)	$e_{ch} = e_s$@0 - ch. Depth	h_T wrt ch = $h_T - e_{ch}$	σ
1-0-22	9:01	1.23	1.02	0.69	0.54	0.04
1-0-22	10:05	1.25	1.02	0.69	0.56	0.04
1-0-22	11:21	1.24	1.02	0.69	0.55	0.04
1-0-22	12:03	1.24	1.02	0.69	0.55	0.04
1-0-22	13:20	1.25	1.02	0.69	0.56	0.04
1-0-22	14:25	1.25	1.02	0.69	0.56	0.04
1-0-22	15:19	1.25	1.02	0.69	0.56	0.04
1-5-22	9:05	1.87	1.12	0.69	1.18	0.04
1-5-22	10:11	1.77	1.12	0.69	1.08	0.04
1-5-22	11:15	1.59	1.12	0.69	0.90	0.04
1-5-22	12:08	1.45	1.12	0.69	0.76	0.04
1-5-22	13:16	1.29	1.12	0.69	0.60	0.04
1-5-22	14:28	1.24	1.12	0.69	0.55	0.04
1-5-22	15:14	1.29	1.12	0.69	0.60	0.04
1-15-22	9:09	1.72	1.17	0.69	1.03	0.03
1-15-22	10:15	1.63	1.17	0.69	0.94	0.03
1-15-22	11:10	1.48	1.17	0.69	0.79	0.03
1-15-22	12:12	1.33	1.17	0.69	0.64	0.03
1-15-22	13:11	1.20	1.17	0.69	0.51	0.03
1-15-22	14:31	1.15	1.17	0.69	0.46	0.03
1-15-22	15:09	1.18	1.17	0.69	0.49	0.03
1-25-22	9:11	1.88	1.48	0.69	1.19	0.01
1-25-22	10:20	1.76	1.48	0.69	1.07	0.01
1-25-22	11:03	1.65	1.48	0.69	0.96	0.01
1-25-22	12:19	1.44	1.48	0.69	0.75	0.01
1-25-22	13:05	1.38	1.48	0.69	0.69	0.01
1-25-22	14:34	1.57	1.48	0.69	0.88	0.01
1-25-22	15:05	1.58	1.48	0.69	0.89	0.01

Location	time	h_T (m)	surf. elev. (e_s) (m)	$e_{ch} = e_s$@0 - ch. Depth	h_T wrt ch = $h_T - e_{ch}$	σ
2-0-39						
2-0-39	10:15	1.81	0.84	0.26	1.55	0.03
2-0-39	11:20	1.68	0.84	0.26	1.42	0.03
2-0-39	12:25	1.51	0.84	0.26	1.25	0.03
2-0-39	13:30	1.35	0.84	0.26	1.09	0.03
2-0-39	14:50	1.29	0.84	0.26	1.03	0.03
2-0-39	15:40	1.33	0.84	0.26	1.07	0.03
2-5-39						
2-5-39	10:30	1.56	0.98	0.26	1.30	0.02
2-5-39	11:15	1.58	0.98	0.26	1.32	0.02
2-5-39	12:20	1.53	0.98	0.26	1.27	0.02
2-5-39	13:20	1.41	0.98	0.26	1.15	0.02
2-5-39	14:45	1.36	0.98	0.26	1.10	0.02
2-5-39	15:30	1.38	0.98	0.26	1.12	0.02
2-15-39						
2-15-39	10:02	1.72	1.03	0.26	1.46	0.03
2-15-39	11:10	1.73	1.03	0.26	1.47	0.03
2-15-39	12:10	1.70	1.03	0.26	1.44	0.03
2-15-39	13:02	1.67	1.03	0.26	1.41	0.03
2-15-39	14:30	1.65	1.03	0.26	1.39	0.03
2-15-39	15:20	1.64	1.03	0.26	1.38	0.03
2-25-39	flooded		1.06	0.26		
2-25-39	flooded		1.06	0.26		
2-25-39	flooded		1.06	0.26		
2-25-39	flooded		1.06	0.26		
2-25-39	flooded		1.06	0.26		
2-25-39	flooded		1.06	0.26		
2-25-39	flooded		1.06	0.26		

Appendix C: Calculations of uncertainty in q'

The following tables show the break-down of the calculation of uncertainty for values of q'. Piezometric head measurements shown were made on November 27, 2003. Exact measurement times are included in the tables. At locations where the hydraulic conductivity (K) was too fast to be measured using the slug-test method, a value of 1.80×10^{-1} m/hr was used.

A negative value of q' indicates that horizontal groundwater flux is away from the channel. It was assumed that the direction of flux was correct, so in cases where uncertainties suggested that the direction of flux could have been in either direction, the magnitude of the uncertainty was adjusted so that the range of possible q' values was either all positive or all negative (uncertainties could not cause the range of values to cross zero).

'h_T wrt ch' is total hydraulic head measured with respect to the adjacent channel bottom. The σ-values associated with these measurements are the uncertainty in the elevation estimation (from Table 1 in the Materials and Methods section) plus a measurement error of +/- 0.005 m, which includes the uncertainty in the measurement of the channel depth and the uncertainty in the head measurement. The uncertainties in the geometric mean (GM) K-values given in cm/s are based on the largest spread of K-measurements made at a single piezometer location and are +505% of the GM K and -20% of the GM K. To convert GM K from cm/s to m/hr, the K-value was multiplied by 36. Therefore, uncertainties associated with GM K in m/hr are equal to the uncertainties associated with the GM K-value in cm/s multiplied by 36. The average K values shown in the table are the geometric mean of the two GM K values at the piezometers between which flux is being measured. Because the average is equal to ½ the sum of the two GM K values, the uncertainty associated with the average K = (1/2)*sqrt(error in GMK_1^2 + error in GMK_2^2) (Taylor, 1997). q' is equal to -½ * K * $((h_2^2 - h_1^2)/L)$ where h is hydraulic head and L is the distance between the two piezometers. Therefore, the uncertainty in q' was calculated in multiple steps. The uncertainty in $h^2 = 2*h^{(1)}*E_h$, where E_h is the uncertainty in the head value. The uncertainty in $h_2^2 - h_1^2 = sqrt(E_{h2}^2 + E_{h1}^2)$, where E_{h2} is the uncertainty in h_2 and E_{h1} is the uncertainty in h_1. The uncertainty in $(h_2^2 - h_1^2)/L$ is equal to the value of the uncertainty in $h_2^2 - h_1^2$ divided by the distance between the two piezometers. And, finally, the uncertainty in q' = (1/2)*sqrt($(E_G*K)^2$ + $(E_K*G)^2$), where K is the average K and E_K is the uncertainty in that value, and G = abs $(h_2^2 - h_1^2)/L$ and E_G is the uncertainty in that value. '+' and '-' are the magnitude of uncertainty in either the positive or negative direction and 'upper bound' and 'lower bound' stipulate the actual range of possible q' values.

Appendix C: Calculations of uncertainty in q'

location	time	h_T wrt ch $= h_T - e_{ch}$	σ	GM K (cm/s)	+	-	GM K (m/hr)	+	-	avg. K (m/hr)	+	-	q' (m^2/hr)	error in h_2^2	error in h_1^2	error in $h_2^2 - h_1^2$	$(h_2^2 - h_1^2)/L$	error in $(h_2^2 - h_1^2)/L$	error in q': +	-	upper bound	lower bound	From:
1-0-11	9:01	1.15	0.04	too fast			2.E-01	9.E-01	4.E-02	2.E-01	6.E-01	3.E-02	3.24E-03	0.09	0.10	1.34E-01	3.60E-02	2.69E-02	1.18E-02	2.46E-03	1.51E-02	7.78E-04	5 to 0
	10:05	1.03	0.04	too fast			2.E-01	9.E-01	4.E-02	2.E-01	6.E-01	3.E-02	3.89E-03	0.08	0.09	1.22E-01	4.32E-02	2.44E-02	1.41E-02	2.27E-03	1.79E-02	1.62E-03	5 to 0
	11:21	0.82	0.04	too fast			2.E-01	9.E-01	4.E-02	2.E-01	6.E-01	3.E-02	4.78E-03	0.07	0.08	1.01E-01	5.31E-02	2.03E-02	1.72E-02	1.94E-03	2.20E-02	2.84E-03	5 to 0
	12:03	0.76	0.04	too fast			2.E-01	9.E-01	4.E-02	2.E-01	6.E-01	3.E-02	1.82E-03	0.06	0.07	8.99E-02	2.02E-02	1.80E-02	6.70E-03	1.64E-03	8.51E-03	1.80E-04	5 to 0
	13:20	0.61	0.04	too fast			2.E-01	9.E-01	4.E-02	2.E-01	6.E-01	3.E-02	1.26E-03	0.05	0.05	7.25E-02	1.40E-02	1.45E-02	4.67E-03	1.26E-03	5.93E-03	0.00E+00	5 to 0
	14:25	0.56	0.04	too fast			2.E-01	9.E-01	4.E-02	2.E-01	6.E-01	3.E-02	1.16E-03	0.05	0.05	6.70E-02	1.29E-02	1.34E-02	4.32E-03	1.16E-03	5.48E-03	0.00E+00	5 to 0
	15:19	0.32	0.04	too fast			2.E-01	9.E-01	4.E-02	2.E-01	6.E-01	3.E-02	6.17E-03	0.03	0.05	5.93E-02	6.86E-02	1.19E-02	2.21E-02	1.38E-03	2.82E-02	4.80E-03	5 to 0
1-5-11	9:05	1.23	0.04	too fast			2.E-01	9.E-01	4.E-02	1.E-01	5.E-01	2.E-02	-8.27E-04	0.10	0.07	1.20E-01	1.64E-02	1.20E-02	6.26E-04	3.95E-03	-2.01E-04	-4.77E-03	15 to 5
	10:11	1.13	0.04	too fast			2.E-01	9.E-01	4.E-02	1.E-01	5.E-01	2.E-02	-1.30E-03	0.09	0.06	1.09E-01	2.57E-02	1.09E-02	6.00E-04	6.15E-03	-7.01E-04	-7.45E-03	15 to 5
	11:15	0.97	0.04	too fast			2.E-01	9.E-01	4.E-02	1.E-01	5.E-01	2.E-02	-9.99E-04	0.08	0.05	9.29E-02	1.98E-02	9.29E-03	5.05E-04	4.73E-03	-4.94E-04	-5.73E-03	15 to 5
	12:08	0.83	0.04	too fast			2.E-01	9.E-01	4.E-02	1.E-01	5.E-01	2.E-02	-2.03E-03	0.07	0.03	7.33E-02	4.03E-02	7.33E-03	5.30E-04	9.60E-03	-1.50E-03	-1.16E-02	15 to 5
	13:16	0.67	0.04	too fast			2.E-01	9.E-01	4.E-02	1.E-01	5.E-01	2.E-02	-6.54E-04	0.05	0.03	6.32E-02	1.30E-02	6.32E-03	3.42E-04	3.10E-03	-3.13E-04	-3.76E-03	15 to 5
	14:28	0.62	0.04	too fast			2.E-01	9.E-01	4.E-02	1.E-01	5.E-01	2.E-02	-5.06E-04	0.05	0.03	5.89E-02	1.00E-02	5.89E-03	3.12E-04	2.40E-03	-1.94E-04	-2.91E-03	15 to 5
	15:14	0.67	0.04	too fast			2.E-01	9.E-01	4.E-02	1.E-01	5.E-01	2.E-02	-1.12E-03	0.05	0.03	6.05E-02	2.21E-02	6.05E-03	3.70E-04	5.27E-03	-7.47E-04	-6.39E-03	15 to 5
1-15-11	9:09	1.16	0.03	2.E-03	8.E-03	3.E-04	6.E-02	3.E-01	1.E-02	6.E-02	2.E-01	9.E-03	7.65E-04	0.07	0.03	7.38E-02	2.48E-02	7.38E-03	2.76E-03	2.53E-04	3.53E-03	5.12E-04	25 to 15
	10:15	1.01	0.03	2.E-03	8.E-03	3.E-04	6.E-02	3.E-01	1.E-02	6.E-02	2.E-01	9.E-03	7.75E-04	0.06	0.02	6.45E-02	2.51E-02	6.45E-03	2.80E-03	2.28E-04	3.58E-03	5.48E-04	25 to 15
	11:10	0.86	0.03	2.E-03	8.E-03	3.E-04	6.E-02	3.E-01	1.E-02	6.E-02	2.E-01	9.E-03	8.91E-04	0.05	0.02	5.53E-02	2.89E-02	5.53E-03	3.21E-03	2.13E-04	4.11E-03	6.78E-04	25 to 15
	12:12	0.53	0.03	2.E-03	8.E-03	3.E-04	6.E-02	3.E-01	1.E-02	6.E-02	2.E-01	9.E-03	1.34E-03	0.03	0.02	3.59E-02	4.34E-02	3.59E-03	4.83E-03	2.21E-04	6.16E-03	1.12E-03	25 to 15
	13:11	0.56	0.03	2.E-03	8.E-03	3.E-04	6.E-02	3.E-01	1.E-02	6.E-02	2.E-01	9.E-03	9.94E-04	0.03	0.02	3.73E-02	3.22E-02	3.73E-03	3.58E-03	1.83E-04	4.58E-03	8.11E-04	25 to 15
	14:31	0.53	0.03	2.E-03	8.E-03	3.E-04	6.E-02	3.E-01	1.E-02	6.E-02	2.E-01	9.E-03	1.19E-03	0.03	0.02	3.59E-02	3.85E-02	3.59E-03	4.28E-03	2.02E-04	5.47E-03	9.86E-04	25 to 15
	15:09	0.47	0.03	2.E-03	8.E-03	3.E-04	6.E-02	3.E-01	1.E-02	6.E-02	2.E-01	9.E-03	1.92E-03	0.03	0.02	3.39E-02	6.24E-02	3.39E-03	6.93E-03	2.94E-04	8.86E-03	1.63E-03	25 to 15
1-25-11	9:11	1.26	0.01	2.E-03	1.E-02	4.E-04	7.E-02	3.E-01	1.E-02														
	10:20	1.13	0.01	2.E-03	1.E-02	4.E-04	7.E-02	3.E-01	1.E-02														
	11:03	1.01	0.01	2.E-03	1.E-02	4.E-04	7.E-02	3.E-01	1.E-02														
	12:19	0.84	0.01	2.E-03	1.E-02	4.E-04	7.E-02	3.E-01	1.E-02														
	13:05	0.80	0.01	2.E-03	1.E-02	4.E-04	7.E-02	3.E-01	1.E-02														
	14:34	0.82	0.01	2.E-03	1.E-02	4.E-04	7.E-02	3.E-01	1.E-02														
	15:05	0.92	0.01	2.E-03	1.E-02	4.E-04	7.E-02	3.E-01	1.E-02														

Appendix C: Calculations of uncertainty in q'

(page 3 of 5)

location	time	h_T wrt ch = $h_T - e_{ch}$	σ	GM K (cm/s)	+	-	GM K (m/hr)	+	-	avg. K (m/hr)	+	-	q' (m^2/hr)	error in h_2^2	error in h_1^2	error in $h_2^2 - h_1^2$	$(h_2^2 - h_1^2)/L$	error in $(h_2^2 - h_1^2)/L$	error in q': +	-	upper bound	lower bound	From:
1-0-22	9:01	0.54	0.04	5.E-04	2.E-03	9.E-05	2.E-02	8.E-02	3.E-03	2.E-03	4.E-02	2.E-03	1.91E-04	0.04	0.09	1.04E-01	2.18E-01	2.07E-02	4.57E-03	1.82E-04	4.76E-03	8.66E-06	5 to 0
	10:05	0.56	0.04	5.E-04	2.E-03	9.E-05	2.E-02	8.E-02	3.E-03	2.E-03	4.E-02	2.E-03	1.51E-04	0.04	0.09	9.76E-02	1.73E-01	1.95E-02	3.63E-03	1.45E-04	3.78E-03	6.59E-06	5 to 0
	11:21	0.55	0.04	5.E-04	2.E-03	9.E-05	2.E-02	8.E-02	3.E-03	2.E-03	4.E-02	2.E-03	8.75E-05	0.04	0.07	8.45E-02	1.00E-01	1.69E-02	2.10E-03	8.45E-05	2.19E-03	3.09E-06	5 to 0
	12:03	0.55	0.04	5.E-04	2.E-03	9.E-05	2.E-02	8.E-02	3.E-03	2.E-03	4.E-02	2.E-03	4.80E-05	0.04	0.06	7.49E-02	5.49E-02	1.50E-02	1.15E-03	4.75E-05	1.20E-03	5.64E-07	5 to 0
	13:20	0.56	0.04	5.E-04	2.E-03	9.E-05	2.E-02	8.E-02	3.E-03	2.E-03	4.E-02	2.E-03	9.21E-06	0.04	0.05	6.57E-02	1.05E-02	1.31E-02	2.21E-04	9.21E-06	2.30E-04	0.00E+00	5 to 0
	14:25	0.56	0.04	5.E-04	2.E-03	9.E-05	2.E-02	8.E-02	3.E-03	2.E-03	4.E-02	2.E-03	-1.27E-06	0.04	0.04	6.31E-02	1.45E-03	1.26E-02	1.27E-06	3.23E-05	0.00E+00	-3.36E-05	5 to 0
	15:19	0.56	0.04	5.E-04	2.E-03	9.E-05	2.E-02	8.E-02	3.E-03	2.E-03	4.E-02	2.E-03	6.73E-06	0.05	0.05	6.57E-02	7.70E-03	1.31E-02	1.62E-04	6.73E-06	1.69E-04	0.00E+00	5 to 0
1-5-22	9:05	1.18	0.04	5.E-06	3.E-05	1.E-06	2.E-04	9.E-04	4.E-05	1.E-04	5.E-04	2.E-05	-2.32E-06	0.09	0.06	1.13E-01	3.20E-02	1.13E-02	8.87E-07	8.80E-06	-1.43E-06	-1.11E-05	15 to 5
	10:11	1.08	0.04	5.E-06	3.E-05	1.E-06	2.E-04	9.E-04	4.E-05	1.E-04	5.E-04	2.E-05	-2.09E-06	0.09	0.06	1.04E-01	2.88E-02	1.04E-02	8.13E-07	7.91E-06	-1.27E-06	-1.00E-05	15 to 5
	11:15	0.90	0.04	5.E-06	3.E-05	1.E-06	2.E-04	9.E-04	4.E-05	1.E-04	5.E-04	2.E-05	-1.33E-06	0.07	0.05	8.62E-02	1.83E-02	8.62E-03	6.55E-07	5.05E-06	-6.73E-07	-6.38E-06	15 to 5
	12:08	0.76	0.04	5.E-06	3.E-05	1.E-06	2.E-04	9.E-04	4.E-05	1.E-04	5.E-04	2.E-05	-1.25E-06	0.06	0.04	7.17E-02	1.72E-02	7.17E-03	5.52E-07	4.75E-06	-6.98E-07	-6.00E-06	15 to 5
	13:16	0.60	0.04	5.E-06	3.E-05	1.E-06	2.E-04	9.E-04	4.E-05	1.E-04	5.E-04	2.E-05	-7.53E-07	0.05	0.03	5.72E-02	1.04E-02	5.72E-03	4.29E-07	2.87E-06	-3.23E-07	-3.62E-06	15 to 5
	14:28	0.55	0.04	5.E-06	3.E-05	1.E-06	2.E-04	9.E-04	4.E-05	1.E-04	5.E-04	2.E-05	-6.66E-07	0.04	0.03	5.24E-02	9.19E-03	5.24E-03	3.93E-07	2.54E-06	-2.74E-07	-3.21E-06	15 to 5
	15:14	0.60	0.04	5.E-06	3.E-05	1.E-06	2.E-04	9.E-04	4.E-05	1.E-04	5.E-04	2.E-05	-8.76E-07	0.05	0.03	5.60E-02	1.21E-02	5.60E-03	4.26E-07	3.33E-06	-4.49E-07	-4.20E-06	15 to 5
1-15-22	9:09	1.03	0.03	3.E-06	2.E-05	6.E-07	1.E-04	6.E-04	2.E-05	3.E-03	1.E-01	6.E-03	4.70E-05	0.06	0.02	6.63E-02	3.64E-02	6.63E-03	2.66E-03	4.70E-05	2.70E-03	0.00E+00	25 to 15
	10:15	0.94	0.03	3.E-06	2.E-05	6.E-07	1.E-04	6.E-04	2.E-05	3.E-03	1.E-01	6.E-03	3.38E-05	0.06	0.02	6.05E-02	2.62E-02	6.05E-03	1.91E-03	3.38E-05	1.95E-03	0.00E+00	25 to 15
	11:10	0.79	0.03	3.E-06	2.E-05	6.E-07	1.E-04	6.E-04	2.E-05	3.E-03	1.E-01	6.E-03	3.83E-05	0.05	0.02	5.12E-02	2.97E-02	5.12E-03	2.17E-03	3.83E-05	2.21E-03	0.00E+00	25 to 15
	12:12	0.64	0.03	3.E-06	2.E-05	6.E-07	1.E-04	6.E-04	2.E-05	3.E-03	1.E-01	6.E-03	1.99E-05	0.04	0.01	4.09E-02	1.54E-02	4.09E-03	1.13E-03	1.99E-05	1.15E-03	0.00E+00	25 to 15
	13:11	0.51	0.03	3.E-06	2.E-05	6.E-07	1.E-04	6.E-04	2.E-05	3.E-03	1.E-01	6.E-03	2.77E-05	0.03	0.01	3.36E-02	2.14E-02	3.36E-03	1.56E-03	2.77E-05	1.59E-03	0.00E+00	25 to 15
	14:31	0.46	0.03	3.E-06	2.E-05	6.E-07	1.E-04	6.E-04	2.E-05	3.E-03	1.E-01	6.E-03	7.23E-05	0.03	0.02	3.30E-02	5.60E-02	3.30E-03	4.09E-03	7.23E-05	4.16E-03	0.00E+00	25 to 15
	15:09	0.49	0.03	3.E-06	2.E-05	6.E-07	1.E-04	6.E-04	2.E-05	3.E-03	1.E-01	6.E-03	7.18E-05	0.03	0.02	3.42E-02	5.56E-02	3.42E-03	4.06E-03	7.18E-05	4.13E-03	0.00E+00	25 to 15
1-25-22	9:11	1.19	0.01	2.E-03	8.E-03	3.E-04	6.E-02	3.E-01	1.E-02														
	10:20	1.07	0.01	2.E-03	8.E-03	3.E-04	6.E-02	3.E-01	1.E-02														
	11:03	0.96	0.01	2.E-03	8.E-03	3.E-04	6.E-02	3.E-01	1.E-02														
	12:19	0.75	0.01	2.E-03	8.E-03	3.E-04	6.E-02	3.E-01	1.E-02														
	13:05	0.69	0.01	2.E-03	8.E-03	3.E-04	6.E-02	3.E-01	1.E-02														
	14:34	0.88	0.01	2.E-03	8.E-03	3.E-04	6.E-02	3.E-01	1.E-02														
	15:05	0.89	0.01	2.E-03	8.E-03	3.E-04	6.E-02	3.E-01	1.E-02														

Appendix C: Calculations of uncertainty in q’

		h_T wrt ch		GM K			GM K			avg.			q'	error in	error in	error in		error in	error in q':		upper	lower	
location	time	$= h_T - e_{ch}$	σ	(cm/s)	+	-	(m/hr)	+	-	K (m/hr)	+	-	(m^2/hr)	h_2^2	h_1^2	$h_2^2 - h_1^2$	$(h_2^2 - h_1^2)/L$	$(h_2^2 - h_1^2)/L$	+	-	bound	bound	From:
2-0-19	9:35	1.60	0.03	too fast			2.E-01	9.E-01	4.E-02	1.E-01	5.E-01	2.E-02											
	10:15	1.57	0.03	too fast			2.E-01	9.E-01	4.E-02	1.E-01	5.E-01	2.E-02	-2.68E-03	0.09	0.06	1.11E-01	5.06E-02	2.23E-02	1.28E-03	1.22E-02	-1.41E-03	-1.49E-02	5 to 0
	11:20	1.37	0.03	too fast			2.E-01	9.E-01	4.E-02	1.E-01	5.E-01	2.E-02	2.51E-04	0.08	0.06	9.91E-02	4.73E-03	1.98E-02	1.55E-03	2.51E-04	1.80E-03	0.00E+00	5 to 0
	12:25	1.20	0.03	too fast			2.E-01	9.E-01	4.E-02	1.E-01	5.E-01	2.E-02	-3.23E-04	0.07	0.05	8.65E-02	6.10E-03	1.73E-02	3.23E-04	1.73E-03	0.00E+00	-2.05E-03	5 to 0
	13:30	1.07	0.03	too fast			2.E-01	9.E-01	4.E-02	1.E-01	5.E-01	2.E-02	1.95E-04	0.06	0.04	7.71E-02	3.68E-03	1.54E-02	1.20E-03	1.95E-04	1.40E-03	0.00E+00	5 to 0
	14:50	1.03	0.03	too fast			2.E-01	9.E-01	4.E-02	1.E-01	5.E-01	2.E-02	5.46E-05	0.06	0.04	7.41E-02	1.03E-03	1.48E-02	8.24E-04	5.46E-05	8.78E-04	0.00E+00	5 to 0
	15:40	1.11	0.03	too fast			2.E-01	9.E-01	4.E-02	1.E-01	5.E-01	2.E-02	-1.28E-05	0.07	0.04	7.98E-02	2.41E-04	1.60E-02	1.28E-05	8.47E-04	0.00E+00	-8.60E-04	5 to 0
2-5-19			0.02	2.E-03	9.E-03	3.E-04	6.E-02	3.E-01	1.E-02	3.E-03	2.E-01	6.E-03											
	10:30	1.49	0.02	2.E-03	9.E-03	3.E-04	6.E-02	3.E-01	1.E-02	3.E-03	2.E-01	6.E-03	2.15E-05	0.06	0.09	1.10E-01	1.61E-02	1.10E-02	1.26E-03	2.15E-05	1.28E-03	0.00E+00	15 to 5
	11:15	1.38	0.02	2.E-03	9.E-03	3.E-04	6.E-02	3.E-01	1.E-02	3.E-03	2.E-01	6.E-03	-8.37E-06	0.06	0.08	9.84E-02	6.27E-03	9.84E-03	8.37E-06	4.91E-04	0.00E+00	-4.99E-04	15 to 5
	12:20	1.19	0.02	2.E-03	9.E-03	3.E-04	6.E-02	3.E-01	1.E-02	3.E-03	2.E-01	6.E-03	-5.03E-07	0.05	0.07	8.58E-02	3.77E-04	8.58E-03	5.03E-07	3.16E-05	0.00E+00	-3.21E-05	15 to 5
	13:20	1.08	0.02	2.E-03	9.E-03	3.E-04	6.E-02	3.E-01	1.E-02	3.E-03	2.E-01	6.E-03	-6.51E-06	0.04	0.06	7.64E-02	4.88E-03	7.64E-03	6.51E-06	3.81E-04	0.00E+00	-3.88E-04	15 to 5
	14:45	1.03	0.02	2.E-03	9.E-03	3.E-04	6.E-02	3.E-01	1.E-02	3.E-03	2.E-01	6.E-03	-1.11E-05	0.04	0.06	7.22E-02	8.31E-03	7.22E-03	1.11E-05	6.50E-04	-4.07E-20	-6.61E-04	15 to 5
	15:30	1.11	0.02	2.E-03	9.E-03	3.E-04	6.E-02	3.E-01	1.E-02	3.E-03	2.E-01	6.E-03	-1.54E-05	0.04	0.06	7.71E-02	1.15E-02	7.71E-03	1.54E-05	9.01E-04	0.00E+00	-9.16E-04	15 to 5
2-15-19	9:30	1.56	0.03	3.E-06	2.E-05	6.E-07	1.E-04	6.E-04	2.E-05	3.E-03	2.E-01	8.E-03											
	10:02	1.54	0.03	3.E-06	2.E-05	6.E-07	1.E-04	6.E-04	2.E-05	3.E-03	2.E-01	8.E-03											
	11:10	1.36	0.03	3.E-06	2.E-05	6.E-07	1.E-04	6.E-04	2.E-05	3.E-03	2.E-01	8.E-03											
	12:10	1.19	0.03	3.E-06	2.E-05	6.E-07	1.E-04	6.E-04	2.E-05	3.E-03	2.E-01	8.E-03											
	13:02	1.05	0.03	3.E-06	2.E-05	6.E-07	1.E-04	6.E-04	2.E-05	3.E-03	2.E-01	8.E-03											
	14:30	0.99	0.03	3.E-06	2.E-05	6.E-07	1.E-04	6.E-04	2.E-05	3.E-03	2.E-01	8.E-03											
	15:20	1.05	0.03	3.E-06	2.E-05	6.E-07	1.E-04	6.E-04	2.E-05	3.E-03	2.E-01	8.E-03											
2-25-19		flooded	0.01	2.E-03	1.E-02	4.E-04	8.E-02	4.E-01	2.E-02														
		flooded	0.01	2.E-03	1.E-02	4.E-04	8.E-02	4.E-01	2.E-02														
		flooded	0.01	2.E-03	1.E-02	4.E-04	8.E-02	4.E-01	2.E-02														
		flooded	0.01	2.E-03	1.E-02	4.E-04	8.E-02	4.E-01	2.E-02														
		flooded	0.01	2.E-03	1.E-02	4.E-04	8.E-02	4.E-01	2.E-02														
		flooded	0.01	2.E-03	1.E-02	4.E-04	8.E-02	4.E-01	2.E-02														
		flooded	0.01	2.E-03	1.E-02	4.E-04	8.E-02	4.E-01	2.E-02														

Appendix C: Calculations of uncertainty in q’

(page 5 of 5)

location	time	h_T wrt ch = h_T - e_{ch}	σ	GM K (cm/s)	+	-	GM K (m/hr)	+	-	avg. K (m/hr)	+	-	q' (m^2/hr)	error in h_2^2	error in h_1^2	error in $h_2^2 - h_1^2$	$(h_2^2 - h_1^2)/L$	error in $(h_2^2 - h_1^2)/L$	error in q': +	-	upper bound	lower bound	From:
2-0-39	9:35	1.56	0.03	1.E-03	5.E-03	2.E-04	4.E-02	2.E-01	7.E-03	4.E-02	2.E-01	6.E-03											
	10:15	1.55	0.03	1.E-03	5.E-03	2.E-04	4.E-02	2.E-01	7.E-03	4.E-02	2.E-01	6.E-03	-3.03E-03	0.09	0.05	1.06E-01	1.39E-01	2.13E-02	6.42E-04	1.12E-02	-2.39E-03	-1.43E-02	5 to 0
	11:20	1.42	0.03	1.E-03	5.E-03	2.E-04	4.E-02	2.E-01	7.E-03	4.E-02	2.E-01	6.E-03	-1.16E-03	0.08	0.05	9.99E-02	5.33E-02	2.00E-02	4.68E-04	4.33E-03	-6.94E-04	-5.49E-03	5 to 0
	12:25	1.25	0.03	1.E-03	5.E-03	2.E-04	4.E-02	2.E-01	7.E-03	4.E-02	2.E-01	6.E-03	2.68E-04	0.07	0.05	9.05E-02	1.23E-02	1.81E-02	1.07E-03	2.68E-04	1.33E-03	0.00E+00	5 to 0
	13:30	1.09	0.03	1.E-03	5.E-03	2.E-04	4.E-02	2.E-01	7.E-03	4.E-02	2.E-01	6.E-03	5.95E-04	0.07	0.05	7.99E-02	2.73E-02	1.60E-02	2.23E-03	3.59E-04	2.82E-03	2.36E-04	5 to 0
	14:50	1.03	0.03	1.E-03	5.E-03	2.E-04	4.E-02	2.E-01	7.E-03	4.E-02	2.E-01	6.E-03	6.53E-04	0.06	0.04	7.62E-02	3.00E-02	1.52E-02	2.44E-03	3.46E-04	3.10E-03	3.08E-04	5 to 0
	15:40	1.07	0.03	1.E-03	5.E-03	2.E-04	4.E-02	2.E-01	7.E-03	4.E-02	2.E-01	6.E-03	4.65E-04	0.06	0.04	7.83E-02	2.13E-02	1.57E-02	1.76E-03	3.48E-04	2.22E-03	1.17E-04	5 to 0
2-5-39			0.02	1.E-03	7.E-03	3.E-04	5.E-02	3.E-01	1.E-02	8.E-04	1.E-01	5.E-03											
	10:30	1.30	0.02	1.E-03	7.E-03	3.E-04	5.E-02	3.E-01	1.E-02	8.E-04	1.E-01	5.E-03	1.86E-05	0.05	0.09	1.02E-01	4.50E-02	1.02E-02	3.01E-03	1.86E-05	3.02E-03	0.00E+00	15 to 5
	11:15	1.32	0.02	1.E-03	7.E-03	3.E-04	5.E-02	3.E-01	1.E-02	8.E-04	1.E-01	5.E-03	1.77E-05	0.05	0.09	1.03E-01	4.28E-02	1.03E-02	2.86E-03	1.77E-05	2.88E-03	0.00E+00	15 to 5
	12:20	1.27	0.02	1.E-03	7.E-03	3.E-04	5.E-02	3.E-01	1.E-02	8.E-04	1.E-01	5.E-03	1.89E-05	0.05	0.09	1.00E-01	4.57E-02	1.00E-02	3.06E-03	1.89E-05	3.08E-03	0.00E+00	15 to 5
	13:20	1.15	0.02	1.E-03	7.E-03	3.E-04	5.E-02	3.E-01	1.E-02	8.E-04	1.E-01	5.E-03	2.75E-05	0.05	0.08	9.63E-02	6.66E-02	9.63E-03	4.45E-03	2.75E-05	4.48E-03	0.00E+00	15 to 5
	14:45	1.10	0.02	1.E-03	7.E-03	3.E-04	5.E-02	3.E-01	1.E-02	8.E-04	1.E-01	5.E-03	3.00E-05	0.04	0.08	9.46E-02	7.26E-02	9.46E-03	4.85E-03	3.00E-05	4.88E-03	0.00E+00	15 to 5
	15:30	1.12	0.02	1.E-03	7.E-03	3.E-04	5.E-02	3.E-01	1.E-02	8.E-04	1.E-01	5.E-03	2.69E-05	0.04	0.08	9.41E-02	6.50E-02	9.41E-03	4.34E-03	2.69E-05	4.37E-03	0.00E+00	15 to 5
2-15-39	9:30	1.47	0.03	4.E-07	2.E-06	7.E-08	1.E-05	7.E-05	3.E-06	1.E-05	5.E-05	2.E-06											
	10:02	1.46	0.03	4.E-07	2.E-06	7.E-08	1.E-05	7.E-05	3.E-06	1.E-05	5.E-05	2.E-06											
	11:10	1.47	0.03	4.E-07	2.E-06	7.E-08	1.E-05	7.E-05	3.E-06	1.E-05	5.E-05	2.E-06											
	12:10	1.44	0.03	4.E-07	2.E-06	7.E-08	1.E-05	7.E-05	3.E-06	1.E-05	5.E-05	2.E-06											
	13:02	1.41	0.03	4.E-07	2.E-06	7.E-08	1.E-05	7.E-05	3.E-06	1.E-05	5.E-05	2.E-06											
	14:30	1.39	0.03	4.E-07	2.E-06	7.E-08	1.E-05	7.E-05	3.E-06	1.E-05	5.E-05	2.E-06											
	15:20	1.38	0.03	4.E-07	2.E-06	7.E-08	1.E-05	7.E-05	3.E-06	1.E-05	5.E-05	2.E-06											
2-25-39		flooded	0.01	4.E-07	2.E-06	8.E-08	1.E-05	7.E-05	3.E-06														
		flooded	0.01	4.E-07	2.E-06	8.E-08	1.E-05	7.E-05	3.E-06														
		flooded	0.01	4.E-07	2.E-06	8.E-08	1.E-05	7.E-05	3.E-06														
		flooded	0.01	4.E-07	2.E-06	8.E-08	1.E-05	7.E-05	3.E-06														
		flooded	0.01	4.E-07	2.E-06	8.E-08	1.E-05	7.E-05	3.E-06														
		flooded	0.01	4.E-07	2.E-06	8.E-08	1.E-05	7.E-05	3.E-06														
		flooded	0.01	4.E-07	2.E-06	8.E-08	1.E-05	7.E-05	3.E-06														

Appendix D: Head response to change in tidal stage. The following graphs show the hydraulic head measurements that where used in the calculation of q', along with the tidal stage and ground surface elevation at the given piezometer location. At most piezometer locations, head changes seem to roughly follow the change in tidal stage while the site is flooded. During non-flooding times, head remains within a few centimeters of the ground surface. Piezometers 1-0-22, 2-5-39 and 2-15-39 do not show this tidal response.

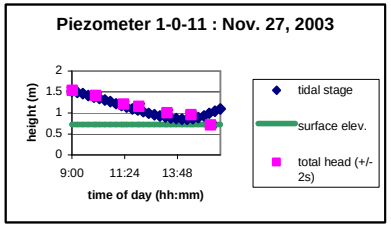

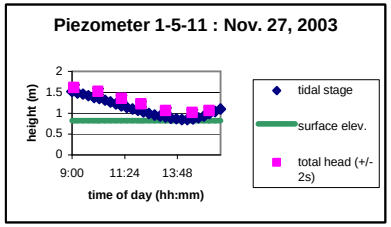

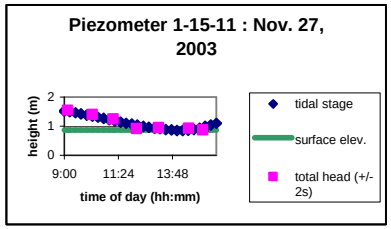

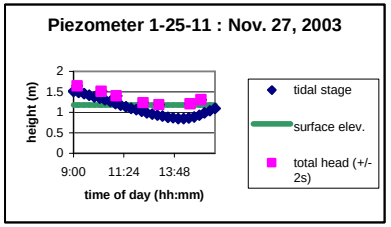

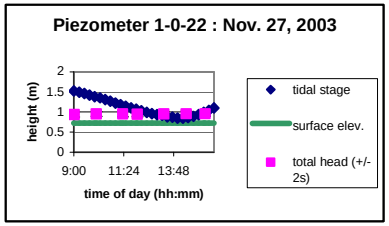

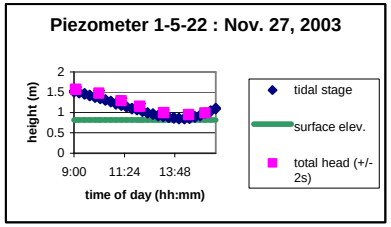

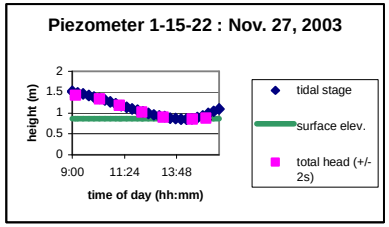

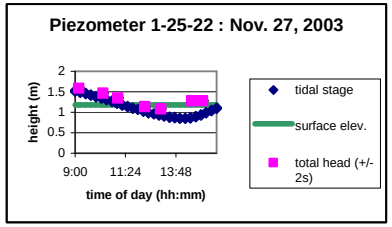

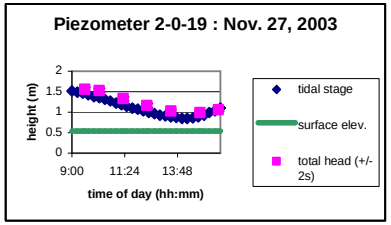

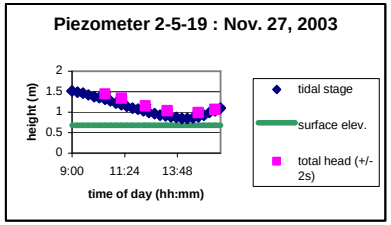

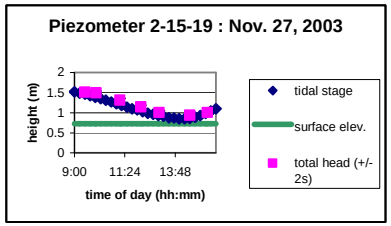

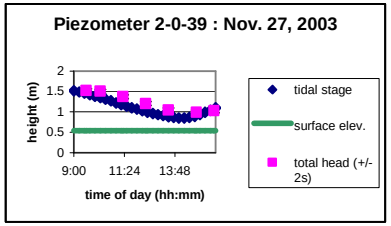

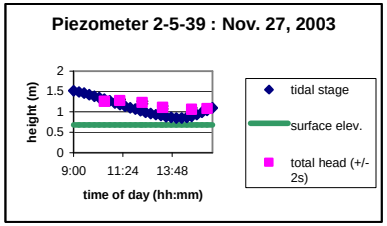

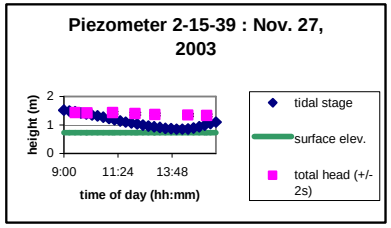

REFERENCES

Agosta, K. 1985. The effect of tidally induced changes in the creekbank water table on pore water chemistry. *Estuarine, Coastal and Shelf Science* 21: 389-400.

Baird, A.J. 1995. Hydrological investigations of soil water and groundwater processes in wetlands, pp. 111-129 In J.M.R. Hughes and A.L. Heathwaite (eds.), Hydrology and Hydrochemistry of British Wetlands. John Wiley & Sons, Chichester, UK.

Baird, A.J. and S.W. Gaffney. 1994. Cylindrical piezometer responses in a humified fen peat. *Nordic Hydrology* 25: 167-182.

Brand, E.W. and J. Premchitt. 1980. Shape factors of cylindrical piezometers. *Geotechnique* 30: 369-384.

Chason, D.B. and D.I. Siegel. 1986. Hydraulic conductivity and related physical properties of peat, Lost River Peatland, Northern Minnesota. *Soil Science* 142: 91-99.

Chesapeake Bay Foundation, The. 2002. "2002 State of the Bay Report." < http://www.cbf.org/site/PageServer?pagename=sotb_2002_index>

Comin, F.A., J.A. Romero, V. Astorga and C. García **.** 1997**.** Nitrogen removal and cycling in restored wetlands used as filters of nutrients for agricultural runoff**.** *Water Science and Technology* 35(5): 255-261.

Craft, C., S. Broome and C. Campbell. 2002. Fifteen years of vegetation and soil development after brackish-water marsh creation. *Restoration Ecology* 10(2): 248-258.

Dunne, T. and L.B. Leopold. 1978. Water in Environmental Planning. W.H. Freeman and Company, New York. 818pp.

Erskine, A.D. 1991. The effect of tidal fluctuation on a coastal aquifer in the UK. *Ground Water* 29(4): 556-562.

Fetter, C.W. 1988. Applied Hydrogeology. Macmillan Publishing Company, New York. Second edition. 592pp.

Hanschke, T. and A.J. Baird. 2001. Time-lag errors associated with the use of simple standpipe piezometers in wetland soils. *Wetlands* 21(3): 412-421.

Harvey, J.W., P.F. Germann and W.E. Odum. 1987. Geomorphological control of subsurface hydrology in the creekbank zone of tidal marshes. *Estuarine Coastal Shelf Science* 25: 677-691.

Harvey, J.W. and W.E. Odum. 1990. The influence of tidal marshes on upland groundwater discharge to estuaries. *Biogeochemistry* 10: 217-236.

Harvey, J.W. and W.K. Nuttle. 1995. Fluxes of water and solute in a coastal wetland sediment. 2. Effect of macropores on solute exchange with surface water. *Journal of Hydrology* 164: 109-125.

Hassen, M.B. 2001. Spatial and temporal variability in nutrients and suspended material processing in the Fier d'Ars Bay (France). *Estuarine, Coastal and Shelf Science* 52: 457-469.

Hemond, H.F., W.K. Nuttle, R.W. Burke and K.D. Stolzenbach. 1984. Surface infiltration in salt marshes: Theory, measurement, and biogeochemical implications. *Water Resources Research* 20(5): 591-600.

Hemond, H.F. and J.C. Goldman. 1985. On non-Darcian waterflow in peat. *Journal of Ecology* 73: 579-584.

Horton, R.E. 1945. Erosional developments of streams and their drainage basins; hydrophysical approach to quantitative morphology. *Geological Society of America Bulletin* 56: 275-370.

Hughes, C.E., P. Binning and G.R. Willgoose. 1998. Characterisation of the hydrology of an estuarine wetland. *Journal of Hydrology* 211: 34-49.

Hvorslev, M.J. 1951. Time Lag and Soil Permeability in Ground-water Observations. U.S. Army Corps of Engineers, Vicksburg, MS. Waterways Experimentation Station Bulletin 36.

Ingram, H.A.P., D.W. Rycroft and D.J.A. Williams. 1974. Anomalous transmission of water through certain peats. *Journal of Hydrology* 22: 213-218.

Jordan, T.E. and D.L. Correll. 1985. Nutrient chemistry and hydrology of interstitial water in brackish tidal marshes of Chesapeake Bay. *Estuarine, Coastal and Shelf Science* 21: 45-55.

Jordan, T.E. and D.L. Correll. 1991. Continuous automated sampling of tidal exchanges of nutrients by brackish marshes. *Estuarine, Coastal and Shelf Science* 32: 527-545.

Kastler, J.A. and P.L. Wiberg. 1996. Sedimentation and boundary changes of Virginia salt marshes. *Estuarine, Coastal and Shelf Science* 42: 683-700.

Katyl, N.L. 1995. Processes that influence iron and sulfur fluxes into and out of a freshwater wetland. University of Maryland, M.S. thesis. 98 p.

Kearney, M.S. and L.G. Ward. 1986. Accretion rates in brackish marshes of a Chesapeake Bay estuarine tributary. *Geo-Marine Letters* 6: 41-49.

Knighton, D. 1998. Fluvial Forms and Processes: A New Perspective. Oxford University Press, Inc., New York. 383pp.

Knott, J.F., W.K. Nuttle and H.F. Hemond. 1987. Hydrologic parameters of salt marsh peat. *Hydrological Processes* 1(2): 211-220.

Lau, S.S.S. 2000. The significance of temporal variability in sediment quality for contamination assessment in a coastal wetland. *Water Research* 34(2): 387-394.

Leeper, G.W. and N.C. Uren. 1993. Soil Science: An Introduction. Melbourne University Press, Victoria. Fifth edition. 300pp.

Leonard, L.A. and M.E. Luther. 1995. Flow hydrodynamics in tidal wetland canopies. *Limnology and Oceanography* 40(8): 1474-1484.

Leopold, L.B, J.N. Collins and L.M. Collins. 1993. Hydrology of some tidal channels in estuarine marshland near San Francisco. *Catena* 20(5): 469-493.

Muriceak, D.R. 1996. Spatial and temporal variations in hydrologic processes, frequency of bankfull stage, and factors influencing flow resistance in a cypress swamp. University of Maryland, M.S. thesis. 124 p.

Nuttle, W.K. 1986. Elements of salt marsh hydrology. Massachusetts Institute of Technology, PhD. Dissertation. 241 p.

Nuttle, W.K. 1988. The extent of lateral water movement in the sediments of a New England salt marsh. *Water Resources Research* 24(12): 2077-2085.

Nuttle, W.K. and J.W. Harvey. 1995. Fluxes of water and solute in a coastal wetland sediment. 1. The contribution of regional groundwater discharge. *Journal of Hydrology* 164: 89-107.

Pasternack, G.B., W.B. Hilgartner and G.S. Brush. 2000. Biogeomorphology of an upper Chesapeake Bay river-mouth tidal freshwater wetland. *Wetlands* 20(3): 520-537.

Premchitt, J. and E.W. Brand. 1981. Pore pressure equalisation of piezometers in compressible soils. *Geotechnique* 31: 105-123.

Priestley, C.H.B. and R.J. Taylor. 1972. On the assessment of surface heat flux and evaporation using large-scale parameters. *Monthly Weather Review* 100(2): 81-92.

Schultz, G. and C. Ruppel. 2002. Constraints on hydraulic parameters and implications for groundwater flux across the upland-estuary interface. *Journal of Hydrology*

260: 255-269.

Schumm, S.A. 1960. The shape of alluvial channels in relation to sediment type. USGS Professional Paper 352(B): 17-30.

Seitzinger, S.P. 1988. Denitrification in freshwater and coastal marine ecosystems: Ecological and geochemical significance. *Limnology and Oceanography* 33(4, part 2): 702-724.

Serway, R.A. 1996. Physics for Scientists and Engineers, Volume 1. Saunders College Publishing, Philadelphia. Fourth edition. 645pp.

Smith-Hall, L. 2002. Channel network and morphology in a tidal freshwater wetland in the Patuxent River. University of Maryland, Geology Department Senior Thesis. 62 p.

Stoddart, D.R., D.J. Reed and J.R. French. 1989. Understanding salt-marsh accretion, Scott Head Island, Norfolk, England. *Estuaries* 12: 228-236.

Taylor, J.R. 1997. An Introduction to Error Analysis: The Study of Uncertainties in Physical Measurements. University Science Books, Sausalito. Second edition. 327pp.

Tobias, C.R., J.W. Harvey and I.C. Anderson. 2001. Quantifying groundwater discharge through fringing wetlands to estuaries: Seasonal variability, methods comparison, and implications for wetland-estuary exchange. *Limnology and Oceanography* 46(3): 604-615.

Vaithiyanathan, P. and C.J. Richardson. 1997. Nutrient profiles in the everglades: examination along the eutrophication gradient. *The Science of the Total Environment* 205(1): 81-95.

Valiela, I., J.M. Teal, S. Volkmann, D. Shafer and E.J. Carpenter. 1978. Nutrient and particulate fluxes in a salt marsh ecosystem: Tidal exchanges and inputs by precipitation and groundwater. *Limnology and Oceanography* 23(4): 798-812.

Ward, L.G., M.S. Kearney and J.C. Stevenson. 1998. Variations in sedimentary environments and accretionary patterns in estuarine marshes undergoing rapid submergence, Chesapeake Bay. *Marine Geology* 151: 111-134.

Weight, W.D. and J.L. Sonderegger. 2001. Manual of Applied Field Hydrogeology. McGraw-Hill, New York. 608pp.

Williams, G.D. 1997. The physical, chemical and biological monitoring of Los

Penasquitos Lagoon. Los Penasquitos Lagoon Foundation Annual Report: 20 September 1996 – 20 September 1997. <http://www.torreypine.org/Lagoon/gw97lpl.htm>

Williams, G.D. and J.B. Zedler. 1999. Fish assemblage composition in constructed and natural tidal marshes of San Diego Bay: Relative influence of channel morphology and restoration history. *Estuaries* 22(3A): 702-716.

Williams, P.B., M.K. Orr and N.J. Garrity. 2002. Hydraulic geometry: A geomorphic design tool for tidal marsh channel evolution in wetland restoration projects. *Restoration Ecology* 10(3): 577-590.

Wise, W.R and R.D. Myers. 2002. Modified falling head permeameter analyses of soils from two South Florida wetlands. *Journal of the American Water Resources Association* 38(1): 111-117.